2010

Prototype electron phantom for radiographic and radiochromic film dosimetry

Chad Joseph Robertson
Louisiana State University and Agricultural and Mechanical College, crobe56@gmail.com

PROTOTYPE ELECTRON PHANTOM FOR RADIOGRAPHIC AND RADIOCHROMIC FILM DOSIMETRY

A Thesis

Submitted to the Graduate Faculty of the
Louisiana State University and
Agricultural and Mechanical College
in partial fulfillment of the
requirements for the Degree of
Master of Science

in

The Department of Physics & Astronomy

by
Chad Joseph Robertson
B.S. Louisiana Tech University, 2006
May 2010

Acknowledgements

I would like to thank Dr. Kenneth Hogstrom for the opportunity to study medical physics at LSU, and for whose example has taught me to be a professional person and physicist. I also thank Dr. Michael Price for his time and patience in assisting me throughout the project, especially during the writing process. I am also grateful for the rest of my Supervisory Committee Members for their valuable assistance: Drs. Brent Parker, Erno Sajo, and Greg Stacy.

I would also like to thank everyone associated with the graduate education program within the Department of Medical Physics at LSU/Mary Bird Perkins Cancer Center. Thanks to Yvonne Thomas and Davelyn Zachary for their kind willingness to assist me in all secretarial matters.

I would like to thank Mr. Ken Freeman at Gammex-RMI for fabricating the prototype film phantom's used in this study. Finally, I thank Mr. David Perrin for his helpful communications throughout the length of the project. Finally, I thank the clinical staff at Mary Bird Perkins Cancer Center, led by Dr. John Gibbons, for always taking their time to answer my questions.

Table of Contents

List of Tables

List of Figures

Abstract

Purpose: The purpose of this work is to develop a solid electron beam film phantom for use with radiographic film (RGF) and radiochromic film (RCF) to measure relative dose distributions in a principal plane containing the central axis for 6–20MeV electron beams. It was hypothesized that relative dose distributions measured using film will agree with corresponding diode measurements within ±2% of the central-axis maximum dose or ±1mm distance-to-agreement (DTA).

Method and Materials: Three prototype film phantoms were designed at Mary Bird Perkins Cancer Center and constructed by Gammex-RMI, Inc. Relative dose measurements, planar (2D) dose distributions containing central-axis, were acquired in the phantom using both Kodak-XV RGF and GafChromic-EBT RCF. Correspondingly, diode measurements were acquired utilizing a Scanditronix-Wellhofer 2D-water phantom. For prototype 3, dose distributions were measured at 100-cm SSD using a 15x15-cm^2 field-size at 6, 9, 12, 16, and 20 MeV, as well as 2x2-cm^2 and 4x4-cm^2 field-sizes at 9 and 16 MeV. Relative dose differences were evaluated with respect to regional criteria of acceptability: (1) high dose, low dose-gradient region (≤ 2 % dose), (2) high dose-gradient region (≤ 2 mm DTA), and (3) low-dose, low dose-gradient region (≤ 2 % dose).

Results: RGF depth-dose measurements agreed with diode measurements within all criteria for all measurements conditions. 2D dose distributions were in agreement with over 98% of measured dose points agreeing within ±2% dose or ±1mm DTA for all energies (6–20MeV, 15x15-cm^2). RCF depth-dose measurements agreed for all measurement conditions in all regions excluding the build-up region (<1–2cm depth), where measurements were approximately 3–4% low. 2D dose distributions reflected differences seen in the depth-doses with 90% of data points within criteria.

Conclusions: With appropriate modifications, the prototype 3 phantom is capable of accurately measuring relative electron dose distributions using RGF sufficiently for clinical use. RCF measurements acquired in the same phantom consistently underestimated diode measurements by 3–4% at depths <2-cm. The cause of this systematic error, believed to be a combination of film-edge misalignment and RCF depth-dependency, must be resolved before prototype phantom 3 with appropriate modifications would be acceptable for clinical use.

Chapter. 1 Introduction

1.1 Background and Significance

1.1.1 Electron Beam Commissioning

Due to characteristically sharp surface dose build-up (<10 mm), relatively uniform dose plateau, and steep distal dose fall-off, electron beams are utilized in radiotherapy to irradiate superficial targets while minimizing dose to underlying critical structures (Tapley 1982; Hogstrom 1991; Hogstrom 2003). Prior to clinical use, medical radiotherapy accelerator electron beams must be commissioned for treatment planning by measuring output and relative dose distributions for multiple combinations of energy, field size, and source-to-surface distance (SSD) (Das *et al.* 2008). Utilizing this data, treatment planning systems (TPS) are able to calculate dose distributions delivered to a patient's body for arbitrary electron fields (Das *et al.* 2008). As such, the accuracy of TPS dose calculations is highly dependent on the quality of the beam data collected during the electron beam commissioning process.

Per the recommendation of the American Association of Physicists in Medicine (AAPM) Task Group 25 (Khan *et al.* 1991), electron beam commissioning measurements should be measured in water using an ion chamber, the accepted standard, or silicon diode. Ion chambers measure directly the charge liberated by radiation in a known volume of air. By applying multiple correction factors, dose that would be absorbed by an equivalent volume of water can be determined from these measurements. Conversely, silicon diode detectors are relative dosimeters. They are useful for electron beam dosimetry since, unlike ion chamber measurements, they do not require stopping-power corrections to obtain the percent depth-dose (PDD). Furthermore, diode detectors are more sensitive than ion chambers ($\approx 10^{3}$) while having a much smaller active region ($\approx 10^{-3}$) (Khan 2003). As with any relative dosimeter, its ability to accurately measure relative dose must be demonstrated by comparison to the "gold" standard ion

chamber. Silicon diodes, TLD, and film have been shown accurate to within 2 % if properly used (Ten Haken *et al.* 1987; Wong 1987).

Electron beam commissioning requires measurements of PDD profiles along the beam's central-axis (CAX) using a scanning diode or ion chamber in water. Off-axis dose profiles are required to construct two-dimensional dose distributions and are measured by scanning the diode laterally across the field, in a plane including the central-axis point perpendicular to the incident beam edge, at multiple depths. A typical clinical linear accelerator produces electron beams for several different nominal energies, which are delivered utilizing differing field-size applicators with Cerrobend inserts and variable collimation systems. Thus, a large number of beam measurement conditions are necessary for commissioning. Due to the set-up time and number of measurements required, the commissioning of a clinical electron treatment planning system using a water phantom and scanning diode/ion chamber is a time-intensive process.

The use of film in a phantom composed of water-equivalent material is an alternative, less time-intensive method of collecting electron beam dose measurements (Khan *et al.* 1991) applicable for beam commissioning, patient-specific "spot" measurements, testing new technology (e.g. electron bolus), and research. Such a water-equivalent phantom has the same electron scattering characteristics as water. Although, this phantom-type requires significantly less time for set-up than a water phantom, it still allows for the acquisition of high resolution data at multiple depths. Film's ability to measure PDD and off-axis dose profiles in a single radiation exposure decreases beam-on time compared to equivalent measurements performed using a scanning diode.

1.1.2 Radiographic Film

Radiographic film (RGF) is used as a reliable dosimeter to create permanent records of high resolution dosimetric data in a 2-D plane with a single radiation exposure (Pai *et al.* 2007).

RGF consists of a transparent film base that has been coated with an emulsion containing crystals of silver bromide. When high-energy radiation, or visible light, interacts with the emulsion the crystals are ionized and a latent image is formed. This image is developed by washing off the unaffected silver bromide crystals, revealing the clear base, and leaving the darkened silver ions through a wet developing process. The amount of darkening on the film is directly related to the amount of radiation absorbed by the film emulsion. Placed in a solid phantom, RGF has been used to measure relative dose distributions for electron beams. These measurements have been shown to agree well with measurements taken using an ion chamber in water (Bova 1990; Shiu *et al.* 1989). Shiu *et al.* reported both depth-dose and off-axis dose measurements using RGF that were in agreement to equivalent measurements acquired using an ion chamber/water phantom within ± 1 % relative dose or ± 1 mm distance-to-agreement for PDD and off-axis dose measurements at depths > 10 mm. For depths < 10 mm, film measurements systematically underestimated diode measurements by 2.5 – 3 %.

Disadvantages of RGF include its sensitivity to visible light and development requirements. RGF must be handled in a light-tight environment, and Cerenkov radiation can be an issue that depends on the phantom (Fujisaki *et al.* 2003) and whether film is bare or in a jacket (Perrin *et al.* 2007). The wet developing process requires specialized equipment that can introduce systematic errors and artifacts. The repeatability of dosimetric measurements between RGF's processed at the same time from the same manufacturing lot has been reported to be within ± 3 %, while variance between films from different batches has been shown to be greater than ± 5 % (Khan *et al.* 1991). Additionally, RGF measurements have been shown to underestimate diode measurements by ≈ 2-3 % at depths < 10 mm due to the high Z silver in the RGF emulsion causing electron side-scatter disequilibrium at the film edge/phantom surface (Pai *et al.* 2007).

1.1.3 Radiochromic Film

Heretofore, radiochromic film (RCF) has not been used as extensively as RGF for electron dose measurements. However, due to the number of facilities decommissioning on-site RGF processor equipment, RCF is rapidly gaining clinical relevance. RCF offers some advantages over RGF for use as a dosimeter. It is nearly insensitive to visible light, eliminating the need for darkroom facilities and allows the film to be easily handled. Also, RCF is self-developing and does not require wet chemical processing, known to be a source or error in RGF measurements (Niroomand-Rad *et al.* 1998).

RCF consists of a thin (7 - 23 μm), radiosensitive layer of monomer crystals dispersed in gelatin bonded onto a Mylar base (Khan 2003). When high-energy radiation interacts with the active layer, the monomer converts to a polymer, changing the color of the dye in proportion to the amount of incident radiation absorbed. The effective atomic number (Z) of the radiochromic film emulsion is similar to that of water, eliminating the errors introduced by the high-Z silver emulsion of RGF. van Battum *et al*. (2008) reported good agreement (<2%) between EBT film and ion chamber measurements taken in a liquid water phantom for a 6 MV photon beam. Currently, there are no known reports in the literature investigating the use of RCF in a solid, water-equivalent phantom for edge-on exposure of high-energy clinical electron beams.

1.1.4 Functional Requirements of Solid Film Phantoms

When designing solid phantoms for use as a radiation dosimetry medium, there are several considerations which should be addressed. First, the phantom must be water equivalent, i.e., having the same linear stopping power and linear angular scattering power as water (Khan *et al.* 1991). Second, the phantom should facilitate sub-millimeter accuracy in alignment of the *en face* film edge with the phantom surface. Misalignments as small as ≈1 mm have been shown to produce dose measurement errors up to 10 % at the film/phantom edge (Dutreix and Dutreix

1969). Third, air gaps between the film and phantom have to be removed, as air gaps of ≈ 0.25 mm can produce errors in the measured PDD curve > 10 % (Dutreix and Dutreix 1969). With air gaps present, errors in the PDD are manifested as an underestimation of dose in the first few mm followed by a sharp overestimation of dose, then following the shape of the PDD after 2-3 cm. Fourth, Cerenkov radiation produced due to electrons traveling faster than the speed of light within the phantom must be either uniform throughout the phantom, a constant fraction of the reading, or a small amount of the reading. Finally, the phantom should be easy to load, meeting the desired alignment criteria, within a light-tight room to meet the requirements for RGF use.

The Bova and Shiu phantoms were shown to fulfill these conditions and to produce accurate dose measurements (Bova 1990; Shiu *et al.* 1989). However, these phantoms were constructed in-house and are not commercially available. Currently, there are no commercially available solid film phantoms proven accurate for RCF or RGF for electron dosimetry. The Solid Water Film Cassette (Model 436-AST), manufactured by Gammex RMI (c.f. Figure 1.1) was evaluated at Mary Bird Perkins Cancer Center and determined to be inadequate for clinical use for several reasons (Perrin *et al.* 2007): (1) The phantom produced air gaps perpendicular to the film when the film was when secured into place. (2) Pins within the phantom, designed to exactly align the RGF edge at the phantom's surface actually positioned the film so that the film edge falls 2 mm short of the phantom's surface. (3) Both halves of the phantom are scored at the surface edge, resulting in an irregular surface around the film for depths < 0.25 mm. (4) Since there are ten screws that must be tightened to secure the phantom's film cassette in place, it is difficult to handle in a darkroom. Gammex RMI offers a second film cassette (Model 436-10) but this cassette was not evaluated as it does not allow for measurements at the phantom surface.

These shortcomings led to the design and construction of a new phantom to fulfill the aforementioned properties for a clinically useful electron beam commissioning film phantom.

Figure 1.1: Gammex Model 436-AST film phantom. The phantom was unsuitable for clinical use due to several design flaws.

The phantom prototypes were designed by Dr. Ken Hogstrom and the electron research team at MBPCC in collaboration with the Gammex-RMI team coordinated by Mr. Ken Freeman, who fabricated the prototypes. The new phantom design adopted features from that of Chi et al (2006), a cylindrical design for electron arc therapy dosimetry. It used a removable film cassette to house bare film, which facilitated easy loading and unloading of the film. Additionally, the new phantom cassette has incorporated mechanics for fine adjustment of the film's edge parallel to the direction of the electron beam to ensure precise film edge/phantom surface alignment. Such feature also allows for inconsistencies in film dimensions as slight variations, up to ≈ 0.5 mm in the length of RCF, have been measured by the author. The removable film cassette is designed to slide into a larger phantom consisting of two, 5-cm thick slabs to provide ample scatter for electron beams. This configuration also compresses the film within the cassette to expel air gaps between the film and phantom cassette. The film cassette was designed to house 10"x12" RGF, while use of 8"x10" RCF is accomplished by placing a spacer on the downstream edge of the film to place the upstream film edge near the phantom surface.

1.2 Purpose

The purpose of this study is to develop in collaboration with Gammex-RMI and to evaluate a prototype film phantom that is clinically applicable and that accepts both 10"x12" RGF and 8"x10" RCF. Evaluation includes the ergonomics of the phantom, and the accuracy of relative dose distributions measured in a principal plane containing the central axis.

1.3 Hypothesis and Specific Aims

Relative central-axis (CAX) depth-dose and off-axis dose profiles measured for square electron fields using radiographic and radiochromic film in a prototype solid water phantom designed at Mary Bird Perkins Cancer Center will agree with equivalent measurements taken in a water phantom using a diode within ± 2 % of the CAX dose maximum or ± 1 mm distance-to-agreement (DTA).

The hypothesis will be verified by completing the following specific aims:

Aim 1. Measure relative depth-dose and off-axis dose profiles in water using diodes. Relative depth-dose and off-axis profiles for standard electron fields will be measured in water using a diode and Wellhofer (Elimpex-Medizintechnik, Moedling, Austria) scanning system. As recommended by AAPM's TG-70 (Gerbi *et al.* 2009), diode measurement accuracy will be validated by comparing depth-dose measurements acquired using a parallel plate ion chamber in the water phantom.

Aim 2. Measure relative depth-dose and off-axis dose profiles in the prototype film phantom using radiographic film. Kodak XV radiographic film (Carestream Health Inc., Rochester, NY) will be used in the prototype film phantom to measure relative depth-dose and off-axis dose profiles for standard electron fields.

Aim 3. Measure relative depth-dose and off-axis dose profiles in the prototype film phantom using radiochromic film. GafChromic EBT radiochromic film (International

Specialty Products, Wayne, NJ) will be used in the prototype film phantom to measure relative depth-dose and off-axis dose profiles for standard electron fields.

Aim 4. Compare the measurements taken in Aims 1 – 3. Percent depth-dose curves, off-axis relative dose profiles, and reconstructed 2-D isodose profiles from both types of film will be compared to diode data taken from the water scanning system to verify the accuracy of measurements obtained using the prototype film phantom.

Chapter. 2 Methods and Materials

2.1 Prototype Film Phantom Designs and Refinements

2.1.1 First Prototype Design Characteristics

The first phantom prototype was designed at Mary Bird Perkins Cancer Center (MBPCC) and fabricated by Gammex-RMI (Middleton, WI). The Solid Water® (Gammex-RMI, Middleton, WI) phantom was designed to measure 2D dose distributions in a plane containing the central axis (CAX) (edge-on exposure) for electron beams in the energy range of 6-20 MeV.

Solid Water® is composed of hydrogen (8.1%), carbon (67.2%), nitrogen (2.4%), oxygen (19.9%), chlorine (0.1%), and calcium (2.3%) (Gammex 2009). Solid Water® can be used as a dosimetric surrogate for liquid water as its linear collision stopping power relative to water is 1.00, and its relative linear angular scattering power is 1.02 (Khan *et al.* 1991).

This prototype consisted of two major components: a phantom body and film cassette. (c.f. Figure 2.1).

Figure 2.1: Picture of the first prototype showing the film cassette and phantom body.

The film cassette consisted of two, 1.5-cm thick halves. One half contained a 0.5 cm female recess that matches the external dimensions of a sheet of 10" x 12" (25.4 x 30.5 cm) bare radiographic film (RGF). The other half of the cassette was designed to fit inside the recess, securing the film sheet firmly in place. The phantom body was composed of two 5-cm thick halves that, when assembled, house the film cassette. The cassette was secured within the phantom body using four compression bolts located at each corner. This design served to compress the film cassette, thus removing air gaps between the film and phantom. A metal rod, pushed through a hole located at the downstream edge of the phantom, was used to remove the film cassette from the phantom body. A detailed schematic of the prototype film phantom is shown in the Appendix.

2.1.2 Second Prototype Design Characteristics

The second prototype, also fabricated by Gammex-RMI, consisted of an updated film cassette designed to be inserted within the first prototype's phantom body. The inner surface of the second prototype cassette was milled in a manner to reduce optical speckling when compared to the first prototype. It was suspected that these imperfections caused non-uniform Cerenkov radiation contamination in film measurements acquired using the first prototype cassette. A comparison of the first and second prototype inner cassette surfaces are shown in Figure 2.2.

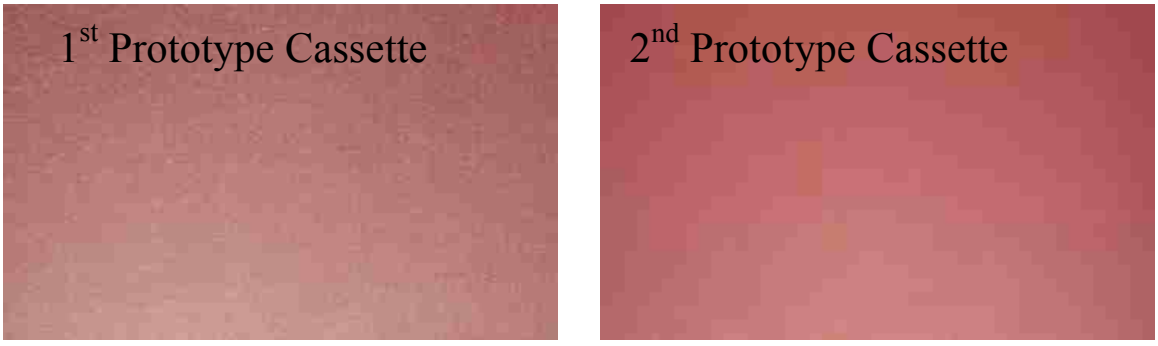

Figure 2.2: Inner cassette surfaces of both the first and second prototype film phantoms. The milling process used in the second prototype phantom resulted in an optically less speckled surface.

The second prototype film cassette was ≈ 1.0 mm wider than the first prototype's cassette and as a result could not fit inside the phantom body. Therefore, measurements were acquired with the phantom body disassembled and the film cassette placed between the two phantom body halves as shown in Figure 2.3. The gantry head was rotated to 90^{o}, and the treatment couch was set to 270^{o}.

Figure 2.3: Second prototype film phantom measurement set-up. The cassette was placed between the two slabs of phantom housing. The gantry was rotated to 90^{o} and the couch was placed at 270^{o}.

2.1.3 Third Prototype Design Characteristics

The third prototype phantom was designed at MBPCC and fabricated by Gammex-RMI. The design of the phantom cassette and housing was similar to that used in the first and second prototype phantoms. However, the third prototype phantom featured an adjustable cam located within the film cassette at the downstream edge of the film. This adjustable cam was utilized to reproducibly position the film edge at the phantom surface accurately (c.f. Figure 2.4). The

rotating cam provided fine adjustment of the film edge with respect to the *en face* phantom surface. Due to the smaller dimensions of radiochromic film (RCF), a cardboard spacer (4.8 x 28 cm) was placed between the distal edge of the film and the adjustable cam (c.f. Figure 2.4). Upon receipt of the third prototype cassette, it was discovered that the film cassette's inner surface was milled in a similar fashion as for the first prototype. The resulting inhomogeneous inner cassette surface can be seen in Figure 2.5.

Figure 2.4: Third prototype film cassette. The film edge can be displaced ≤ 3.7 cm to allow precise alignment of the film edge with the phantom surface for different sized films. A spacer was used for RCF to account for the films' shorter length.

Figure 2.5: Close-up of the third prototype phantom's inner cassette surface. Milling was performed in a similar fashion as the first prototype resulting in an optically speckled surface.

2.1.4 Impact of Cerenkov Radiation

2.1.4.1 First Prototype Film Phantom

When bare RGF was irradiated with an electron beam, edge-on, in the first prototype phantom (20 MeV, 15x15 cm^2), local variations akin to high frequency noise were observed in the high-dose region of the measured percent depth-dose (PDD) curves. These variations were reproducible, and an example of this measured phenomenon is shown in Figure 2.6. It was thought that these artifacts were due to optical non-uniformities present in the milled surface of the Solid Water film cassette, which vary the amount of Cerenkov light reaching the film. This conclusion was based on the film variations being reproducible with depth on repeated, independent film exposures.

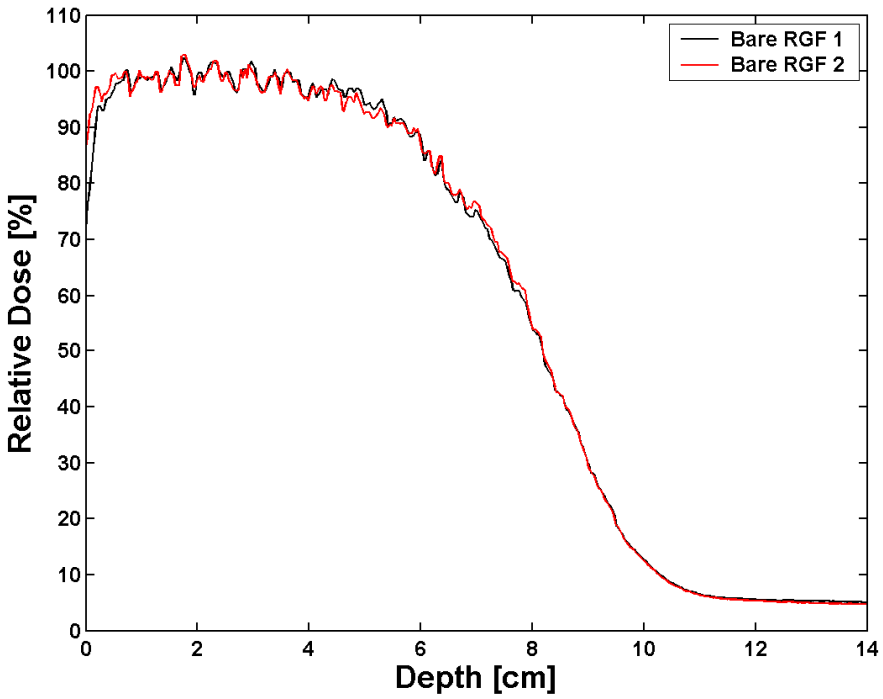

Figure 2.6: Comparison of CAX PDDs (20 MeV, 15x15 cm^2) measured using two separate RGFs in the first prototype cassette. Curves RGF 1 and RGF 2 demonstrate the reproducibility of Cerenkov variations in the first prototype cassette due to optical non-uniformities present in the film cassettes inner surface.

To remove the Cerenkov radiation contamination, prior to irradiation, the film was placed between two pieces of thin black paper cut to the exact size of the film cassette recess. The measured RGF PDD curve acquired with the film placed between sheets of black paper is shown in Figure 2.7. Due to the paper's opacity, the Cerenkov light contamination observed for bare film measurements are not present, while the shape of the curve is retained. This further supports the conclusion that the variations seen in the PDD are due to non-uniform changes in the milled surface of the film cassette.

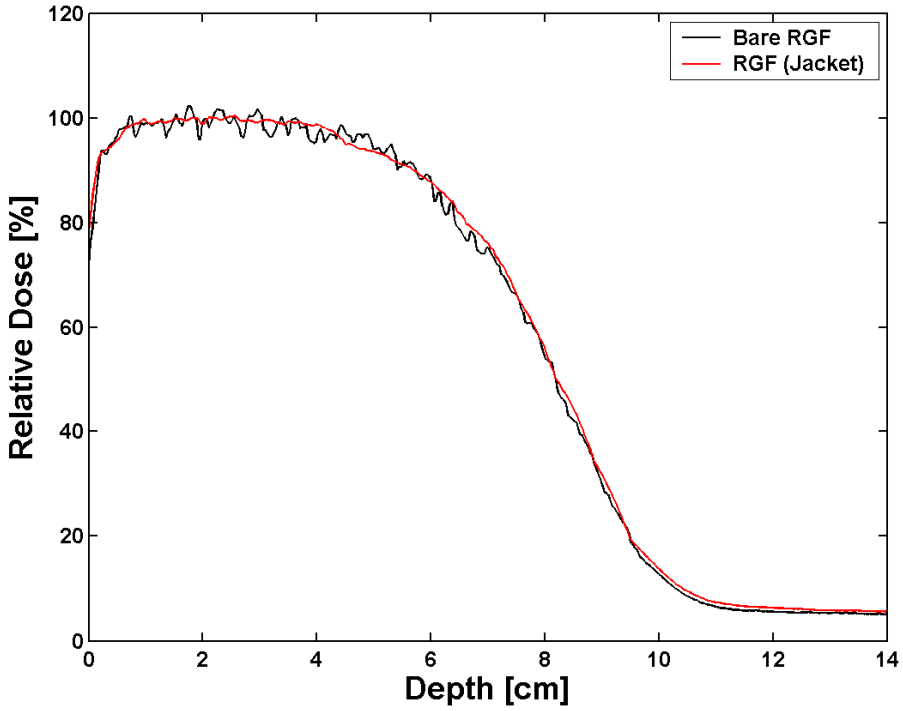

Figure 2.7: Comparison of CAX PDD measurements (20 MeV, 15x15 cm^2) for bare film and film contained in the light tight jacket within the first prototype film cassette.

2.1.4.2 Second Prototype Film Phantom

To observe the difference in the Cerenkov variations produced in the second prototype cassette due to the different milling process used, bare RGF was irradiated (16 MeV, 15x15 cm^2) within the second prototype cassette in the configuration shown in Figure 2.4 (c.f. Figure 2.8).

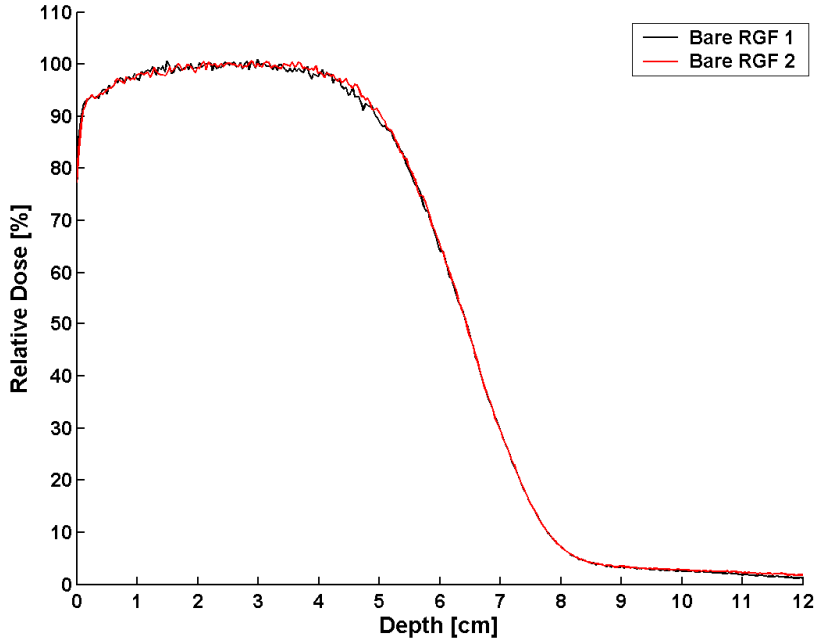

Figure 2.8: Comparison of CAX PDDs (16 MeV, 15x15 cm^2) measured using two separate RGFs in the second prototype cassette. The Cerenkov variations are reduced in magnitude relative to the first prototype cassette due to increased uniformity in the optical speckling of the film cassettes inner surface.

Cerenkov variations in the measured PDD were reduced in magnitude when compared to PDD measurements acquired using the first prototype cassette. This decrease in Cerenkov variations is due to increased optical uniformity in the inner milled surface of the film cassette causing the amount of Cerenkov light reaching the film to be more constant throughout the phantom. The Cerenkov variations present in the second prototype cassette measurements were removed using two different methods. The first method (c.f. Figure 2.9) smoothed the PDD curve using a smoothing algorithm that performs a least-squares fit of a 3rd order polynomial to a 31-point sliding window (Savitzky and Golay 1964). While the second method involved placing the film between two thin pieces of black photographic paper which shielded the Cerenkov light from reaching the radiographic film (c.f. Figure 2.10).

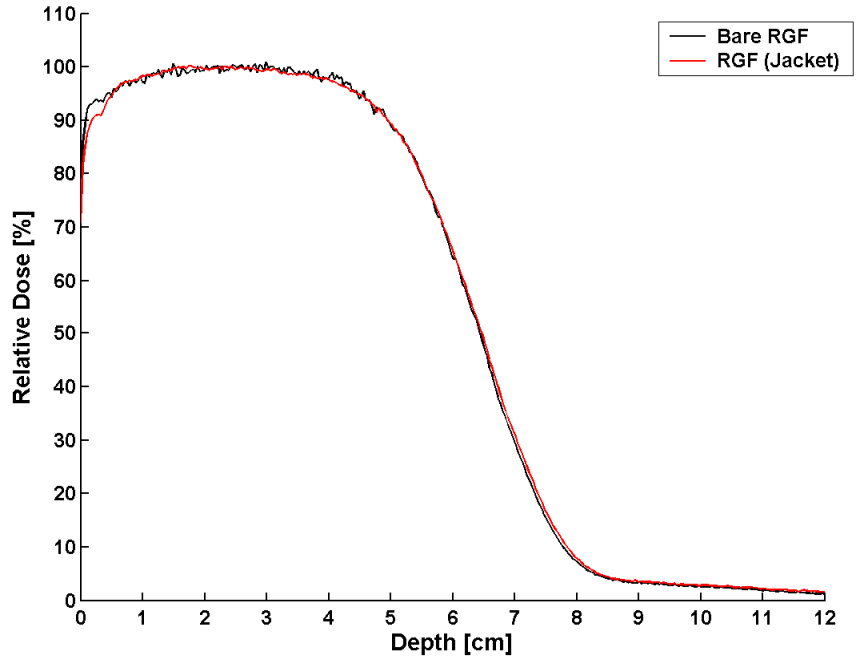

Figure 2.9: Comparison of CAX PDDs (16 MeV, 15x15 cm^2) for bare film compared to film irradiated in the black paper within the second prototype film cassette.

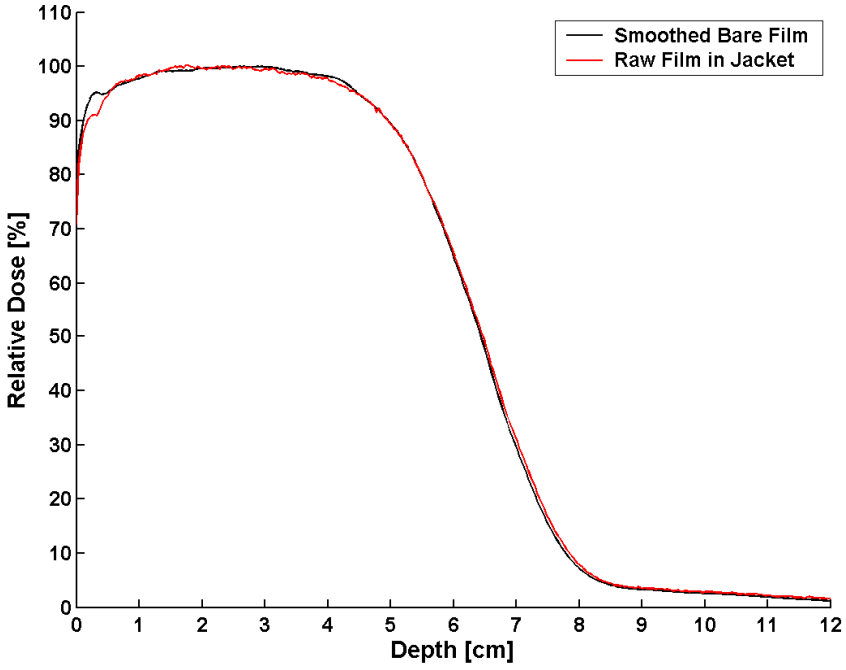

Figure 2.10: Comparison of smoothed CAX PDD data measured using bare film vs. unsmoothed CAX PDD (16 MeV, 15x15 cm^2) measurement for film irradiated within the photographic paper, in the second prototype cassette. Both methods effectively remove the high frequency Cerenkov noise present in the PDD.

Data points less than half the length of the sliding window from the surface were smoothed by extending the data set beyond the surface and inflecting the data about the surface depth. Both the smoothing algorithm and use of the black paper reduced the effect of Cerenkov noise in the PDD. Therefore, it was decided to use the smoothing algorithm to remove the small effect of Cerenkov noise from film measurements made using the second prototype phantom, as it was desired to irradiate bare film to eliminate possible artifacts introduced by use of the black photographic paper.

2.1.4.3 Third Prototype Film Phantom

When bare RGF was irradiated in the third prototype film phantom (16 MeV, 15x15 cm^2), Cerenkov variations are seen in the measured PDD similar to those measured using the first prototype film cassette (c.f. Figure 2.11).

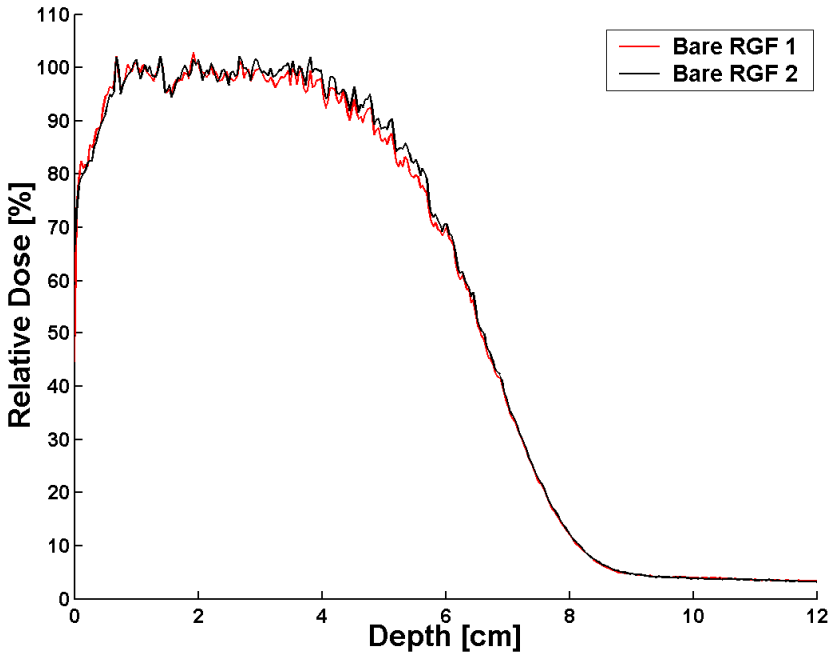

Figure 2.11: Comparison of CAX PDD's (16 MeV, 15x15 cm^2) measured for two separate films irradiated within the third generation film phantom using bare RGF. Reproducible Cerenkov variations are present in the PDD as seen in the first generation film cassette due to non-uniform optical speckling in the film cassette inner surface.

These variations were removed by placing the film between two cut sheets of black paper, as for the first prototype cassette, and the resulting CAX PDD is shown in Figure 2.12.

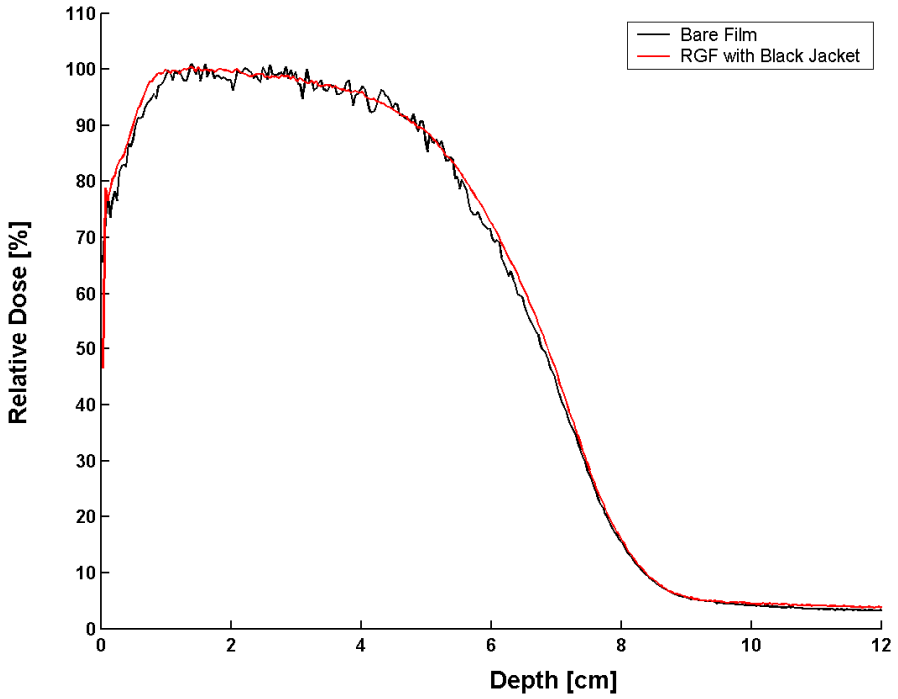

Figure 2.12: Comparison of CAX PDD measurements (16 MeV, 15x15 cm^2) for bare RGF and film contained in the light-tight paper within the third prototype film phantom.

Use of the black paper removes the Cerenkov contamination, therefore all film measurements acquired in the third prototype phantom for comparison to diode measurements were taken with the film placed between the pieces of photographic paper before being inserted into the cassette. The photographic paper was cut to the exact size of the phantom cassette recess by inserting the paper in the phantom so that the edge protruded beyond the phantom surface and using a razor blade to trim the paper flush with the phantom surface. It was decided to not smooth measurements acquired in the third prototype phantom, as done for the second prototype phantom, due to possible errors introduced at the surface measurements for data points less than one-half of the length of the sliding window from the surface.

2.1.5 Impact of Film Edge Alignment

When comparing RGF PDD measurements acquired using the second prototype phantom to diode measured PDDs, agreement was observed for all depths excluding those near the surface (< 1 cm). In this region, film underestimated diode measurements, on average, by ≈ 3%. Figure 2.13 shows an example of this effect for a 16 MeV, 15x15 cm^2 electron field irradiated in the second prototype phantom. It was theorized that these discrepancies were due to misalignment of the film and phantom edges at the phantom's *en face* surface. An illustration of the effects of film misalignment at the phantom surface when film is irradiation edge-on in an electron beam is shown is Figure 2.14 (Dutreix and Dutreix 1969). As shown in the figure, for the film protruding by 1 mm, as dose error of approximately 10 % decrease is introduced in the relative film dose measurement at the phantom surface. Also, the measured penetration for the 1 mm misaligned film is visibly different than that for the aligned film as shown in Figure 2.14 by the surface depth value being placed at a negative depth. For measurements in the second prototype phantom, since error in film dose is an approximately 3 % decrease with insignificant difference in penetration, hence it is believed that misalignment errors are on the order of 0.2 millimeter.

Further film edge alignment issues were encountered since the second prototype film cassette was designed to specifically house 10"x12" RGF sheets. For the use of 8"x10" RCF sheets, a spacer was used to adapt the cassette. The spacer was a 4.8 x 28 cm cardboard strip placed at the downstream film edge to align the irradiated film edge flush with the phantom surface. Use of this rigid spacer resulted in inconsistent alignment of the film edge at the phantom surface due to variations in the dimensions of different sheets of RCF (maximum of ± 0.5 mm in the direction of the incident beam). This variation (σ = 0.43 mm, n = 24) was observed by the author for films taken within the same as well as across different manufacturing lots. Therefore, in order to facilitate accurate and reproducible alignment of slightly different

sized films, a third prototype film cassette was designed that includes a mechanism to allow for fine adjustment of the film edge at the phantom surface (c.f. Figure 2.4).

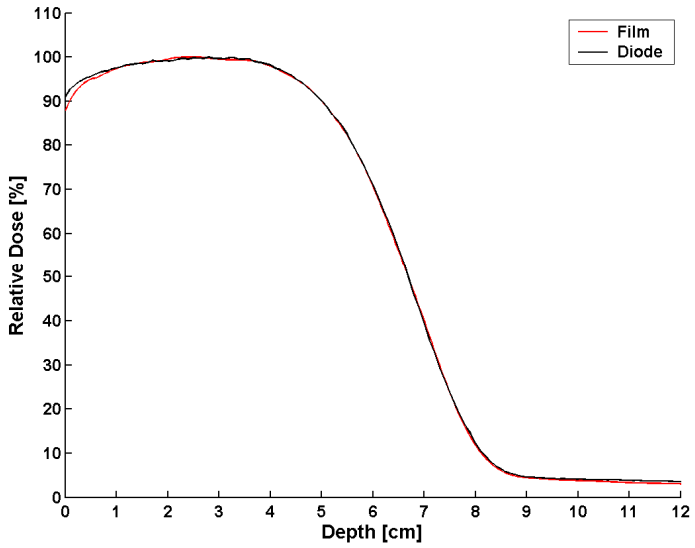

Figure 2.13: Smoothed PDD measured in the second prototype phantom for a 16 MeV, 15x15 cm^2 electron beam. Underestimation of dose by film at the phantom surface is believed to be due to misalignment of the film edge at the phantom surface, e.g. protruding 0.3 mm.

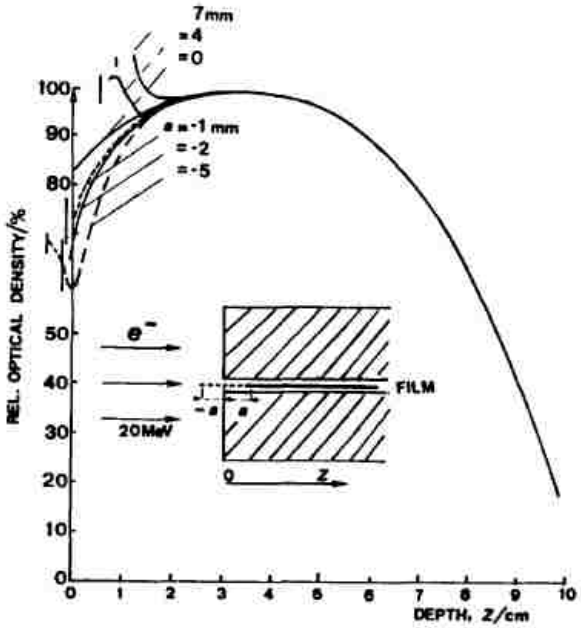

Figure 2.14: Effect of film misalignment at phantom surface on the PDD curve (Dutreix and Dutreix 1969).

2.1.6 Impact of Film-Phantom Air Gap

When comparing RGF PDD measurements using the third prototype phantom and diode measured PDDs, (c.f. Figure 2.15), the shape of the film measured PDD curve suggested that an air gap was present between the film and inner cassette surface. As shown in Figure 2.16, for small air gaps (0.25-0.75 mm), film measurements underestimate the dose at the surface before sharply increasing to overestimate the dose. The curve then matches the shape of the true PDD but penetrates deeper (Dutreix and Dutreix 1969). By comparing this figure to the film measurements acquired in the third prototype phantom, normalizing the Dutreix curves to 100 % at maximum dose, it is estimated that an air gap slightly less than 0.25 mm is present within the film cassette.

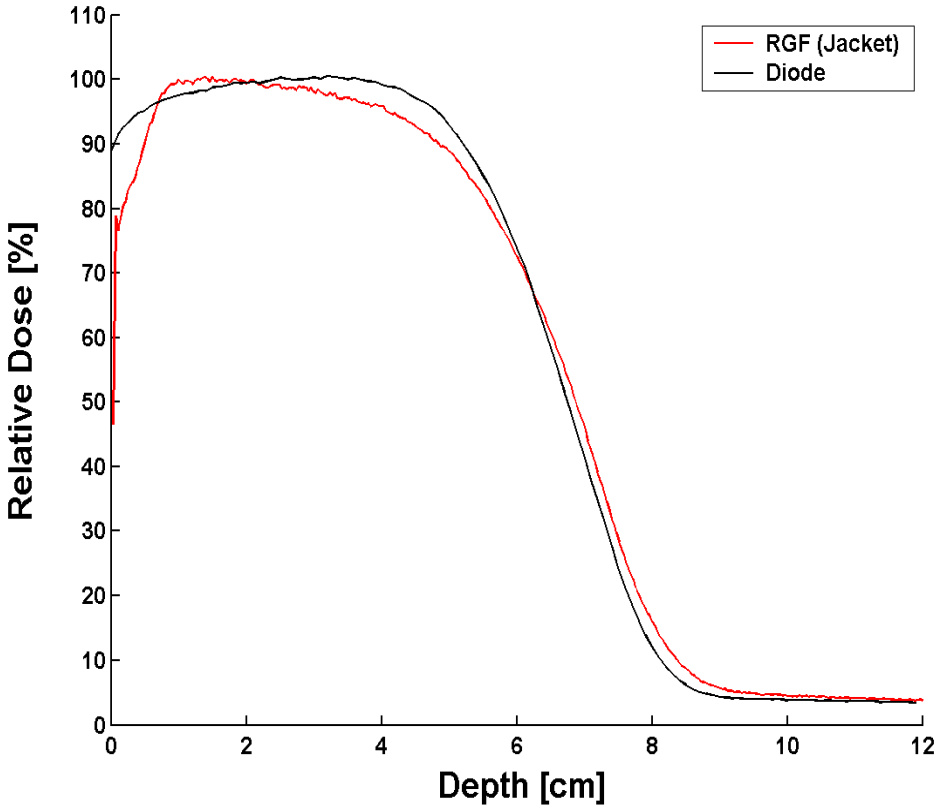

Figure 2.15: Comparison of CAX PDDs measured in the third prototype phantom compared to diode PDD measurement for a 16 MeV, 15x15 cm^2 electron field.

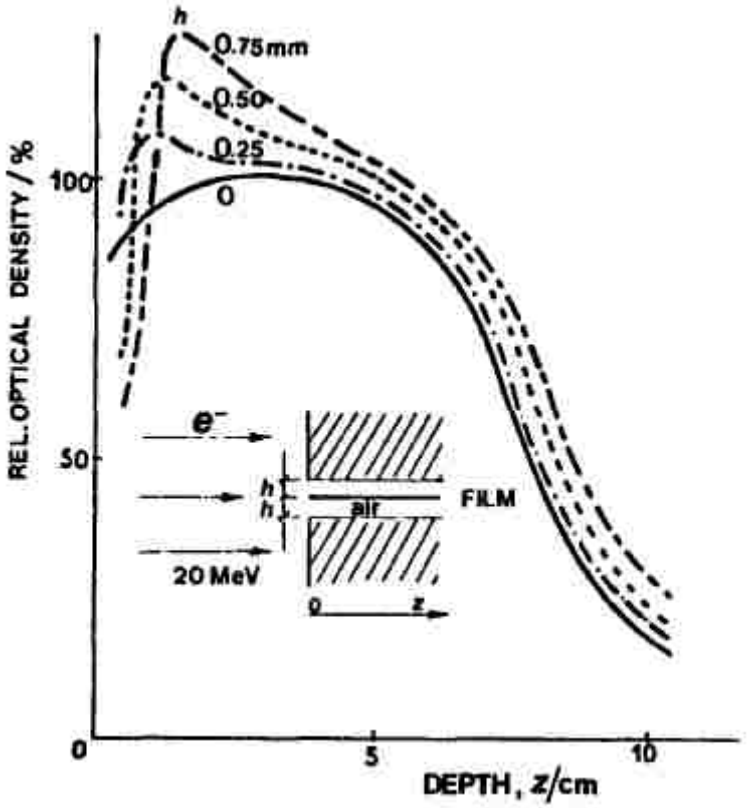

Figure 2.16: Effect of air gap between the film and phantom on the PDD curve (Dutreix and Dutreix 1969).

It was thought that this air gap was produced by the compression bolts located at the corners of the phantom, which caused the center of the film cassette to bow. This created a separation that is largest at the phantom center. To remedy this effect, a C-clamp was fastened around the phantom housing with wooden blocks placed between the clamp arms and phantom housing to more uniformly compress the phantom (c.f. Figure 2.17). The resulting PDD measured with the C-clamp around the phantom is shown in Figure 2.18. The improved agreement between the film and diode lends support to our assessment that an air gap was present within the film cassette. Therefore, all measurements acquired in the third prototype phantom for the purposes of comparison were done with the C-clamp secured around the phantom housing.

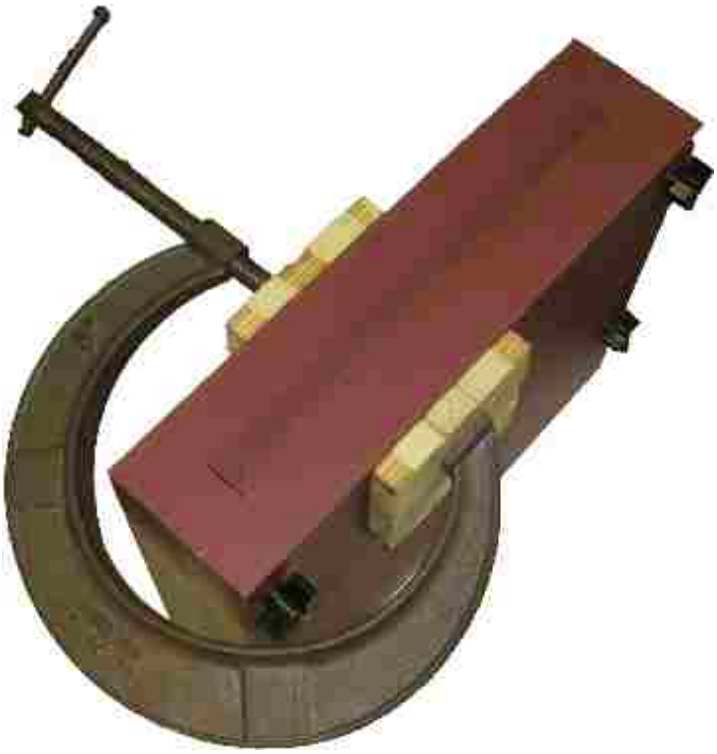

Figure 2.17: C-Clamp used to compress the film and remove air present between the film and third prototype phantom cassette.

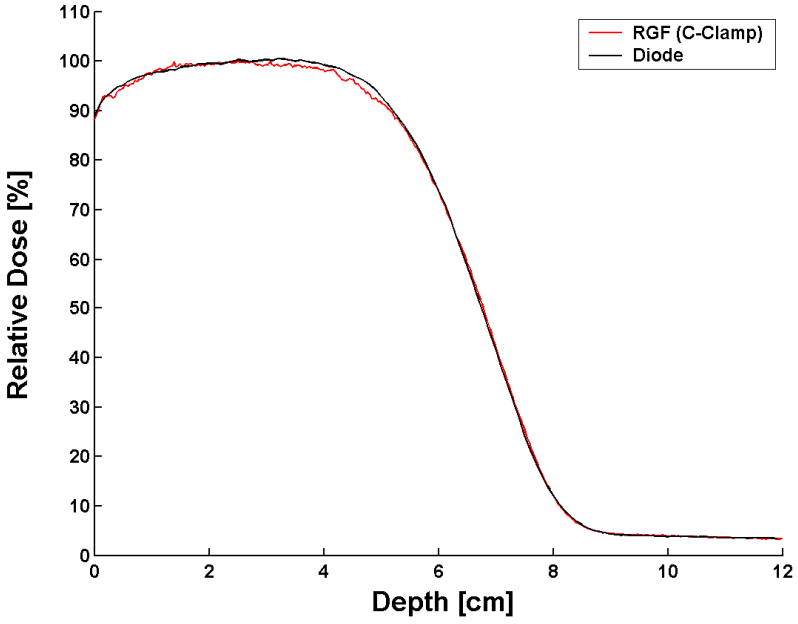

Figure 2.18: 16 MeV, 15x15 cm^2 CAX PDD measured using the third prototype film phantom with RGF placed inside the film packaging and the C-clamp around the phantom compared to diode measured CAX PDD.

2.2 Aim 1: Measurement of Relative Dose in Water

2.2.1 Relative Dose Measurements in Water Using an Ion Chamber

As recommended in the AAPM Task Group 70 (Khan *et al.* 1991), CAX PDDs were acquired using a PTW (PTW, Freiburg, Germany) Roos-style parallel plate ionization chamber (PTWN31001, SN: 0601799) in a 2-D water phantom (WP-700, Wellhofer Dosimtrie, Germany), compared to equivalent diode measurements to verify the accuracy of the diode detectors used in this study for measuring relative dose. The sensitive volume of the ion chamber was specified by the manufacturer to be 0.35 cm^2. To acquire measurements, the ion chamber was affixed to the water phantom's moveable carriage. The upstream surface of the chamber was level and positioned even with the water surface. The chamber was shifted upstream 1.3 mm to account for manufacturer's specified thickness of the chambers entrance window (PTW 2009). A cylindrical ion chamber (PTW TN30013-3114, SN: 0802381), placed upstream within the primary field but outside of the light field was used as a reference chamber to account for variations in the machine output.

Measurements were acquired utilizing the step-by-step measurement mode of the Wellhofer scanning system with a depth resolution of 0.1 cm. Ionization vs. depth along the CAX was measured for all accelerator electron energies (6, 9, 12, 16, 20 MeV) for a 15x15 cm^2 electron field at 100-cm SSD generated by a Varian Clinac 21EX 4/10 linear accelerator (SN: 1412). The relative depth-ionization measurements were converted to relative dose by correcting the measurements using stopping power ratios calculated as described in the AAPM's TG-70 (Gerbi *et al.* 2009). The resulting PDDs were then compared to equivalent diode measurements.

2.2.2 Relative Dose Measurements in Water Using Diode

Relative dose measurements acquired using the diode in the water phantom were performed in accordance with the AAPM Task Group 25 protocol (Khan *et al.* 1991; Almond *et*

al. 1999). Two silicon diode, electron field detectors (EFD, Scanditronix-Wellhofer, Germany) were used in conjunction with a scanning water phantom (WP-700, Wellhofer Dosimtrie, Germany) controlled by Omni-Pro Accept v6.6 software (Madison, SD). A Varian Clinac 21EX 4/10 (SN: 1412) (Varian Medical Systems, Inc., Palo Alto, CA) linear accelerator was used to generate 6, 9, 12, 16, and 20 MeV electron beams with the gantry and collimating jaws rotated to 180^{o}. In this position, the beam is aimed toward the floor. The water tank was placed on top of the treatment couch and aligned in-plane using light field crosshairs and treatment room alignment lasers.

The diode reference detector was positioned above the tank so that it lies just outside the electron beam's path through the electron cone insert, but within the radiation field as defined by the x-ray collimators. The signal detector diode was affixed to the scanner's movable carriage, positioned at the center of the carriage's range of motion. A level was used to ensure the carriage was level with respect to the water surface. The treatment couch was adjusted laterally and longitudinally in order to center the diode field detector within the light field. The couch was then adjusted vertically to position the surface of the water at 100-cm SSD using the optical distance indicator (ODI) for guidance. The accuracy of the ODI was validated using a mechanical distance indicator prior to measurements.

The tip of the diode field detector was visually set even with the water surface. A piece of wax paper was placed on the water surface to eliminate a meniscus from forming around the diode tip. Then, the paper was removed and the carriage was raised 0.4 mm to align the active region of the diode to the water surface, per manufacturer specification. After set-up, an off-axis dose profile was measured (16 MeV, 15x15 cm^2 open applicator) at the depth of maximum dose to ensure the diode was centered in the electron field. A depth-dose profile was measured at the commencement and conclusion of each measurement session to ensure system consistency.

2.2.2.1 PDD Measurements

PDD was measured along the CAX of the electron field to a depth ≥ 4 cm deeper than each beam's practical range (Rp). The scanner's carriage was first positioned at the deepest measurement depth and then moved upstream towards the surface in 0.1 cm increments. Scanning in this direction is recommended to reduce the effect of meniscus formation at the water surface (Gerbi *et al.* 2009). The "dose-rate" mode (step-by-step) was used for measurement scans. In this mode, five diode readings are averaged for each reported reading.

2.2.2.2 Off-Axis Dose Profiles

Off-axis profiles were measured in an in-plane orientation, i.e. in the plane in which the gantry bending magnets redirect the electron beam. Similar to PDD data acquisition, "Dose-rate" data acquisition mode was utilized with a 0.1 cm spatial resolution. Profiles were acquired at ten different depths that varied as a function of electron energy. Using the 15x15 cm^2 PDD curve for each energy, the selection criteria was as follows: (1) minimum possible scan depth (0.2 cm), (2) three evenly spaced depths between the minimum scan depth and R_{90}, (3) R_{90}, (4) half-way between R_{90} and R_{20}, (5) R_{20}, (6) R_{10} + 1 cm, (7) R_{10} + 2 cm, and (8) R_{10} + 5 cm (c.f. Table 2.1).

Table 2.1: Depths [cm] of measurement for off-axis dose profiles using a diode within a scanning water phantom.

Energy	**6 MeV**	**9 MeV**	**12 MeV**	**16 MeV**	**20 MeV**	**9 MeV**	**16 MeV**	**9 MeV**	**16 MeV**
Field Size [cm^2]	**15x15**	**15x15**	**15x15**	**15x15**	**15x15**	**4x4**	**4x4**	**2x2**	**2x2**
Depths [cm]	0.2	0.2	0.2	0.2	0.2	0.2	0.2	0.2	0.2
	0.6	0.8	1.2	1.5	1.7	0.8	1.2	0.6	0.8
	1.0	1.5	2.1	2.7	3.1	1.5	2.2	1.0	1.4
	1.4	2.1	3.1	3.9	4.6	2.1	3.2	1.4	2.1
	1.8	2.8	4.0	5.2	6.1	2.7	4.2	1.9	2.7
	2.2	3.4	4.9	6.4	7.9	3.4	5.9	2.9	4.6
	2.7	4.1	5.7	7.7	9.7	4.1	7.5	3.9	6.6
	3.9	5.3	7.1	9.1	11.4	5.3	9.1	5.2	8.6
	4.9	6.3	8.1	10.1	12.4	6.3	10.2	6.2	9.6
	7.9	9.3	11.1	13.1	15.4	9.3	13.1	9.2	12.6

2.3 Aim 2: Measurement of Relative Dose in Prototype Phantoms Using Radiographic Film

2.3.1 Radiographic Film (RGF) Specifications

Kodak X-Omat V RGF (Carestream Health Inc., Rochester, NY) was utilized for electron beam measurements due its lack of energy-dependence in the range of electron beam energies utilized in this work (Pai *et al.* 2007). Kodak XV film is double sided with an AgBr/AgI crystal emulsion, and is approximately 0.18 mm thick. This film is suitable for dose measurements within the range of 0 to 80 cGy, corresponding to optical densities between 0 and 4 (Pai *et al.* 2007). Sheets of 10"x12" were utilized in this study.

2.3.2 RGF Calibration

A single calibration curve was measured for each batch of radiographic film (Bos *et al.* 2002). Curves were generated using eleven bare films placed inside the phantom cassette and irradiated to the following doses: 1.2, 5.5, 8.9, 13.3, 16.7, 22.2, 27.8, 33.3, 44.4, 55.4, and 66.7 cGy. Three other films from the same batch were left unirradiated and were developed to provide the background + fog optical density level for the film. Pixel intensity values for the transmitted light varied from approximately 278 to 37210 Vidar scanner values for the dose range 67 cGy to 0 cGy, respectively. The standard deviation of the three background film measurements was 108 Vidar scanner values, corresponding to a relative standard deviation of 0.3 % which indicates satisfactory consistency in the background level between films. Irradiated films were placed in an orientation perpendicular to a 16 MeV electron beam, collimated by a 15x15 cm^2 open applicator. Films were placed at a water equivalent depth of 3 cm (Plastic Water® [1.5 cm] + phantom cassette [1.5 cm Solid Water]) atop of 5 cm of Plastic Water® to provide sufficient backscatter. The top of the 1.5-cm Plastic Water® sheet was set to 100 cm SSD using the accelerator's optical distance indicator (ODI). Dose delivered to the center of the films was

measured prior to irradiation using a Roos style (PTWN31001) parallel-plate ion chamber (SN: 0057) irradiated in Plastic Water® (Elimpex) at a depth of 3 cm with 5 cm of backscatter. All ionization readings were converted to dose per AAPM Task Group Report 51 (Almond *et al.* 1999).

Exposed films were processed and digitized according to methods presented in section 2.3.4. The average scanner value over a 2x2 cm^2 region (≈ 3100 pixels) in the center of each irradiated field was measured and correlated to the delivered dose for cross calibration. To convert measured optical densities to dose, RIT ver 5.2 scanner software (Colorado Springs, CO) generated a piecewise polynomial fit to the calibration data (Fritsch and Carlson 1980). The measured data and resulting fit are shown in Figure 2.19.

Both the linear response range of RGF and of the film scanner was taken into consideration to determine the optimal amount of dose to deliver for electron dose profile measurements. Calibration films were digitized using a transmission type scanner (VIDAR DosimetryPRO® *Advantage* (Red), Vidar Systems Corporation, Hendon, Virginia) which correlates the amount of light transmitted through the film to the corresponding dose value to generate a calibration curve. The relationship between optical density, light transmission values, and monitor unit's (MU) delivered to XV film in the calibration setup for the Vidar scanner is shown in Figure 2.20. The solid line was obtained by scanning a calibrated step-wedge with strips of known optical density and measuring the corresponding scanner values. The data points represent measurements of films exposed to the said number of MU's that were read using an manual densitometer (y-axis) and then scanned to determine the Vidar scanner value (x-axis). Due to its logarithmic response, the resolution of the scanner is greatest for a range of optical densities between 0 and 1 (0 – 20 MU). Quantitatively, of the 65,536 possible scanner values measured by the Vidar scanner, ≈ 76 % lie within this range (Pai *et al.* 2007). Therefore, to

deliver dose in the region of greatest resolution, films were exposed to a D_{max} of 20 cGy, corresponding to an optical density of approximately 1 for Kodak X-OmatV RGF.

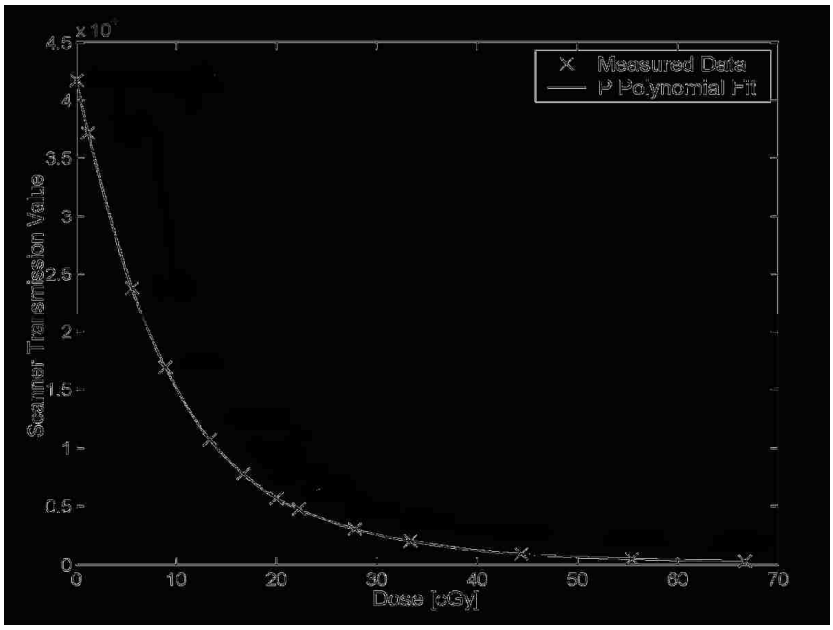

Figure 2.19: Measured calibration dose points and corresponding piecewise polynomial fit used to convert RGF measurements of scanner transmission value to dose.

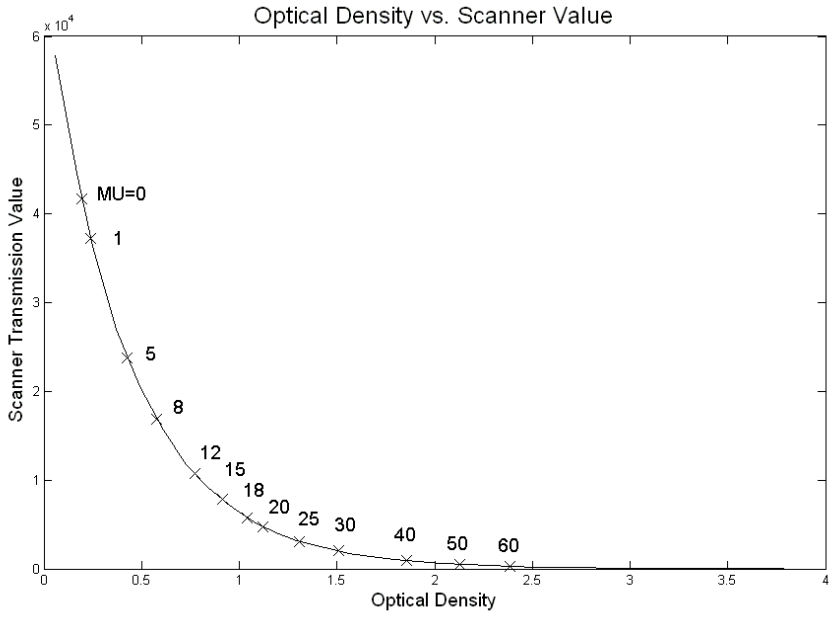

Figure 2.20: Relationship of dose delivered to RGF, optical density, and measured Vidar scanner values. The X's represent the XV film dose points for the given monitor units.

2.3.3 RGF Irradiation Method

RGF was removed from its packaging and positioned within the phantom's film cassette inside of a darkroom for all irradiations. For the first and second prototype phantoms, RGF was seated within the recessed half of the film cassette and no additional effort was used to align the film edge with the phantom surface. For the third prototype, once bare film was inserted into the recessed half of the film cassette the adjustable cam was utilized to precisely align the edge of the RGF to the phantom surface. This was accomplished by placing a flat-plate against the phantom surface and forcing the adjustable cam against the downstream edge of the film to press the film against the plate, effectively aligning the film edge with the phantom surface. Once satisfactory alignment was achieved, the adjustable cam was secured in place via a single Allen bolt located at the cams axis of rotation. This procedure, once done for a single film, did not require readjustment as RGF dimensions were constant for films from the same batch.

The film cassette was then assembled and inserted into the phantom housing. A single piece of light opaque photographic tape was placed along the film edge at the entry phantom surface to prevent light leakage. The loaded phantom was placed on the treatment couch and aligned in an in-plane orientation (i.e. long axis of the film parallel to the plane of electron bending) using the light field crosshairs. Parallel alignment with the plane of the beam was achieved by using the patient set-up lasers to ensure the surface of the phantom was not angled with respect to the incident electron beam. The top of the phantom was set to 100-cm SSD using the accelerator's ODI. Once satisfactory alignment was achieved, the accelerator's electron beam was turned on and 20 MU (D_{max} = 20 cGy) were delivered to the RGF.

2.3.4 RGF Development and Digitization

RGFs were developed using an AFP Mini Medical 90 processor (AFP Imaging Corp., Elmsford, NY). Prior to developing irradiated films, a minimum of four unexposed films were

processed in order to stabilize the developer's temperature and eliminate any abnormal start-up conditions. The RGF orientation was held constant for all scans; the un-irradiated long edge of the film positioned against the edge of the processors loading tray. This placed the irradiated film edge in approximately the center of the processor bed to avoid any artifacts that may be caused by the film abutting against the processor edge.

RGF's were digitized using the Vidar scanner with a pixel size of 0.0356 cm. The scanner uses a red light emitting diode light source and a solid state detector array consisting of 89 μm charge-coupled device (CCD) detector elements. To obtain a pixel size of 356 μm, sixteen (4x4 area) 89 μm pixel readings were averaged. The averaged signal was recorded as a 16-bit (65,536 gray level) scanner value. Digitized films were exported as Matlab v6.0 (The Mathworks, Nattick, MA) files and imported into in-house software used for data manipulation and analysis.

2.4 Aim 3: Measurement of Relative Dose in Prototype Phantoms Using Radiochromic Film

2.4.1 RCF Specifications

GafChromic EBT RCF (International Specialty Products, Wayne, NJ) Lot # 37122-04I was used for this work. This film is specified for the measurement of absorbed dose in the range of 1-800 cGy, corresponding to optical densities between 0-4. Su et al. (2007) reported GafChromic EBTs response is independent of energy, field size, and dose rate for electron beam measurements. AAPM Task Group 63 has published detailed characteristics of RCF, and all handling recommendations suggested in the report were followed (Niroomand-Rad *et al.* 1998). Sheets of 8"x10" were utilized in this study.

2.4.2 RCF Calibration

A single calibration curve was used to calibrate all films from the same manufacturing lot. Calibration curves were determined using 12 measurements obtained using 2.5"x2.5" pieces of film cut from a single sheet. The bottom left corner of each square piece was numbered to allow consistent, identical film orientation for film digitization (Niroomand-Rad *et al.* 1998). Each film piece was placed inside of the film cassette and irradiated at a depth of 3 cm (Plastic Water [1.5 cm] + Cassette [1.5 cm Solid Water]) atop of 5 cm of Plastic Water to provide sufficient backscatter. The top of the Plastic Water was set to 100 cm SSD using the accelerators ODI. The pieces of film were then individually irradiated in the center of a 16 MeV electron beam (d_{max} = 3 cm), collimated by a 15x15 cm^2 open applicator. One piece of film was unirradiated and used to provide background + fog optical density level of the film. To investigate the fluctuation in the background readings between different sheets of RCF, three unirradiated sheets of film were digitized and the average pixel value for a 2x2 cm^2 field in the center of the film was determined. The standard deviation between the readings from the three film sheets was 133 Vidar scanner values which corresponds to a relative standard deviation of 0.3 % indicating an overall satisfactory uniformity in the background variation between films. The remaining film pieces were irradiated to the following doses: 0.6, 1.1, 1.7, 2.2, 2.8, 3.3, 3.9, 4.4, 4.9, 5.6, and 6.1 Gy. Dose delivered to the center of the films was measured prior to film irradiation using a Roos style (PTWN31001) parallel-plate ion chamber (SN: 0057) irradiated in Plastic Water® (Elimpex) at a depth of 3 cm with 5 cm of backscatter. All ionization readings were converted to dose per AAPM Task Group Report 51 (Almond *et al.* 1999).

All calibration films were digitized following methods described in section 2.4.4. The measured scanner value for a 2x2 cm^2 region in the center of each film was correlated to dose, and a piecewise polynomial was fit to the resulting curve to convert film scanner values to dose.

The measured data points and resulting fit are shown in Figure 2.21. Upon inspection of the sensitometric curve, it was decided to irradiate films to 3.5 Gy (350 MU) for electron beam dose profile measurements.

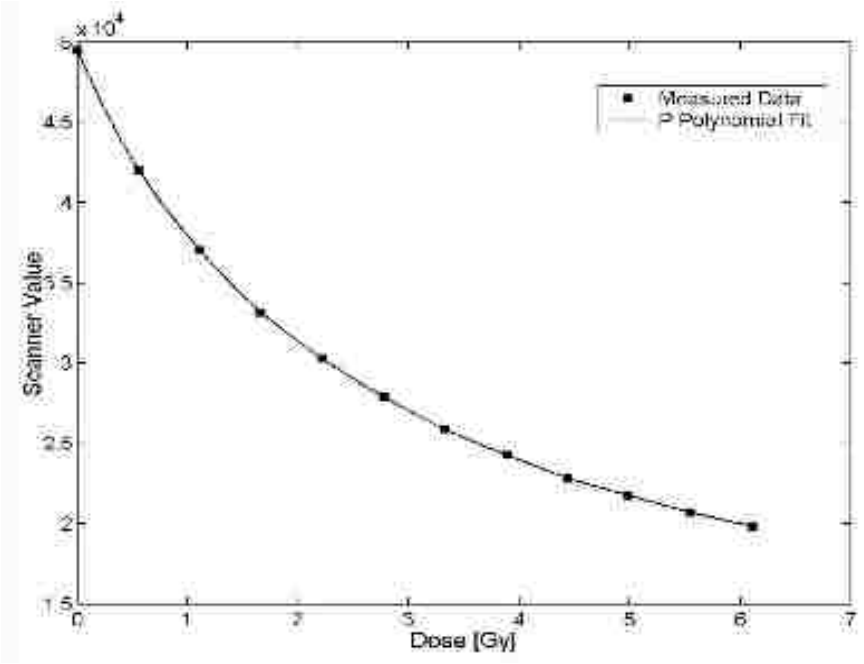

Figure 2.21: RCF measured calibration points and corresponding piecewise polynomial fit used to convert RCF readings to dose.

2.4.3 RCF Irradiation Method

RCF was not irradiated in the first prototype phantom. For the second and third prototype phantoms, RCF sheets were placed inside the recessed half of the film cassette and abutted against the left edge. Since the dimensions of RCF are smaller than the film cassette recess, a spacer was placed against the downstream edge of the film to move the irradiated film edge flush with the phantom surface. Strips of RCF were used as spacers for the second prototype measurements. Due to the small size discrepancies between sheets of RCF, spacers with slightly varying widths were utilized. For the third prototype cassette, a single rigid cardboard shim (4.8x28 cm) was placed between the downstream edge of the film and the adjustable cam. Alignment of the different sized sheets of RCF to the phantom edge was achieved by utilizing

the adjustable cam as described in section 2.3.3. This procedure had to be repeated for each RCF as the dimensions of films within the same batch were not as consistent as for RGF. Once satisfactory edge alignment was achieved, the cassette was assembled and secured inside the phantom body for irradiation.

2.4.4 RCF Digitization

Following exposure, RCFs were stored for at least 12 hours prior to scanning to allow for film development under ambient conditions (temperature ≈ 23^{o} C, relative humidity ≈ 30^{o} C) with nominal exposure to fluorescent room lights. Irradiated films were digitized using an Epson Perfection V700 Photo flatbed scanner (Seiko Epson Corporation, Nagano, Japan). This scanner uses a fluorescent white light source and linear charge-coupled device (CCD) detector array to produce 48-bit red-green-blue (RGB) images in a tagged image file format (TIFF). The 16-bit red channel image was exported for film analysis since the absorption peak of RCF film lies at ≈773 nm, corresponding to the scanners red channel.

A scanning resolution of 72 dpi (≈ 0.353 mm pixel^{-1}) was chosen for RCF digitization, approximately equal to that used for RGF (0.356 mm pixel^{-1}). The EpsonScan software was used to communicate with the scanner in the professional film (positive) mode, with all image manipulation features turned off. All films were scanned in the same orientation in the center of the scanner bed. Prior to scanning irradiated films, a previously scanned film was rescanned and compared to the previous measurements to ensure the scanner was stable and functioning consistently.

It has been reported in the literature that the CCD detector in the type of scanner used in this study exhibits a non-uniform response perpendicular to the scan direction (Menegotti *et al.* 2008). The effect of the non-uniformity can be seen in the measured film data shown in Figure 2.22. One observes as the distance off central-axis increases, the digitized film dose

measurements increasingly overestimate the diode measurements by up to 2.5 % for the 5 % dose contour.

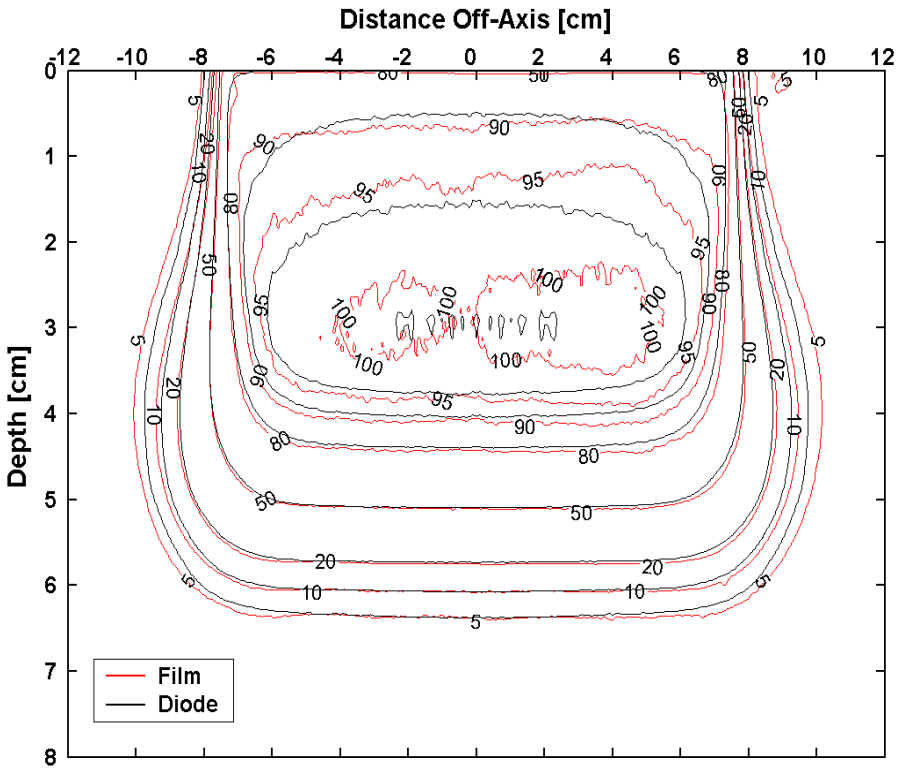

Figure 2.22: Uncorrected 2D relative dose distribution measured for a 12 MeV, 15x15 cm^2 electron field with RCF on the flatbed scanner.

To correct for this non-uniform response, an off-axis dependent correction factor was applied to the scanner values read from the irradiated films. To determine this factor, a single strip (8"x2") of RCF was irradiated by a presumably flat electron beam to 150 MU (16 MeV, 25x25 cm^2, 3 cm depth) and digitized five times using the flatbed scanner in a cross-plane orientation. This dose level was chosen because it results in a value that lies in the middle of the range of scanner values encountered when digitizing irradiated RCFs utilized in this work. The resulting averaged scanner values were fit using a 2^{nd} order polynomial (c.f. Figure 2.23). The polynomial fit was then normalized to 1 at its maximum value and the resulting values were used as the correction factors across the scan field (c.f. Figure 2.24).

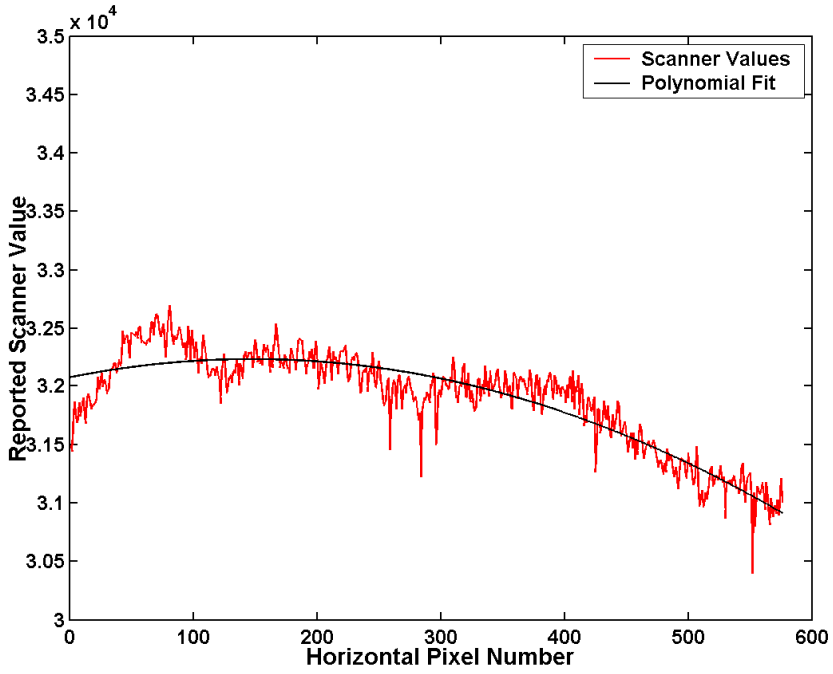

Figure 2.23: Average of scanner values (n=5) measured perpendicular to the scan direction for a 8"x2" strip of RCF digitized using the flatbed scanner.

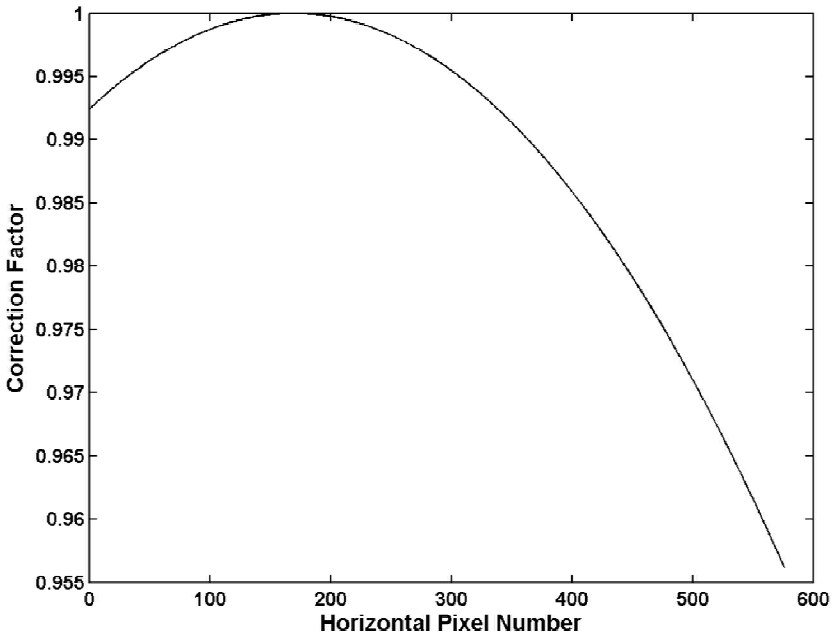

Figure 2.24: Correction factors obtained from polynomial fit of the raw scanner values measured perpendicular to the scan direction for a single piece of RCF digitized using the flatbed scanner.

Each row (cross-plane axis of the film) of measured data was corrected by applying the correction factors determined from the polynomial fit using Equation 2.1:

$$Film_{corrected}(i,j) = \frac{Film_{uncorrected}(i,j)}{CF(i)}, \qquad (2.1)$$

where *i* corresponds to the row or horizontal pixel number and *j* corresponds to the column or vertical pixel number. The corrected 2D dose distribution is shown in Figure 2.25.

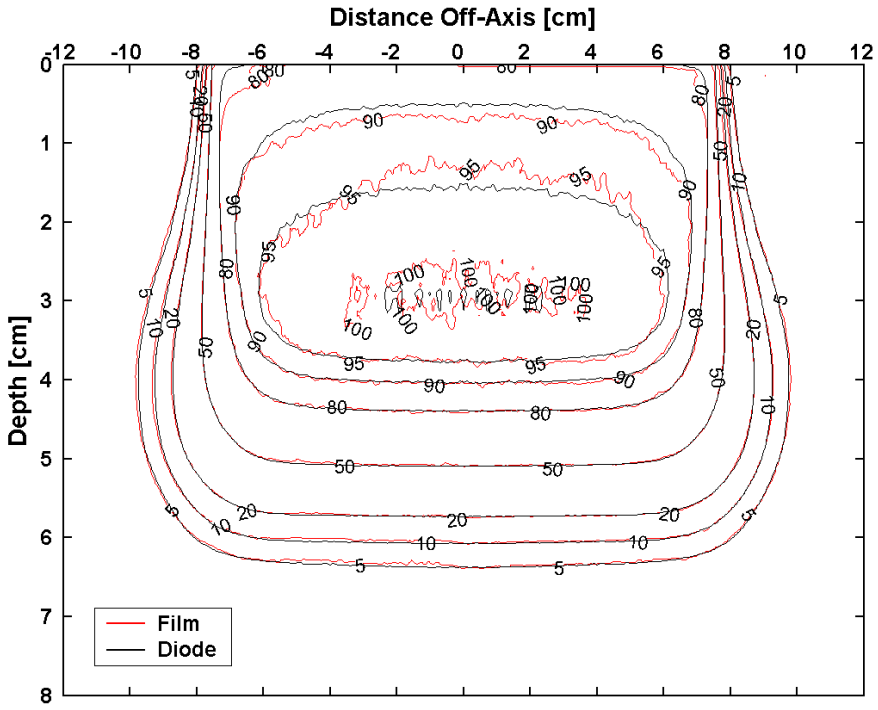

Figure 2.25: Corrected 2D relative dose distribution measured for a 12 MeV, 15x15 cm^2 electron field.

Improved agreement is seen compared to the uncorrected dose distribution as the distance off-axis is increased. Due to the low dose values having the greatest scanner values, a small (3.3 %) correction in scanner values results in a large dose change (33 %). For example, the 7.5 % dose contour of the uncorrected film becomes the 5 % dose contour of the corrected film when a

correction factor of approximately 3.3 % is applied. This is a 33 % change in dose due to a 3.3 % change in pixel values. Both the 7.5 % and 5 % dose lie between the first two measured calibration points where a linear approximation gives a slope of -1.73×10^4 (pixel values)/Gy. The pixel value corresponding to the 7.5 % (uncorrected) dose is 4.37×10^4 and when a correction factor of 0.967 is applied this value becomes 4.52×10^4, corresponding to an absolute change in pixel value of 1.5×10^3. When this difference in pixel values is multiplied by slope^{-1} the corresponding change in dose is -0.087 Gy which is consistent with the difference between the 7.5 % (0.262 Gy) and 5 % relative dose (0.175 Gy).

2.5 Aim 4: Comparison of Film and Diode Relative Dose Measurements

2.5.1 Precision of Measured Data

The average of three measurements was acquired for each electron field measured using both film and diodes and used for all comparisons in this work. The standard deviation, σ, between the three measurements was calculated using Equation 2.2.

$$\sigma = \sqrt{\frac{\sum_{i=1}^{N}(x_i - x_{mean})^2}{N-1}} \qquad (2.2)$$

The standard error, σ_{mean}, was calculated from the standard deviation to determine the precision in the measurements according to Equation 2.3.

$$\sigma_{mean} = \frac{\sigma}{\sqrt{N}} \qquad (2.3)$$

2.5.2 Data Processing

In-house software was written in Matlab v6.0 for all data processing by the author. The code is modular in that it requires no ancillary or third-party data analysis package. The software allowed importation of RIT-generated *.mat* files containing calibrated film dose arrays, normalization of dose distributions to an arbitrary value, and plotting of relative 1D depth-doses,

1D off-axis dose profiles, and 2D isodose distributions. 2D dose distributions were reconstructed from the CAX, PDD and the set of off-axis ratios. A diverging fan-beam interpolation was used to resample the measured off-axis ratios at a depth resolution of 0.1 cm. The resulting off-axis ratios were then multiplied by the value of the CAX PDD curve at the corresponding depths to determine the relative 2D dose array.

The software was also utilized for comparisons of all measured data sets, reporting the number of points within an arbitrary percent agreement as well as distance-to-agreement (DTA). Film measured PDD curves were compared to diode measurements to evaluate the accuracy of measurements acquired utilizing the third prototype film phantom. To do so, the depth-dose curve was divided into three different regions: (1) high-dose, low dose-gradient region corresponding to doses from the surface to R_{90}, (2) high-gradient region, corresponding to dose between R_{90} and R_{10}, and (3) low-dose, low dose-gradient region for dose levels below R_{10}. In regions (1) and (3), criterion for agreement was within ±2% of the CAX maximum dose, while for region (2), agreement criterion was defined as ±1 mm distance-to-agreement (DTA).

To calculate the dose differences in the measured PDD curves, the film data was linearly interpolated to match the depth resolution of the diode data. The relative dose difference between the two curves was calculated for the appropriate depths following Equation 2.4:

$$\Delta Dose[\%] = \left| Diode(d) - Film(d) \right|, \qquad (2.4)$$

Where d is the depth at which the dose difference is being calculated.

To determine the DTA between the curves, the film data was linearly interpolated to match the dose values from the diode data. The DTA was calculated for each film measured dose value according to Equation 2.5:

$$DTA[mm] = \left| Diode(D) - Film(D) \right|, \qquad (2.5)$$

where *D* is the dose value for which the DTA is being calculated.

To quantitatively evaluate the film measured 2D dose distributions, an algorithm was written that compares each pixel in a film dose array to diode measurements using three criteria: (1) 2% dose or 1 mm DTA, (2) 2% dose or 2 mm DTA, and (3) 3% dose or 3 mm DTA. The algorithm first down-samples the film dose array to spatially match the diode dose array. The two data sets are then digitally overlaid on top of each other and correct alignment is ensured by maintaining the same number of pixel's from the first column of each dose array to the pixel corresponding to its CAX. The CAX of each dose array was determined by computing the full-width half-max of the 50 % dose contour. The aligned dose arrays were first subtracted to determine the relative dose difference, and then each pixel with a dose difference greater than the specified criteria was evaluated for DTA, isotropically.

Chapter. 3 Results and Discussion

3.1 Aim 1: Measurement of Relative Dose in Water

3.1.1 Relative Dose Measurements in Water Using an Ion Chamber

Percent depth-dose (PDD) measurements were acquired along the central-axis (CAX) of 6, 9, 12, 16, and 20 MeV, 15x15 cm^2 electron fields using a parallel plate ion-chamber in a liquid water phantom to validate the accuracy of equivalent diode detector measurements. The minimum scanning depth of measurements was 1.3 mm, the depth of the ion chamber's active volume. For lesser depths, the ion chamber surface breaks the plane of the water's surface. PDDs were normalized to the maximum ion chamber reading acquired along the beam's CAX. The measured PDD curves for 9 and 16 MeV are shown in Figure 3.1 and Figure 3.2.

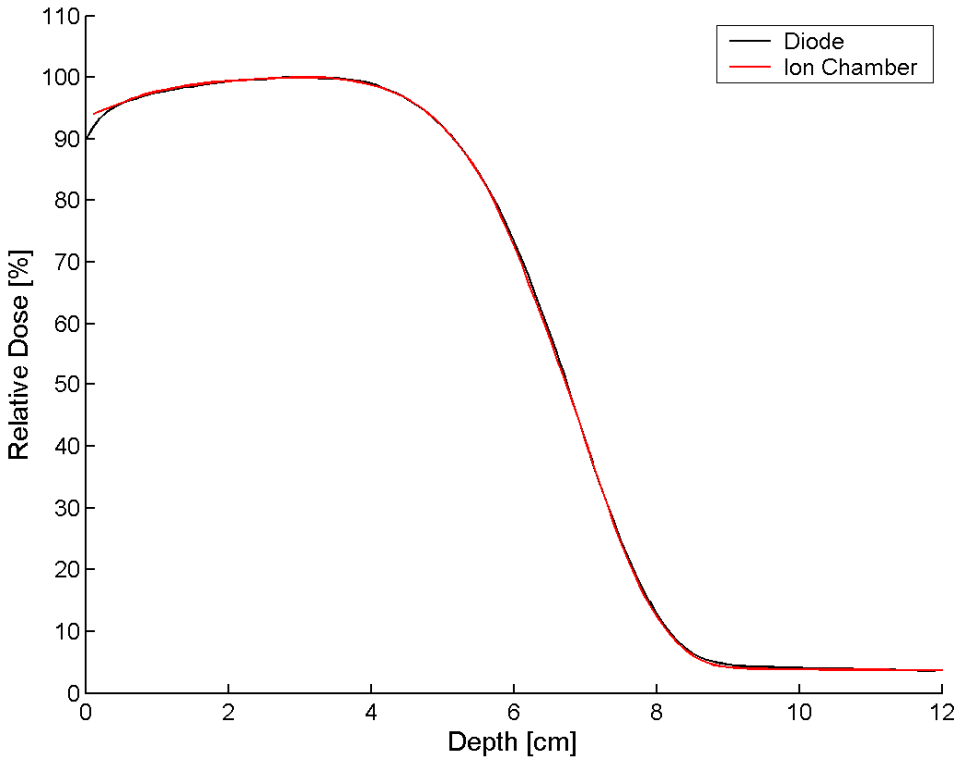

Figure 3.1: Parallel-plate ion chamber vs. diode measured CAX PDD. Curves were acquired in liquid water using a scanning water phantom for a 16 MeV, 15x15 cm^2 electron field.

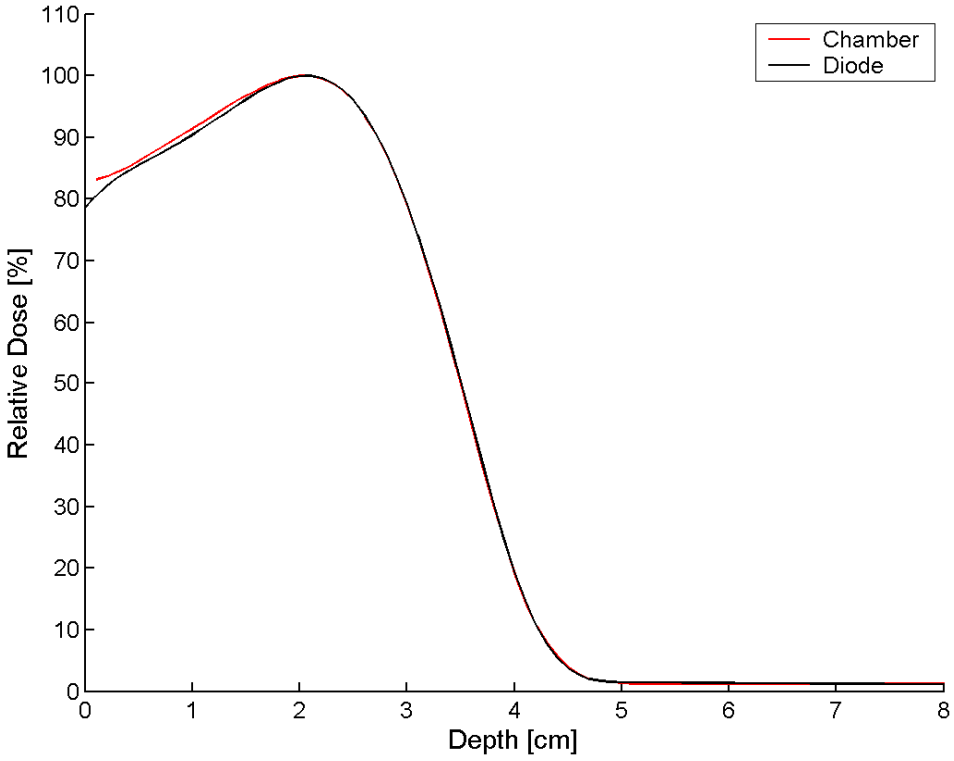

Figure 3.2: Parallel-plate ion chamber vs. diode measured CAX PDD. Curves were acquired in liquid water using a scanning water phantom for a 9 MeV, 15x15 cm^2 electron field.

3.1.2

The greatest difference in measured PDD was observed for depths < 0.25 cm (≈ 2 %). This is attributed to water collecting on the flat surface of the ion chamber as it approached the water surface. Measurements acquired for 6, 12, and 20 MeV electron beams using a 15x15 cm^2 field-size applicator showed similar agreement. For all electron energies, at depths greater than 0.25 cm, ion chamber measurements agreed with diode measurements within ± 1 % dose relative to the CAX maximum or ± 0.5 mm distance-to-agreement (DTA).

3.1.3 Central-Axis, Percent Depth-Dose Measurements Using Diodes

PDD measurements were acquired along the CAX of electron fields using a scanning diode system in a water phantom. Measurements were acquired using a 15x15 cm^2 field size for 6, 9, 12, 16, and 20 MeV electron beams, in addition to 2x2 cm^2 and 4x4 cm^2 fields defined

using Cerrobend cut-outs placed inside a 15x15 cm^2 applicator for both 9 and 16 MeV. Three PDD scans were acquired for each measured electron field to test the reproducibility of diode measurements. PDDs were normalized to the maximum diode reading along the CAX. The resulting 9 and 16 MeV, 15x15 cm^2 PDD curves are displayed in Figure 3.3 and Figure 3.4. The standard deviation and standard error of the mean were calculated for the three regions of the PDD for both 9 and 16 MeV, 15x15 cm^2 (c.f. Table 3.1). Values for standard deviation were similar between the 9 and 16 MeV electron beams and were all within 0.2 % relative dose, or 0.04 mm DTA indicating sufficient precision in the diode measurements. The calculated values for standard error of the mean in the three curve regions were all less than 0.12 % relative dose, and 0.02 mm DTA for both energies shown.

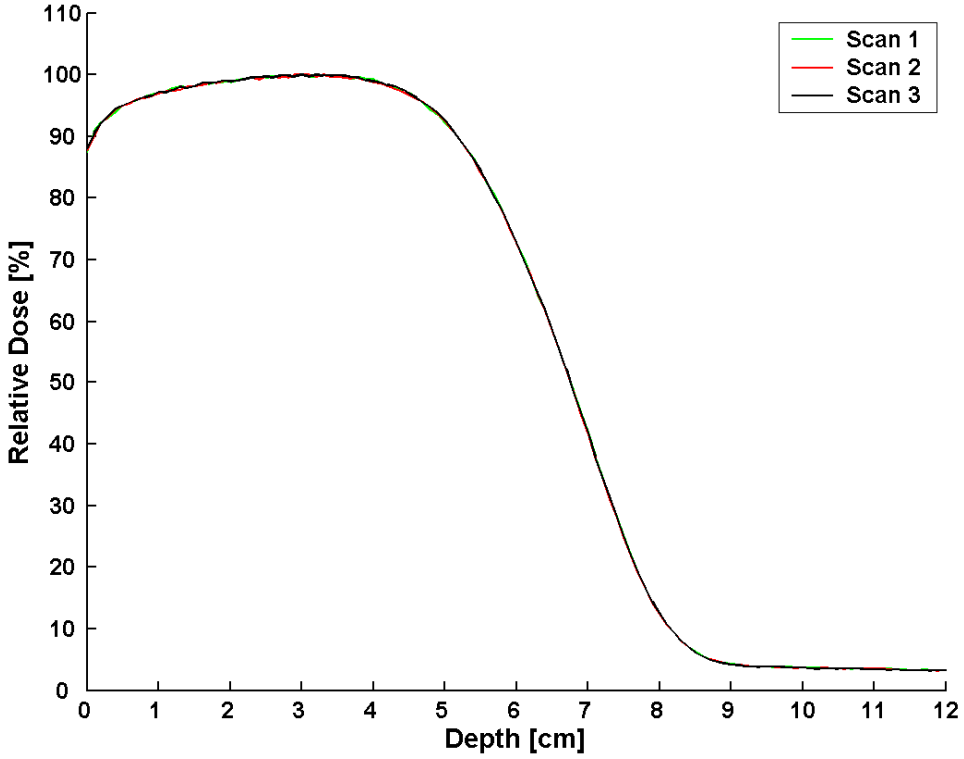

Figure 3.3: Reproducibility of diode measured PDDs acquired within a water phantom for a 16 MeV, 15x15 cm^2 electron field.

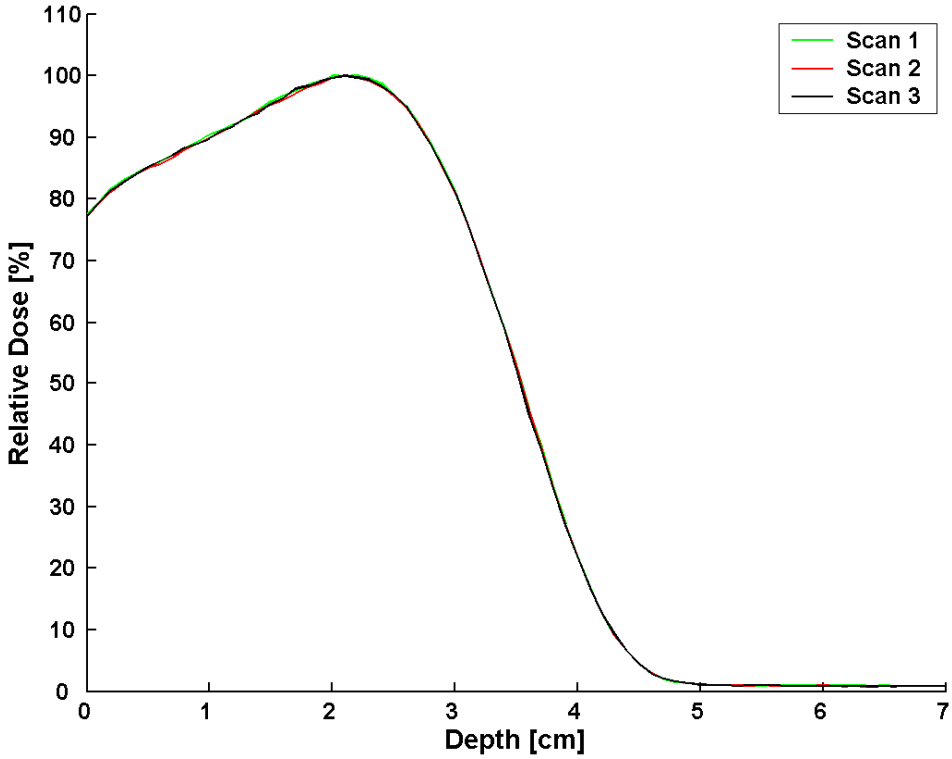

Figure 3.4: Reproducibility of diode measured PDDs acquired within a water phantom for a 9 MeV, 15x15 cm^2 electron field.

Table 3.1: Standard deviation and standard error of the mean determined for the three PDD curve regions for 9 and 16 MeV, 15x15 cm^2 electron fields measured using diodes in a scanning water phantom.

Curve Region	**16 MeV**		**9 MeV**	
	σ	**σ_{err}**	**σ**	**σ_{err}**
0 - R_{90}	0.13 %	0.07 %	0.20 %	0.12 %
R_{90} - R_{10}	0.04 mm	0.02 mm	0.03 mm	0.02 mm
R_{10} + 4 cm	0.04 %	0.03 %	0.02 %	0.01 %

3.1.4 Relative Off-Axis Dose Measurements Using Diode

Off-axis dose profiles were measured in water for the same electron fields listed in section 3.1.2. Three scans were acquired at three different depths for both 9 and 16 MeV, 15x15 cm^2 electron beams (c.f. Figure 3.5 and Figure 3.6). To determine the precision in the diode off-axis relative dose measurements, the standard error of the mean of the three scans at each depth

was determined. The values for each depth were averaged in three regions of the curve, and the results are shown in Table 3.2.

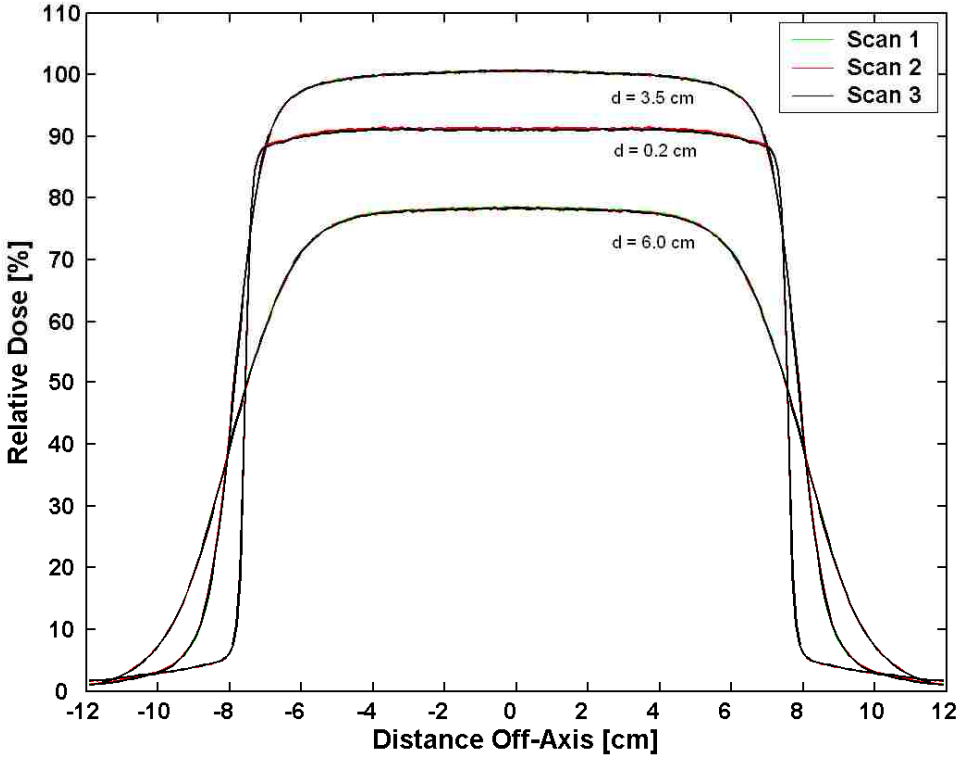

Figure 3.5: Reproducibility of 1D off-axis dose profiles acquired using diodes in a scanning water phantom for a 16 MeV, 15x15 cm^2 electron field. Measurement depths are 0.2, 3.5, and 6.0 cm.

The three regions are defined as follows: low-dose region (LD) corresponding to the tail regions, the high-gradient region (HG) corresponding to the field-edge, and the low-gradient region (LG) of high dose. The values for the standard error of the mean in the low-dose and low-gradient regions are less than 0.1 % except at 3.6 cm for the 9 MeV beam where the standard error of the mean is 0.23 % in the low-gradient region. This is due to differences in the relative dose value in the high-dose region at this depth. In the high-gradient region of the depth-dose curve, small positioning errors in the diode can result in large measurement errors of relative

dose. Since measured dose profiles are normalized during reconstruction of the 2D diode dose arrays, differences in the dose value are minimized. Standard error of the mean calculated for the high-gradient region was all within 0.13 mm which was considered acceptable for this study.

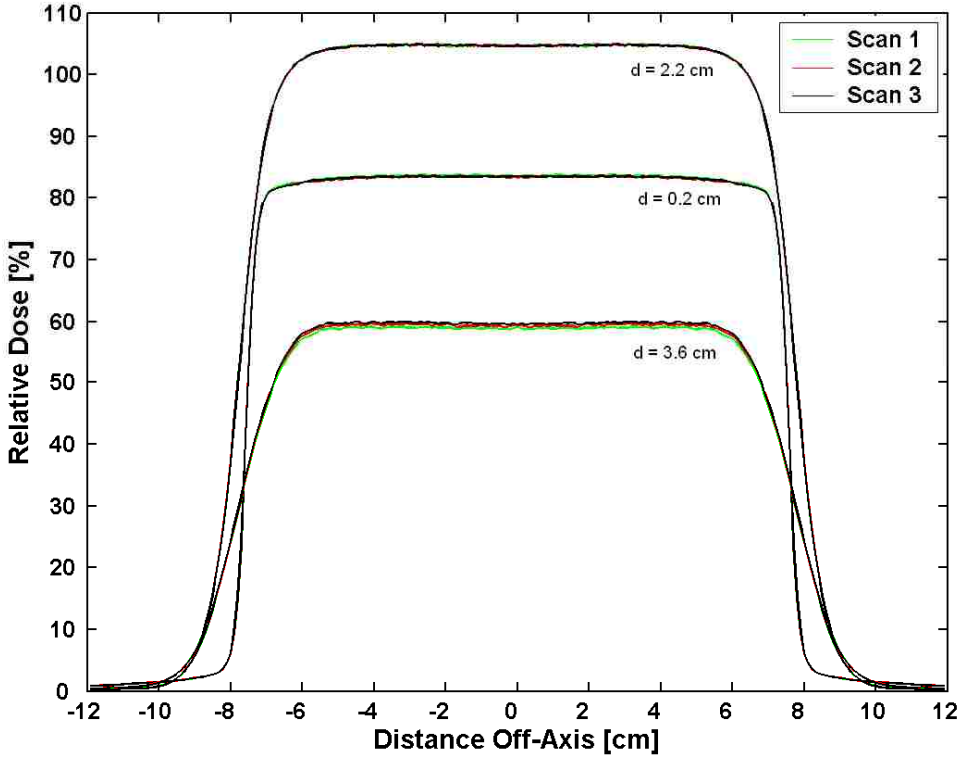

Figure 3.6: Reproducibility of 1D off-axis dose profiles acquired using diodes in a scanning water phantom for a 9 MeV, 15x15 cm^2 electron field. Measurement depths are 0.2, 2.2, and 3.6 cm.

Table 3.2: Standard error of the mean for 9 and 16 MeV, 15x15 cm^2 off-axis dose profiles measured using diodes in a water phantom at the depths shown in Figure 3.5 and Figure 3.6. LD = low-dose region, HG = high-gradient region, LG = low-gradient region.

	9 MeV, σ_{err}			**16 MeV, σ_{err}**		
Depth	LD	HG	LG	LD	HG	LG
0.2 cm	0.01%	.09 mm	0.08%	0.04%	.13 mm	0.10%
2.2, 3.5 cm	0.02%	.12 mm	0.07%	0.04%	.08 mm	0.06%
3.6, 6 cm	0.01%	.08 mm	0.23%	0.02%	.03 mm	0.07%

3.2 Aim 2: Measurement of Relative Dose in Third Prototype Phantom Using Radiographic Film (RGF)

3.2.1 Central-Axis, Percent Depth-Dose Profiles

PDD measurements were acquired using the third prototype film phantom with the RGF placed between sheets of black paper and a C-clamp secured around the phantom (Section 2.3.3). Three films were irradiated for each electron field measured. The resulting PDDs for the 9 and 16 MeV, 15x15 cm^2 electron fields are displayed in Figure 3.7 and Figure 3.8. The three irradiated film data sets were averaged for comparison to diode measurements. To obtain an estimation of the precision in the measurements, the standard deviation and standard error of the mean was calculated for the three PDD regions and the results are summarized in Table 3.3 below.

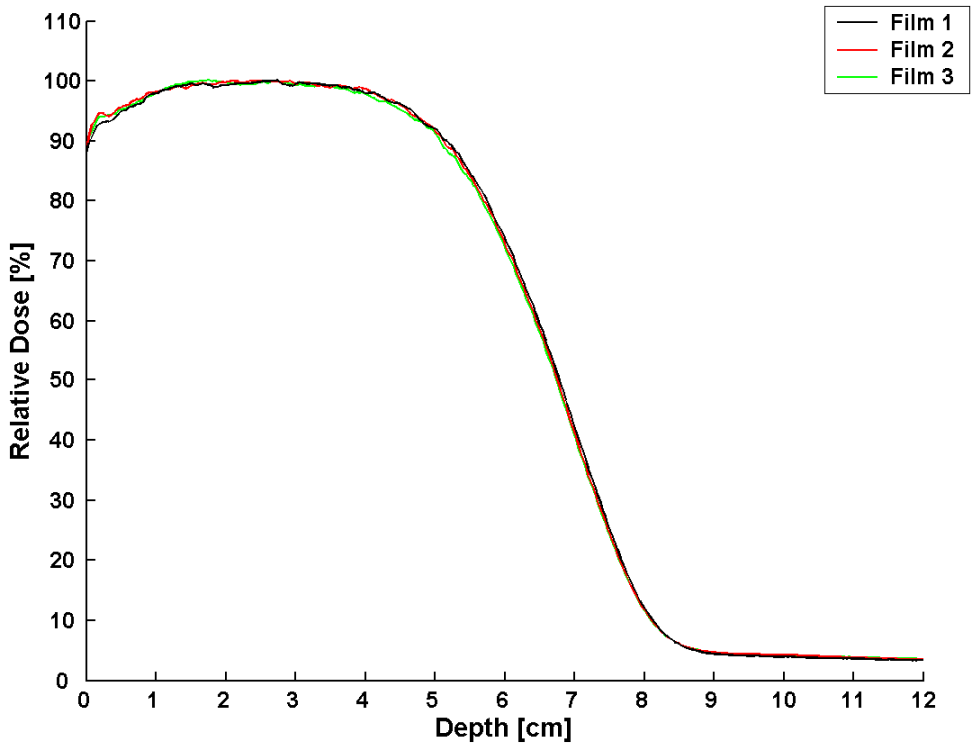

Figure 3.7: Reproducibility of PDDs acquired in the third prototype film phantom using RGF for a 16 MeV, 15x15 cm^2 electron field.

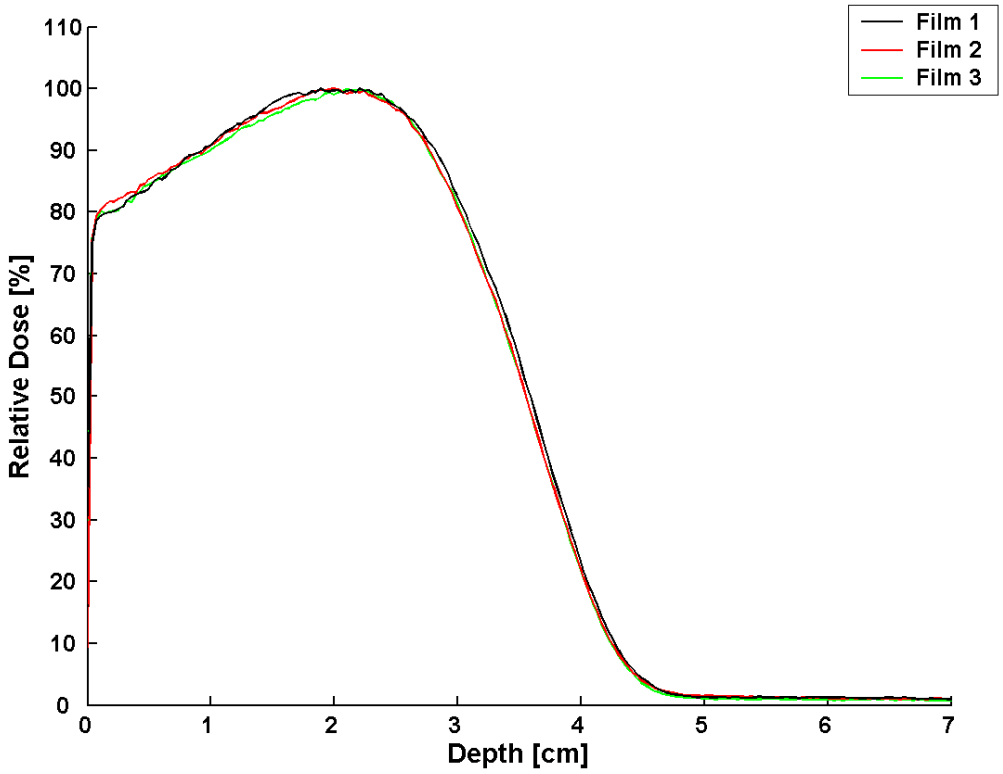

Figure 3.8: Reproducibility of PDDs acquired in the third prototype film phantom using RGF for a 9 MeV, 15x15 cm^2 electron field.

Table 3.3: Standard deviation and standard error of the mean determined for the three PDD curve regions for 9 and 16 MeV, 15x15 cm^2 electron fields measured in the third prototype phantom using RGF.

Curve Region	**16 MeV**		**9 MeV**	
	σ	**σ_{err}**	**σ**	**σ_{err}**
0 - R_{90}	0.53 %	0.31 %	0.52 %	0.30 %
R_{90} - R_{10}	0.25 mm	0.14 mm	0.18 mm	0.10 mm
R_{10} + 4 cm	0.07%	0.04%	0.19 %	0.11 %

Values for standard deviation are similar for both 9 and 16 MeV and are higher in the high-dose, low dose-gradient region than in the low-dose, low dose-gradient region. This is due to the fact that all measurements compared are relative to the CAX maximum, and since the relative dose values of the PDD are higher in the high-dose region, one would expect the standard deviation in this region to be higher as well. In the high-gradient region, standard deviation was evaluated in terms of DTA as this is how the curves are compared to diode

measurements. Values for standard deviation are higher for 16 MeV than for 9 MeV, due to the steeper slope of the 9 MeV PDD in this region. For the 9 MeV PDD film 1 penetrates slightly deeper (≈ 0.25 mm) than film 2 and 3 suggesting a small (0.1 mm) misalignment of the film at the phantom surface.

3.2.2 Off-Axis Dose Profiles

Off-axis dose profiles were derived from films irradiated for PDD measurements. The 9 and 16 MeV, 15x15 cm^2off-axis dose profiles from three different films are shown in Figure 3.9 and Figure 3.10. The standard error of the mean for each depth and curve region was calculated and the averaged values are presented in Table 3.4.

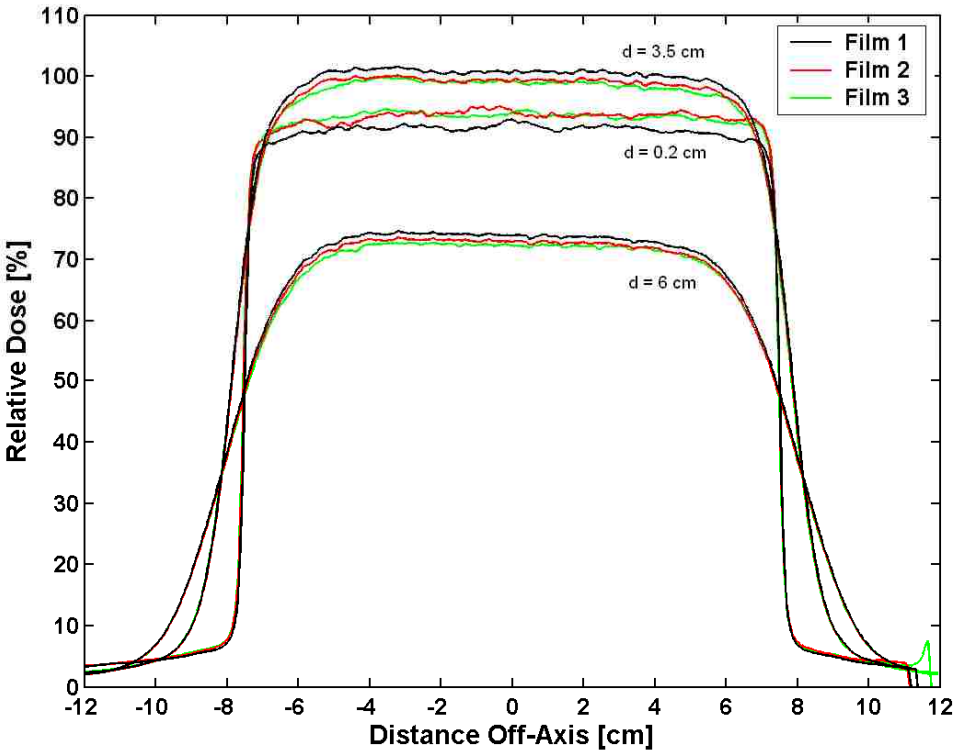

Figure 3.9: Reproducibility of 1D off-axis dose profiles acquired in the third prototype film phantom using RGF for a 16 MeV, 15x15 cm^2 electron beam. Measurement depths are 0.2, 3.5, and 6.0 cm.

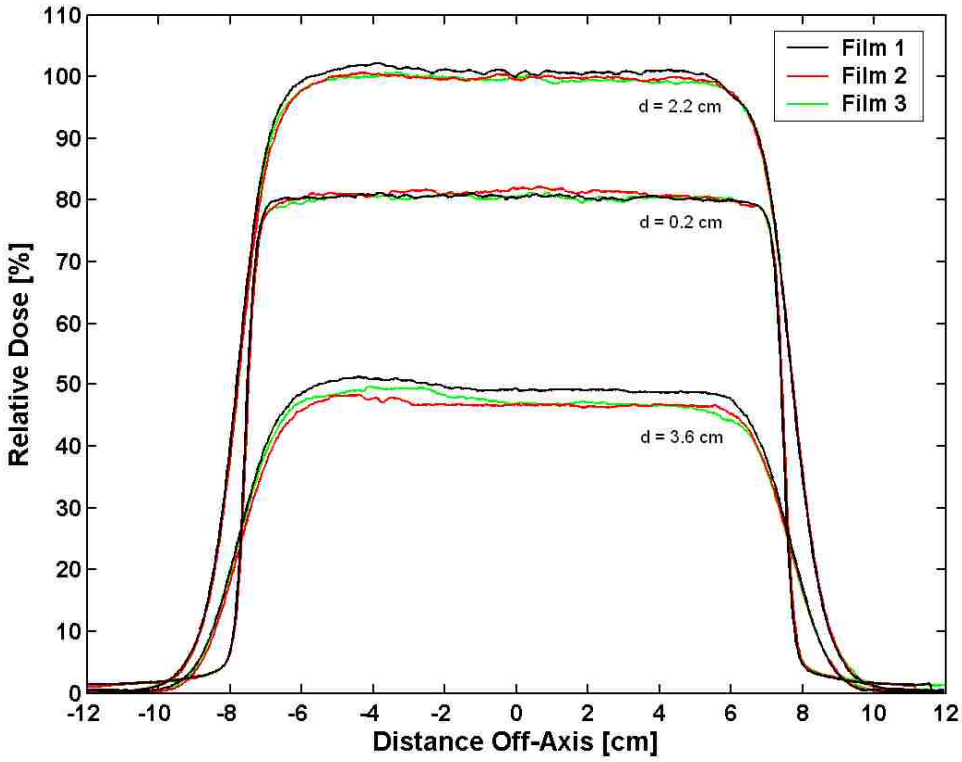

Figure 3.10: Reproducibility of 1D off-axis dose profiles acquired in the third prototype film phantom using RGF for a 9 MeV, 15x15 cm^2 electron field. Measurement depths are 0.2, 2.2, and 3.6 cm.

Table 3.4: Average standard error of the mean for 9 and 16 MeV, 15x15 cm^2 off-axis dose distributions measured in the third prototype phantom using RGF at the depths shown in Figure 3.9 and Figure 3.10. LD = low-dose region, HG = high-gradient region, LG = low-gradient region.

	9 MeV, σ_{err}			**16 MeV, σ_{err}**		
Depth	LD	HG	LG	LD	HG	LG
0.2 cm	0.07%	.08 mm	0.39%	0.30%	.11 mm	0.81%
2.2, 3.5 cm	0.11%	.10 mm	0.28%	0.15%	.11 mm	0.25%
3.6, 6 cm	0.08%	.35 mm	0.75%	0.14%	.09 mm	0.29%

For 9 MeV, the largest value for standard error of the mean is 0.75 % for the low-gradient region of the 3.6 cm depth. This is due to the differences in the PDD in the high-gradient region

of the curve at this depth where a slight shift in the film PDD results in a large dose difference. The largest value for standard error of the mean for 16 MeV was 0.81 % in the low-gradient region at a depth of 0.2 cm. This depth corresponds to the region of greatest dose difference in the PDD curve. In the low-gradient regions of the off-axis profiles standard error of the mean for both energies was below 0.3 %. In the high-gradient region, the largest value is 0.35 mm, and 0.11 mm for 9 MeV and 16 MeV, respectively.

3.3 Aim 3: Measurement of Relative Dose in Third Prototype Phantom Using Radiochromic Film (RCF)

3.3.1 Central-Axis, Percent Depth-Dose Profiles

PDD measurements were acquired using the third prototype film phantom with bare RCF placed inside the phantom cassette and a C-clamp secured around the phantom (Section 2.4.3). Three films were irradiated for each electron field measured. The resulting PDDs for the 9 and 16 MeV, 15x15 cm^2 electron fields are displayed in Figure 3.11 and Figure 3.12. The digitized dose values of the three irradiated films were averaged for comparison to diode measurements. To obtain an estimate of the precision, the standard deviation and standard error of the mean were calculated for the three PDD regions (c.f. Table 3.5).

Values for standard deviation are higher in the high-dose and low-dose regions of the PDD compared to RGF film measurements due to systematic noise inherent in the data which may be introduced by the flatbed scanner during digitization of the RCFs. The standard deviation for the measured16 MeV PDD is higher than for 9 MeV as film 1 slightly underestimates film 2 and 3 between 4 and 6 cm. In this high dose-gradient region, PDDs among the three films are in agreement for both 9 and 16 MeV with the largest standard deviation is for the 9 MeV measurements at 0.17 mm. Values for standard error of the mean are all less than 0.46 % relative dose and 0.1 mm DTA indicating sufficient precision in the measured data.

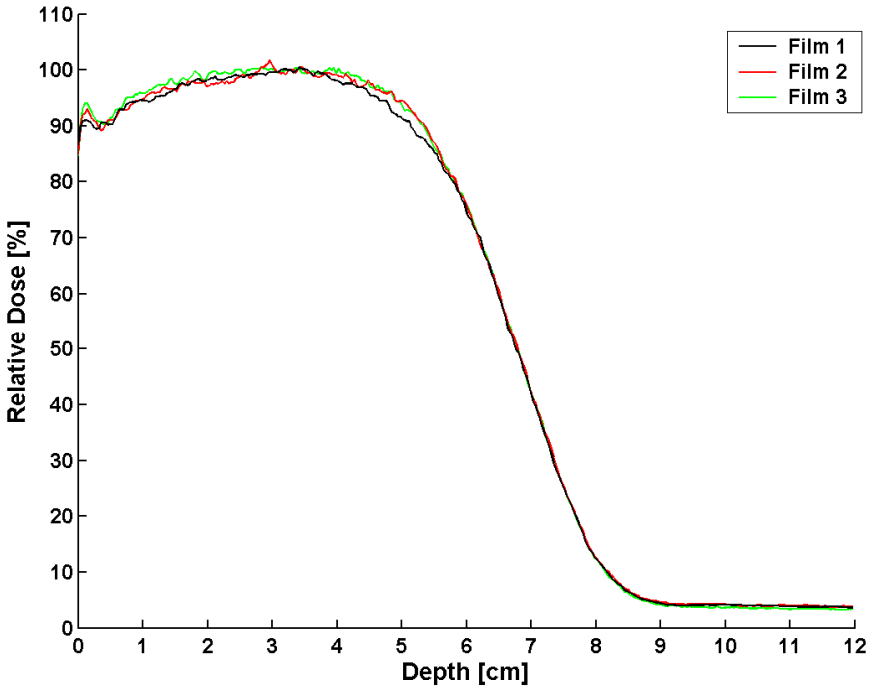

Figure 3.11: Reproducibility of PDDs acquired in the third prototype film phantom using RCF for a 16 MeV, 15x15 cm^2 electron field.

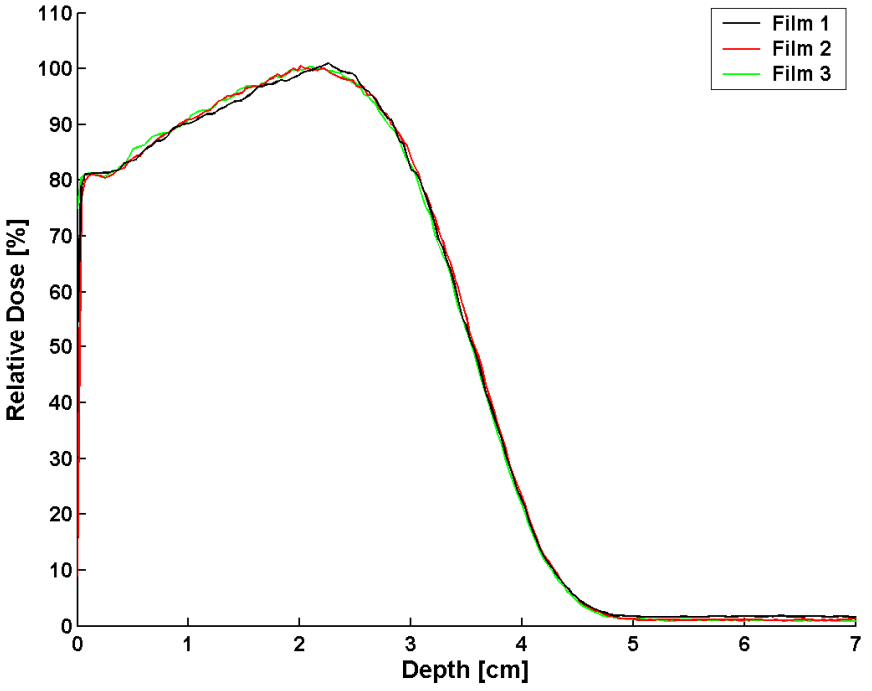

Figure 3.12: Reproducibility of PDDs acquired in the third prototype film phantom using RCF for a 16 MeV, 15x15 cm^2 electron field.

Table 3.5: Standard deviation and standard error of the mean determined for the three PDD curve regions for 9 and 16 MeV, 15x15 cm^2 electron fields measured in the third prototype phantom using RCF.

Curve Region	16 MeV		9 MeV	
	σ	σ_{err}	σ	σ_{err}
0 - R_{90}	0.80 %	0.46 %	0.57 %	0.33 %
R_{90} - R_{10}	0.13 mm	0.08 mm	0.17 mm	0.10 mm
R_{10} + 4 cm	0.27 %	0.15 %	0.33 %	0.19 %

3.3.2 Off-Axis Dose Measurements

Off-axis dose profiles were extracted from the films used to determine the CAX PDD. The 9 and 16 MeV, 15x15 cm^2 off-axis dose profiles are shown in Figure 3.13 and Figure 3.14. The standard error of the mean was calculated for each depth of measurement shown in the high-gradient, low-dose, and low-gradient regions of the curve (c.f. Table 3.6).

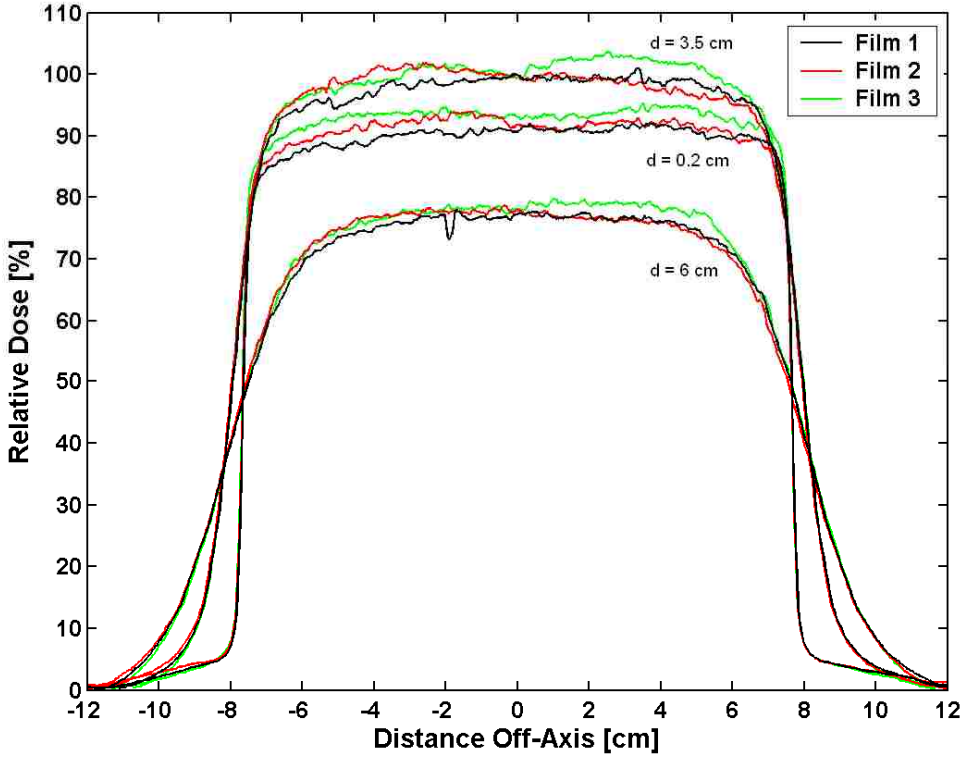

Figure 3.13: Reproducibility of 1D off-axis dose profiles acquired in the third prototype film phantom using RCF for a 16 MeV, 15x15 cm^2 electron field. Measurement depths shown are: 0.5 cm, 3.5 cm, and 6.0 cm.

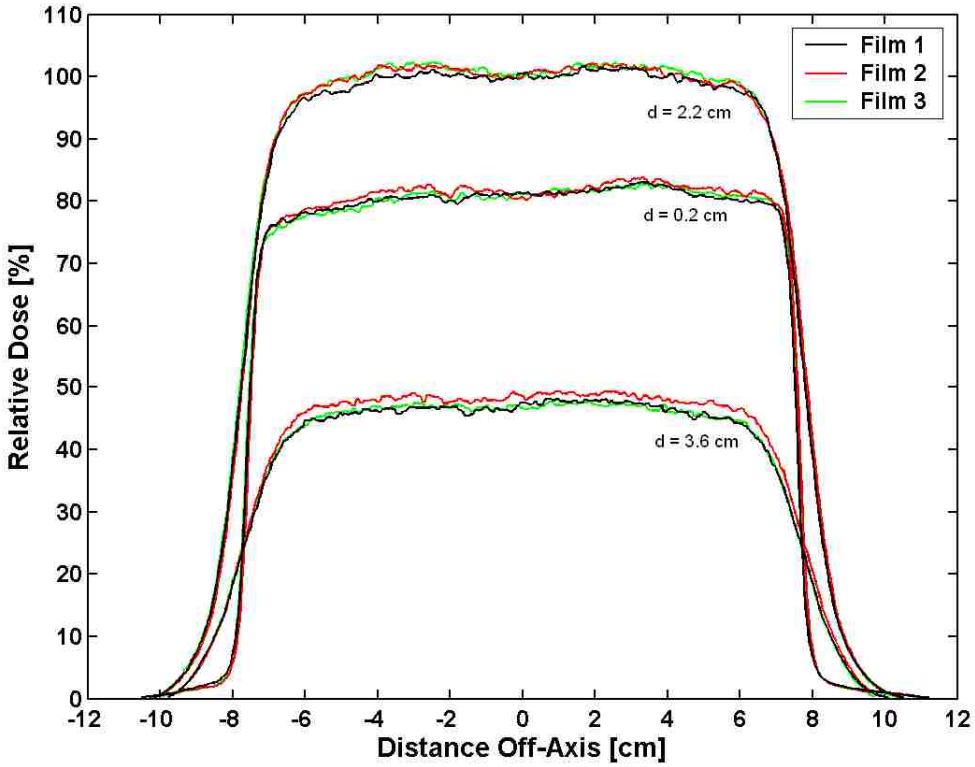

Figure 3.14: Reproducibility of 1D off-axis dose profiles acquired in the third prototype film phantom using RCF for a 9 MeV, 15x15 cm^2 electron field. Measurement depths shown are: 0.5 cm, 2.2 cm, and 3.6 cm.

Table 3.6: Average standard error of the mean for 9 and 16 MeV, 15x15 cm^2 off-axis dose distributions measured in the third prototype phantom using RCF at the depths shown in Figures 3.13 and 3.14. LD = low-dose region, HG = high-gradient region, LG = low-gradient region.

	9 MeV, σ_{err}			**16 MeV, σ_{err}**		
Depth	LD	HG	LG	LD	HG	LG
0.2 cm	0.11%	.17 mm	0.36%	0.30%	.10 mm	1.0%
2.2, 3.5 cm	0.11%	.18 mm	0.42%	0.46%	.11 mm	1.1%
3.6, 6 cm	0.06%	.16 mm	0.80%	0.41%	.16 mm	0.7%

Film measurements show improved uniformity for 9 MeV than for 16 MeV where film 3 overestimates film 1 and 2 at the positive off-axis distances for all depths. It is suggested that this

difference is possibly due to a non-uniform scanner response seen for this scan. For 9 MeV, the off-axis profiles for the three films are within 1 % agreement.

3.4 Aim 4: Comparison of Film and Diode Relative Dose Measurements for the Third Prototype Film Phantom

3.4.1 RGF Relative Dose Measurements

In sections 3.4.1.1 to 3.4.1.9, measured CAX PDD profiles, 1D off-axis dose profiles, and 2D dose distributions acquired using RGF in the third prototype phantom are compared to equivalent scanning diode measurements in water for 6-20 MeV, 15x15 cm^2 in addition to 9 and 16 MeV, 2x2 and 4x4 cm^2 electron fields. All film measurements were normalized to 100% at the CAX maximum and all data is unsmoothed. A discussion of RGF results is presented in Section 3.5.1.

3.4.1.1 20 MeV, 15x15 cm^2

The measured PDD profile agrees within criteria with diode measurements for all regions of the curve (c.f. Figure 3.15). In the high-dose, low dose-gradient region, the maximum measured relative dose difference is 1.3 %. In the high dose-gradient region, the maximum measured DTA is 0.82 mm, and in the low-dose, low dose-gradient region the maximum measured relative dose difference is 0.3 %.

Off-axis dose profiles are shown in Figure 3.16 and the differences between RGF and diode measurements are summarized in Table 3.7. The profiles agree within criteria for all depths except 0.5 cm. At this depth, the film underestimates the diode measurement by as much as 2.17 % in the negative off-axis distances. Also, for the 0.5 cm depth, the film disagrees with the diode measurement by a maximum of 1.03 mm DTA in the high dose-gradient region at the positive off-axis field edge.

The resulting 2D dose distributions (c.f. Figure 3.17) are in agreement with 99.8 % of the RGF measured data points falling within ± 2 % dose or ± 1 mm DTA to the diode measurements. As the agreement criteria is expanded to ± 2 mm DTA, the agreement improves to 99.9 %, while 100 % of the RGF measured data points are within the ± 3 %, ± 3 mm agreement criteria.

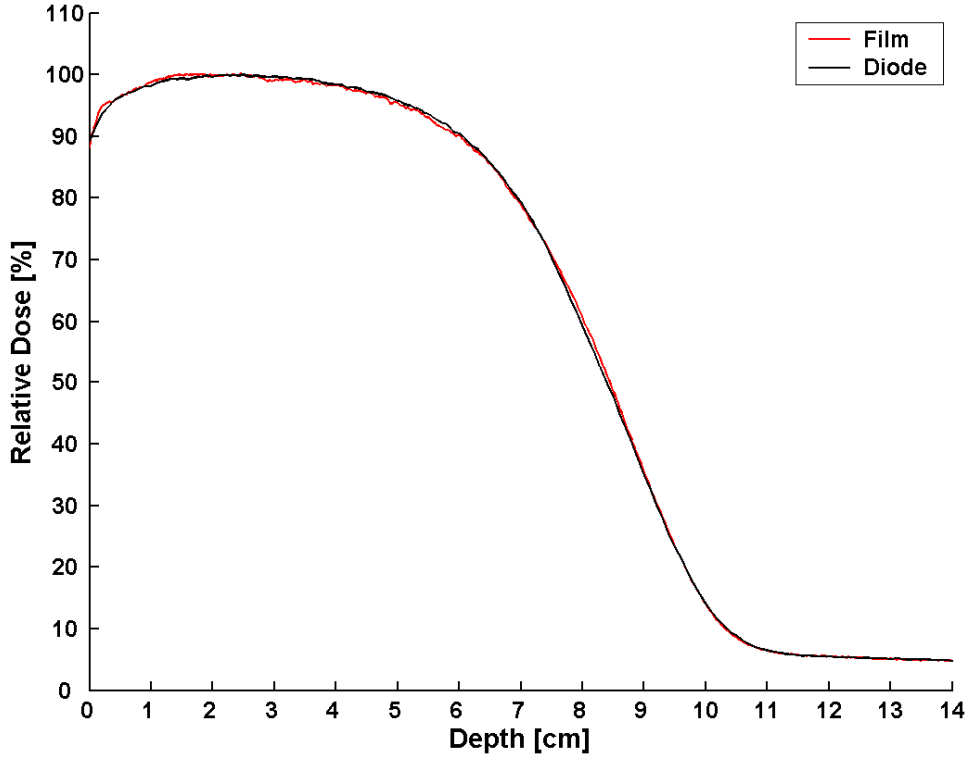

Figure 3.15: PDD measured using RGF in the third prototype phantom compared to diode measurements for a 20 MeV, 15x15 cm^2 electron field. Differences are 1.3 %, 0.82 mm, and 0.3 % in the high-dose, low dose-gradient; high-gradient; and low-dose, low dose-gradient regions, respectively.

Table 3.7: Maximum calculated differences between off-axis dose profiles measured using RGF in the third prototype phantom compared to diode measurements acquired in a water phantom for a 20 MeV, 15x15 cm2 electron field. The sign (+/-) preceding column headers (excluding HDR) indicate position relative to the CAX.

Depth	-DTA [mm]	+DTA [mm]	-LDR [%]	+LDR [%]	HDR [%]
0.5 cm	1.03	0.92	1.61	1.31	2.17
3.05 cm	0.29	0.66	1.31	0.98	1.56
6.1 cm	0.47	0.71	0.92	0.69	1.95

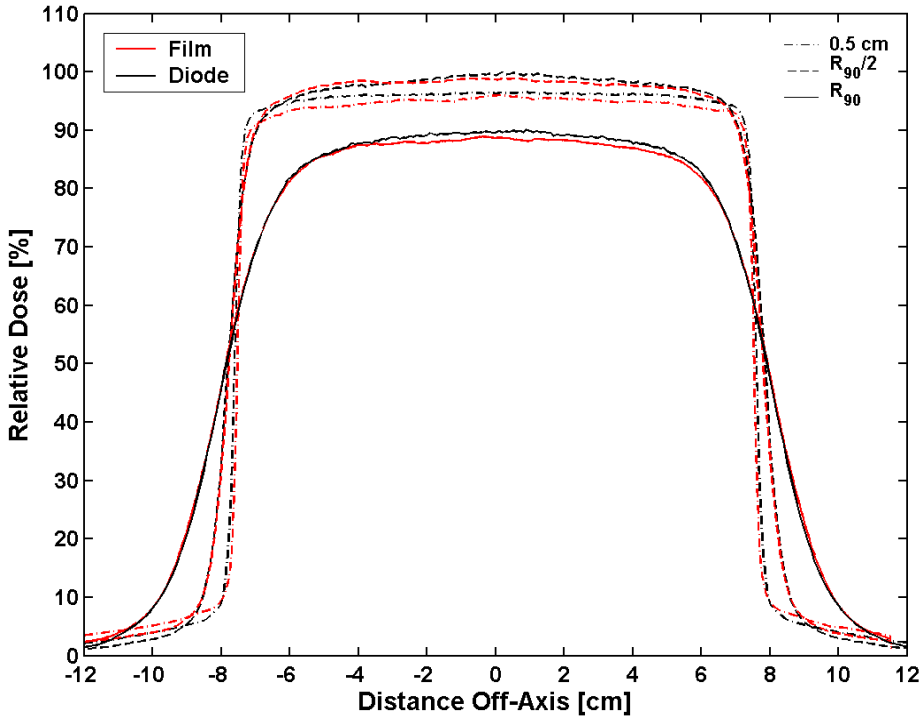

Figure 3.16: Off-axis dose profiles measured using RGF in the third prototype phantom compared to diode measurements for a 20 MeV, 15x15 cm^2 electron field. Depths shown are: 0.5 cm, $R_{90}/2$ = 3.05 cm, R_{90} = 6.1 cm.

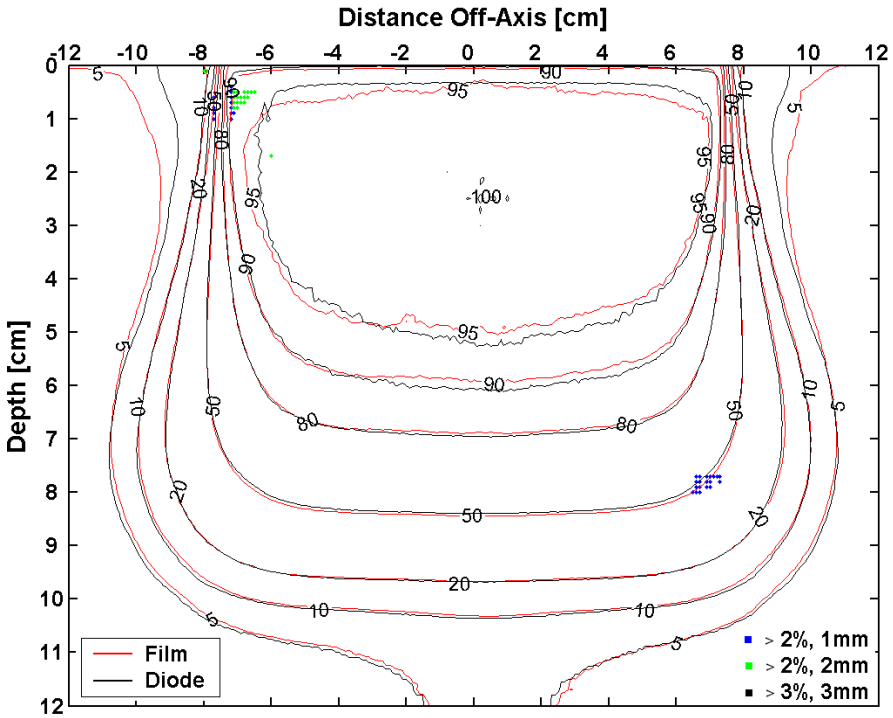

Figure 3.17: 2D dose distributions measured using RGF in the third prototype phantom compared to diode measurements for a 20 MeV, 15x15 cm^2 electron beam.

3.4.1.2 16 MeV, 15x15 cm^2

For the 16 MeV, 15x15 cm^2 RGF and diode PDDs shown in Figure 3.18, agreement is within criteria for all regions of the curves. In the high dose, low dose-gradient region, relative dose agreement is within 1.65 %. In the high dose-gradient region the maximum DTA is 0.44 mm, and in the low dose, low dose-gradient region relative dose agreement is within 0.38 %.

Off-axis dose profile comparisons for this electron beam are shown in Figure 3.19 and the differences calculated for each depth and region of the curve are summarized in Table 3.8. Profiles agree within criteria for all depths shown, excluding 0.5 cm. At this depth, the film disagrees with the diode measurement by as much as 1.04 mm DTA in the high dose-gradient region at the positive off-axis field edge.

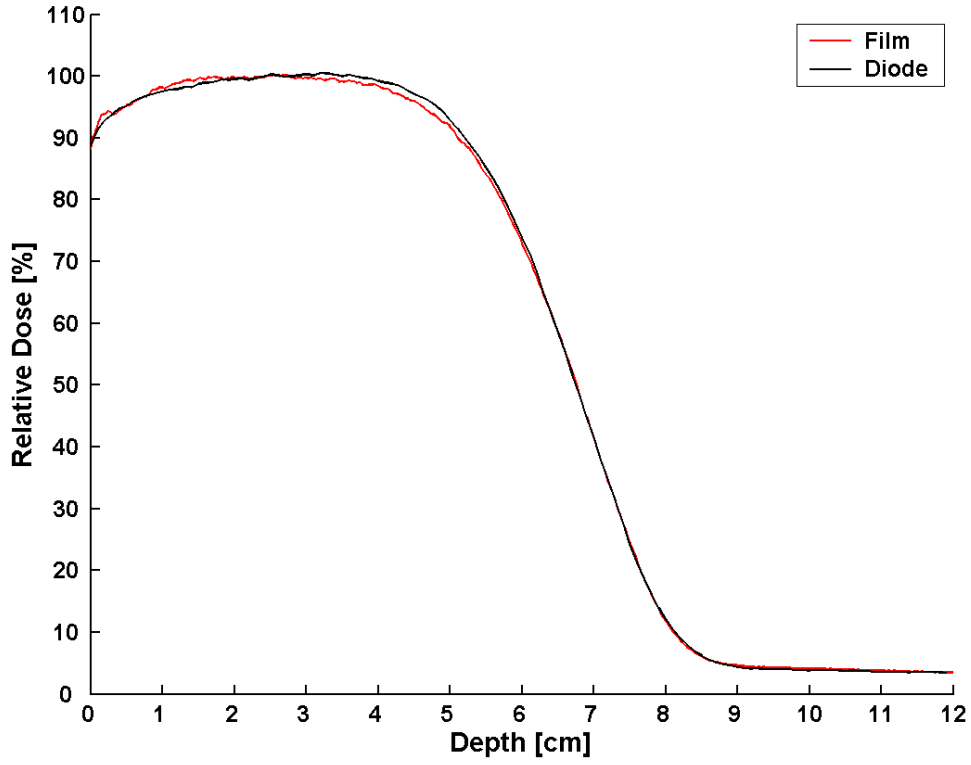

Figure 3.18: PDD measured using RGF in the third prototype phantom compared to diode measurements for a 16 MeV, 15x15 cm^2 electron field. Differences are 1.7 %, 0.44 mm, and 0.4 % in the high-dose, low dose-gradient; high-gradient; and low-dose, low dose-gradient regions, respectively.

Table 3.8: Maximum calculated differences between off-axis dose profiles measured using RGF in the third prototype phantom compared to diode measurements acquired in a water phantom for a 16 MeV, 15x15 cm^2 electron field. The sign (+/-) preceding column headers (excluding HDR) indicate position relative to the CAX.

Depth	-DTA [mm]	+DTA [mm]	-LDR [%]	+LDR [%]	HDR [%]
0.5 cm	0.67	1.04	1.76	1.89	0.82
2.6 cm	0.7	0.73	1.51	1.19	1.72
5.2 cm	1	0.39	1.41	0.43	1.16

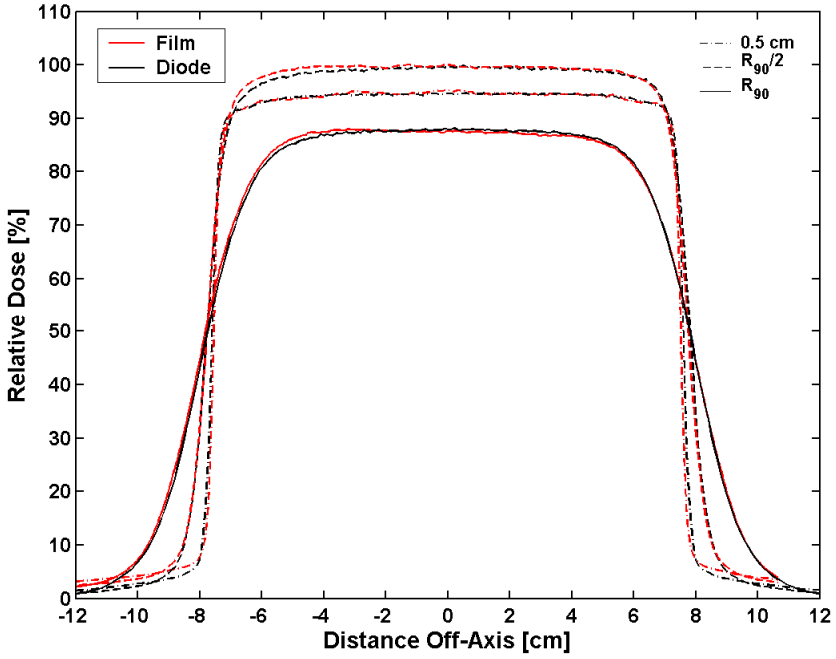

Figure 3.19: Off-axis dose profiles measured using RGF in the third prototype phantom compared to diode measurements for a 16 MeV, 15x15 cm^2 electron field. Depths shown are: 0.5 cm, $R_{90}/2$ = 2.6 cm, R_{90} = 5.2 cm.

As shown in Figure 3.20, 99.1 % of the RGF measured data points fall within ± 2 % dose or ± 1 mm DTA to the diode measurements. As the agreement criteria is expanded to ± 2 mm DTA, the agreement is improved to 99.3 %, while 100 % of the RGF measured data points are within ± 3 %, ± 3 mm agreement.

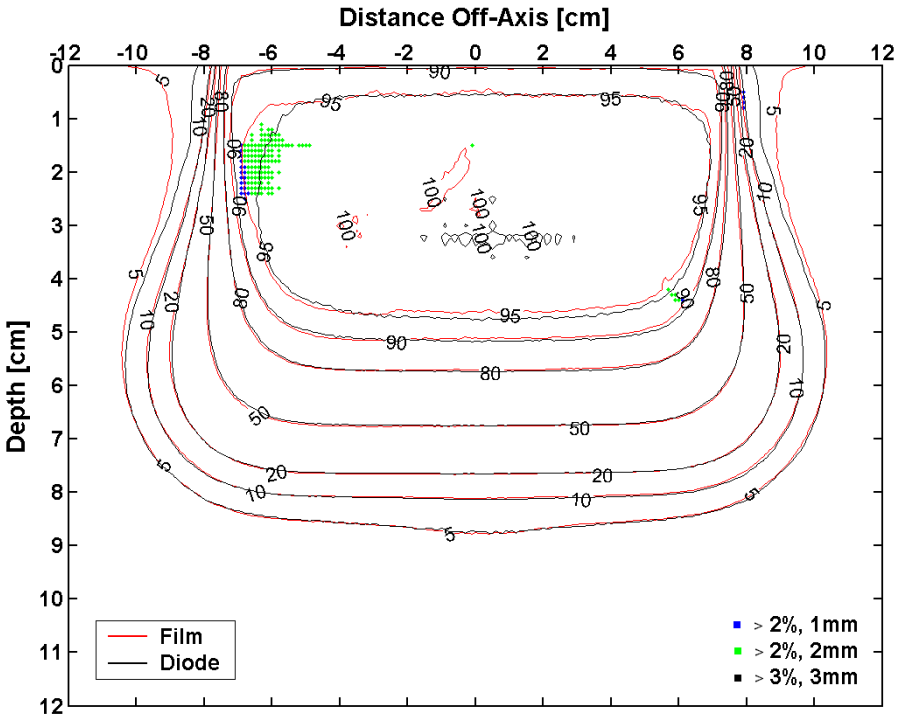

Figure 3.20: 2D dose distributions measured using RGF in the third prototype phantom compared to diode measurements for a 16 MeV, 15x15 cm^2 electron beam.

3.4.1.3 12 MeV, 15x15 cm^2

The RGF PDD measurement agrees with the diode PDD within criteria in all curve regions (c.f. Figure 3.21). In the high dose, low dose-gradient region, relative dose differences are within 1.3 %. In the high-gradient region, the maximum measured DTA is 0.33 mm, and in the low dose, low dose-gradient region relative dose differences are within 0.83 %.

Measured off-axis dose profiles for 12 MeV, 15x15 cm^2 are shown in Figure 3.22 and the differences between RGF and diode measurements for each depth curve region are summarized in Table 3.9. Profiles were in agreement within criteria with diode measurements for all depths except 2.0 cm. For this depth, the film overestimates the diode measurement by as much as 2.95 % relative dose in the negative off-axis distances.

In the 2D dose distributions shown in Figure 3.23, 98.1 % of the RGF measured data points fall within ± 2 % relative dose or ± 1 mm DTA. As the agreement criteria is expanded to ±

2 mm DTA, the agreement is improved to 99.22 %, and 100 % of the points are within ± 3 %, ± 3 mm agreement.

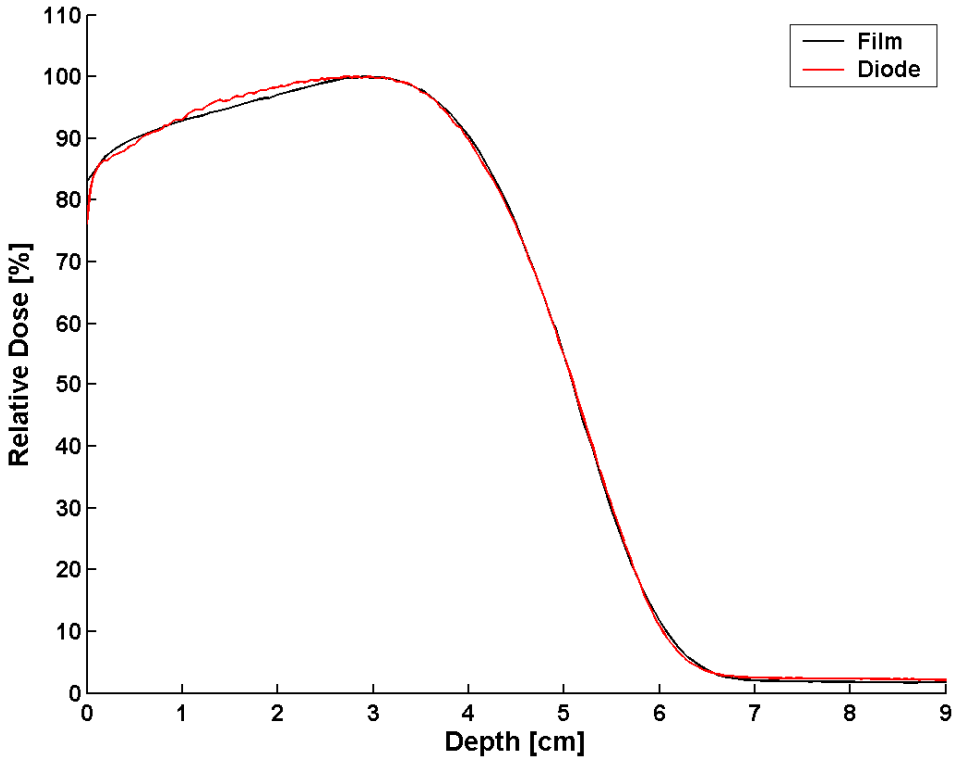

Figure 3.21: PDD measured using RGF in the third prototype phantom compared to diode measurements for a 12 MeV, 15x15 cm^2 electron field. Differences are 1.3 %, 0.33 mm, and 0.8 % in the high-dose, low dose-gradient; high-gradient; and low-dose, low dose-gradient regions, respectively.

Table 3.9: Maximum calculated differences between off-axis dose profiles measured using RGF in the third prototype phantom compared to diode measurements acquired in a water phantom for a 12 MeV, 15x15 cm^2 electron field. The sign (+/-) preceding column headers (excluding HDR) indicate position relative to the CAX.

Depth	-DTA [mm]	+DTA [mm]	-LDR [%]	+LDR [%]	HDR [%]
0.5 cm	0.76	0.54	1.98	1.83	1.12
2.0 cm	1.13	0.38	1.76	1.75	2.95
4.0 cm	0.89	0.76	1.71	1.75	1.65

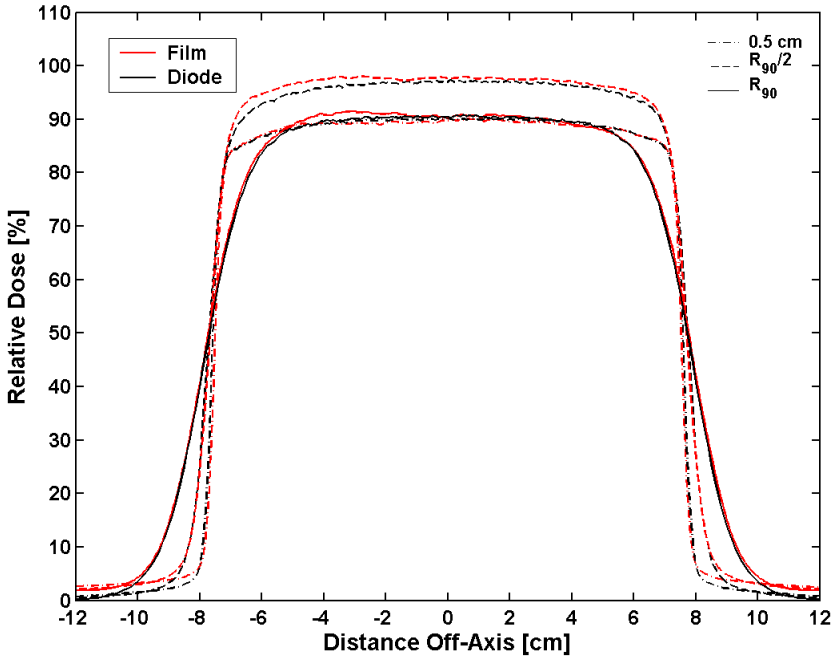

Figure 3.22: Off-axis dose profiles measured using RGF in the third prototype phantom compared to diode measurements for a 12 MeV, 15x15 cm^2 electron field. Depths shown are: 0.5 cm, $R_{90}/2$ = 2.0 cm, R_{90} = 4.0 cm.

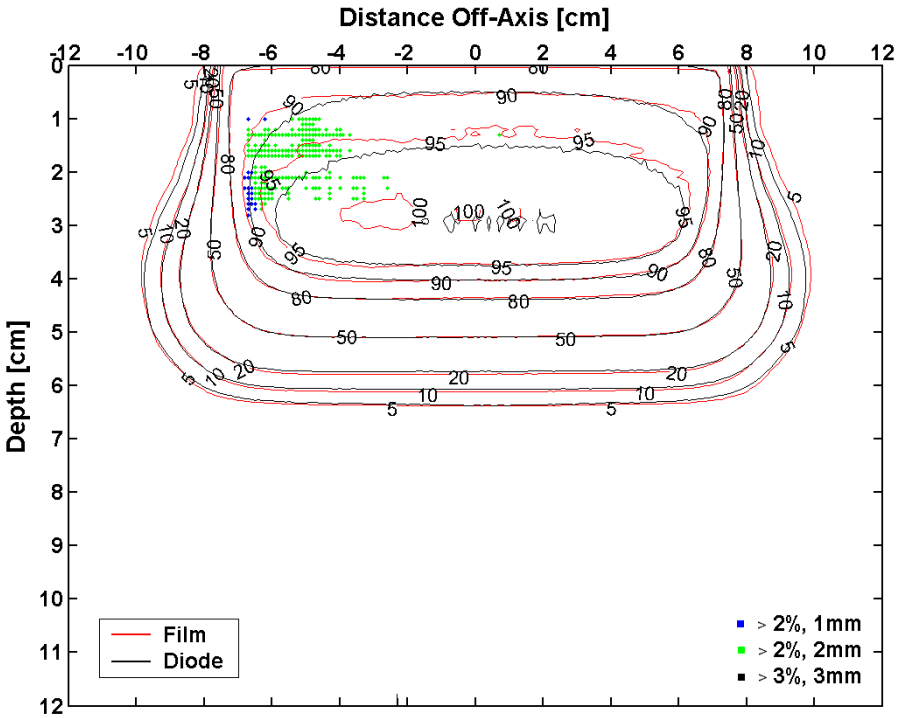

Figure 3.23: 2D dose distributions measured using RGF in the third prototype phantom compared to diode measurements for a 12 MeV, 15x15 cm^2 electron beam.

3.4.1.4 9 MeV, 15x15 cm^2

The 9 MeV, 15x15 cm^2 PDD profile agrees within criteria with diode measurements in all regions of the curve (c.f. Figure 3.24). In the high dose, low dose-gradient region, relative dose agreement is within 1.6 %. In the high-gradient region the maximum measured DTA is 0.28 mm, while in the low dose, low dose-gradient region relative dose differences are up to 1.4 %.

Off-axis dose profile measurements are shown in Figure 3.25 and the maximum differences for each depth and curve region are summarized in Table 3.10. The RGF measured profiles are in agreement within criteria with diode measurements for all depths shown excluding 1.4 cm. For this depth, the film overestimates the diode measurement by as much as 2.55 % relative dose in the negative off-axis distances.

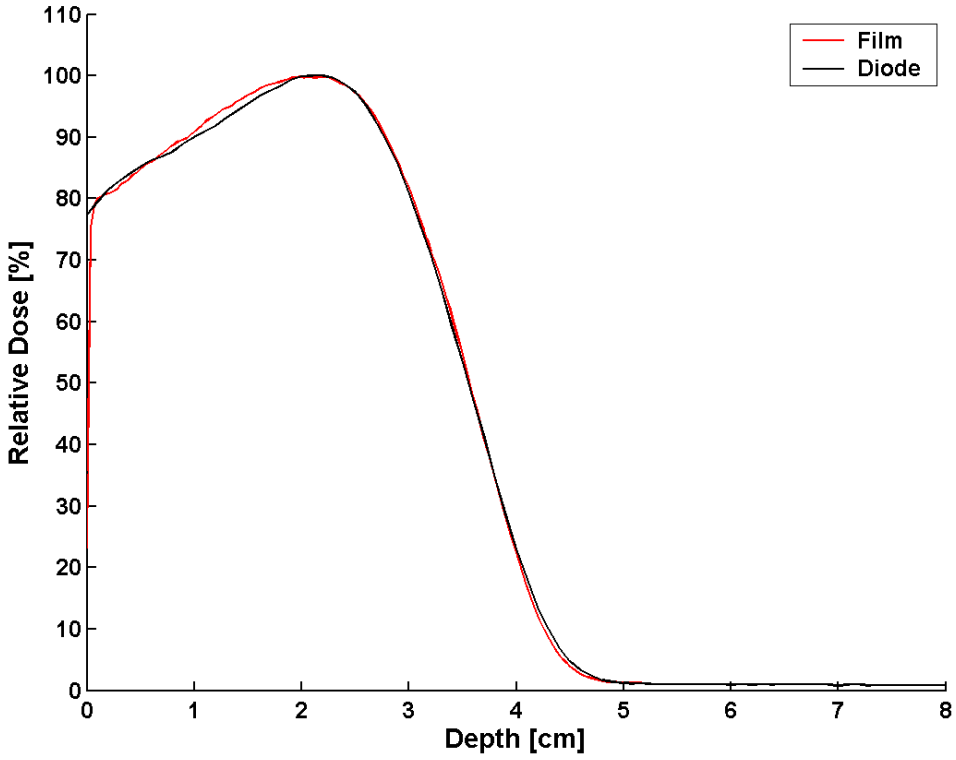

Figure 3.24: PDD measured using RGF in the third prototype phantom compared to diode measurements for a 9 MeV, 15x15 cm^2 electron field. Differences are 1.6 %, 0.28 mm, and 1.4 % in the high-dose, low dose-gradient; high-gradient; and low-dose, low dose-gradient regions, respectively.

Table 3.10: Maximum calculated differences between off-axis dose profiles measured using RGF in the third prototype phantom compared to diode measurements acquired in a water phantom for a 9 MeV, 15x15 cm^2 electron field. The sign (+/-) preceding column headers (excluding HDR) indicate position relative to the CAX.

Depth	-DTA [mm]	+DTA [mm]	-LDR [%]	+LDR [%]	HDR [%]
0.5 cm	0.84	0.52	1.11	0.92	2
1.4 cm	0.36	0.4	0.69	1.27	2.55
2.8 cm	0.72	0.89	0.66	0.71	1.95

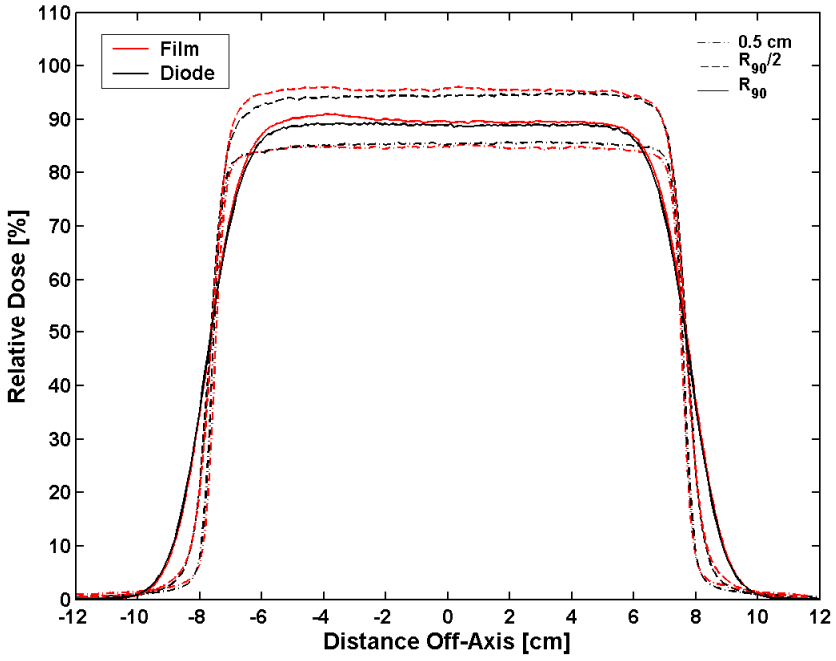

Figure 3.25: Off-axis dose profiles measured using RGF in the third prototype phantom compared to diode measurements for a 9 MeV, 15x15 cm^2 electron field. Depths shown are: 0.5 cm, $R_{90}/2$ = 1.4 cm, R_{90} = 2.8 cm.

As shown in Figure 3.26, 99.1 % of the RGF measured data points fall within ± 2 % dose or ± 1 mm DTA to diode measurements. As the agreement criteria is expanded to ± 2 mm DTA, the percentage of RGF measured data points is increased to 99.73 %, while 100 % of the measured data points are within ± 3 %, ± 3 mm agreement.

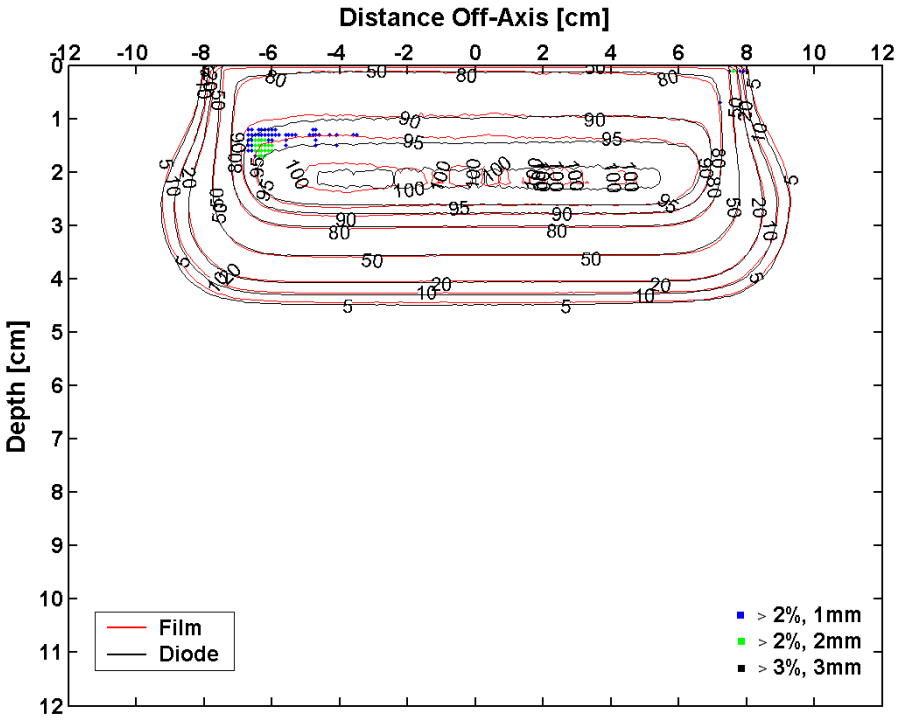

Figure 3.26: 2D dose distributions measured using RGF in the third prototype phantom compared to diode measurements for a 9 MeV, 15x15 cm^2 electron beam.

3.4.1.5 6 MeV, 15x15 cm^2

The 6 MeV, 15x15 cm^2 RGF PDD measurement agrees within criteria in all regions of the curve (c.f. Figure 3.27). In the high dose, low dose-gradient region, relative dose agreement is within 1.9 %. In the high-gradient region, the maximum measured DTA is 0.42 mm, and in the low dose, low dose-gradient region relative dose differences are within 1.4 %.

Off-axis dose profiles are shown in Figure 3.28 and the maximum differences for each depth and curve region are summarized in Table 3.11. Measurements were in agreement within criteria with diode measurements for all depths shown excluding the 1.8 cm depth. For this depth, the film underestimates the diode measurement by as much as 3.6 % relative dose for the positive off-axis distances.

In the 2D dose distributions (c.f. Figure 3.29), 99.0 % of the RGF measured data points are within ± 2 % relative dose or ± 1 mm DTA. As the agreement criteria is expanded to ± 2 mm

DTA, the agreement is improved to 99.74 %, while 100 % of the points pass for the ± 3 %, ± 3 mm agreement criteria.

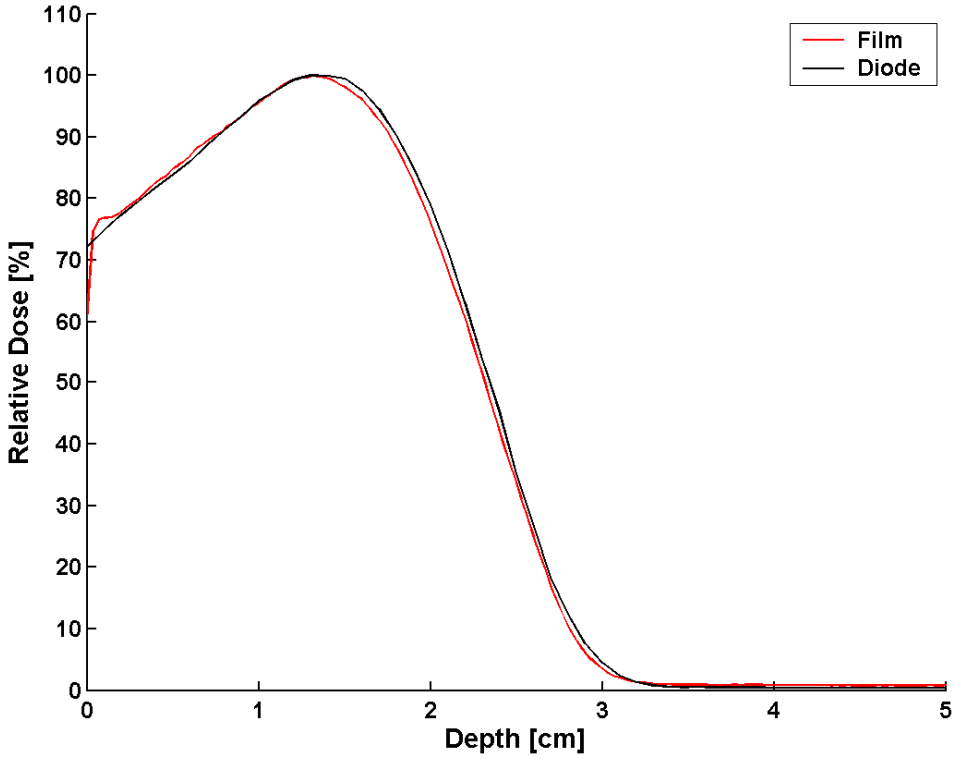

Figure 3.27: PDD measured using RGF in the third prototype phantom compared to diode measurements for a 6 MeV, 15x15 cm^2 electron field. Differences are 1.9 %, 0.43 mm, and 1.4 % in the high-dose, low dose-gradient; high-gradient; and low-dose, low dose-gradient regions, respectively.

Table 3.11: Maximum calculated differences between off-axis dose profiles measured using RGF in the third prototype phantom compared to diode measurements acquired in a water phantom for a 6 MeV, 15x15 cm^2 electron field. The sign (+/-) preceding column headers (excluding HDR) indicate position relative to the CAX.

Depth	-DTA [mm]	+DTA [mm]	-LDR [%]	+LDR [%]	HDR [%]
0.5 cm	0.53	0.49	0.89	0.85	1.75
0.9 cm	0.9	0.6	0.9	0.74	1.64
1.8 cm	0.84	0.9	1.21	0.7	3.61

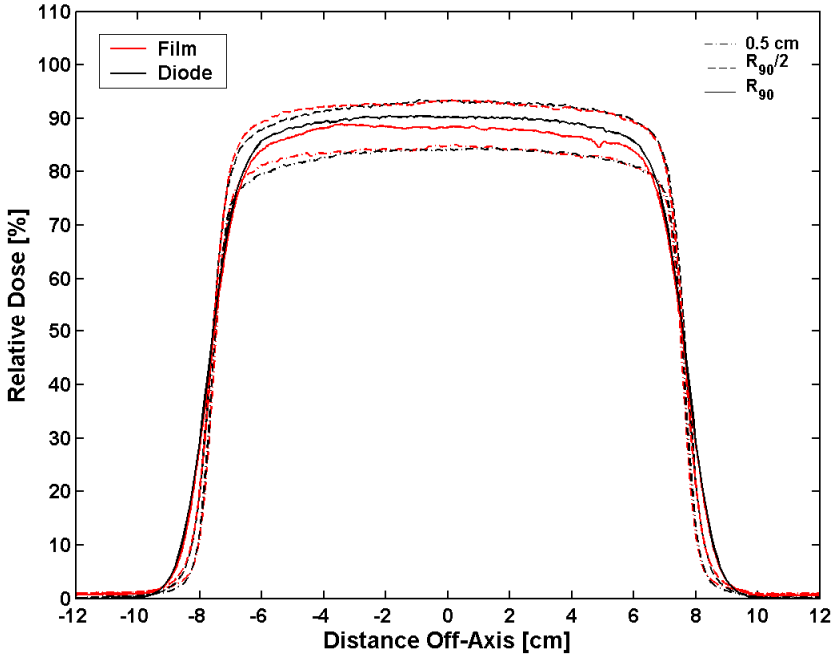

Figure 3.28: Off-axis dose profiles measured using RGF in the third prototype phantom compared to diode measurements for a 6 MeV, 15x15 cm^2 electron field. Depths shown are: 0.5 cm, $R_{90}/2$ = 0.9 cm, R_{90} = 1.8 cm.

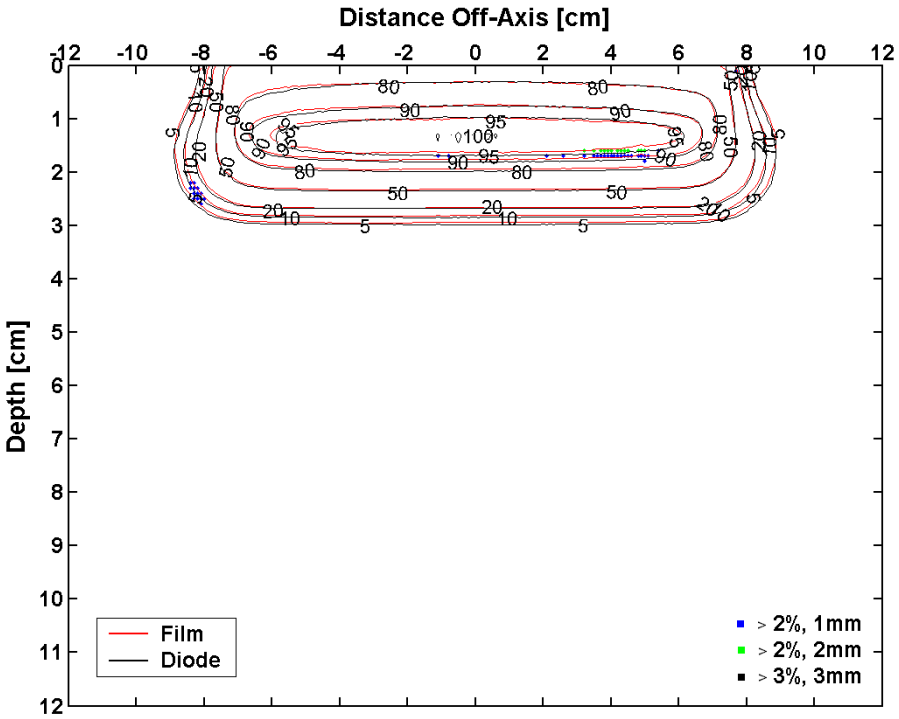

Figure 3.29: 2D dose distributions measured using RGF in the third prototype phantom compared to diode measurements for a 6 MeV, 15x15 cm^2 electron beam.

3.4.1.6 16 MeV, 4x4 cm^2

PDD measurements are shown Figure 3.30 and RGF is in agreement to diode measurements in all regions of the curve. In the high-dose, low dose-gradient region agreement is within 1.3 %. In the high dose-gradient region, the DTA is within 0.74 mm, while in the low-dose, low dose-gradient region the relative dose difference is within 0.9 %.

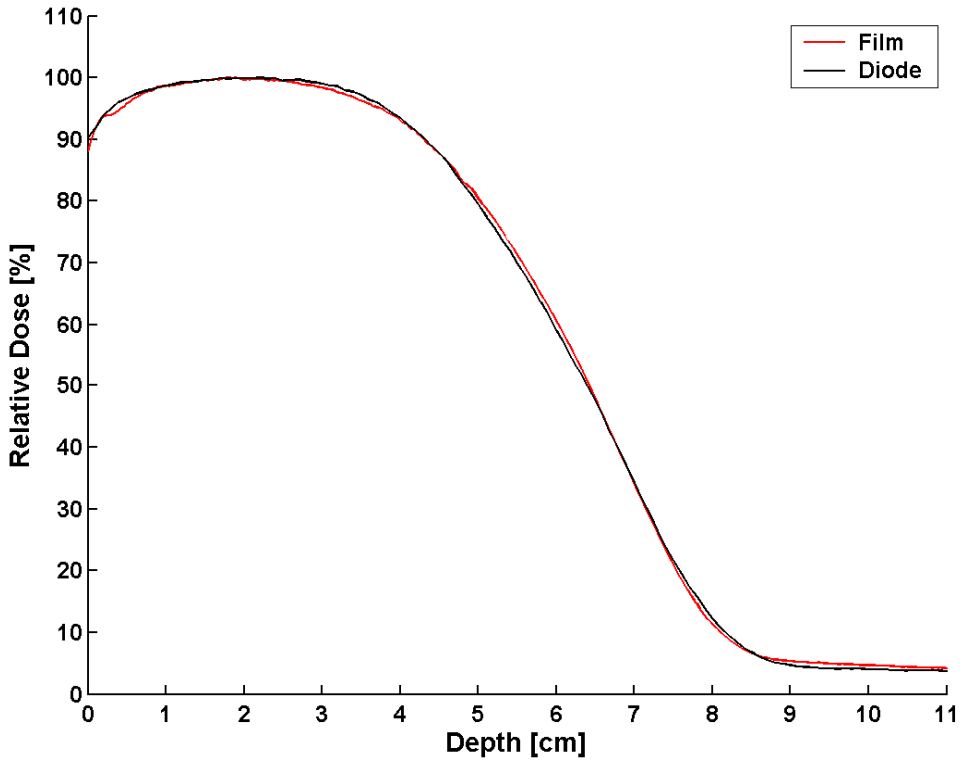

Figure 3.30: PDD measured using RGF in the third prototype phantom compared to diode measurements for a 16 MeV, 4x4 cm^2 electron field. Differences are 1.3 %, 0.74 mm, and 0.9 % in the high-dose, low dose-gradient; high-gradient; and low-dose, low dose-gradient regions, respectively.

Off-axis dose profile comparisons for this electron field are shown in Figure 3.31 and the differences calculated for each depth and region of the curve are summarized in Table 3.12. Agreement is within criteria in the high-gradient regions at both the 0.5 cm and 2.05 cm depths. At the 4.1 cm depth, the maximum differences in this region are 1.92 mm and 1.83 mm in the

negative and positive off-axis distances, respectively. Measurements are within criteria in the high-dose region of the curve for all depths shown. In the low-dose, low dose-gradient curve regions, film measurements consistently overestimate diode measurements at each depth with a maximum relative dose difference of 3.43 % in the positive low-dose region at 0.5 cm.

Table 3.12: Maximum calculated differences between off-axis dose profiles measured using RGF in the third prototype phantom compared to diode measurements acquired in a water phantom for a 16 MeV, 4x4 cm^2 electron field. The sign (+/-) preceding column headers (excluding HDR) indicate position relative to the CAX.

Depth	-DTA [mm]	+DTA [mm]	-LDR [%]	+LDR [%]	HDR [%]
0.5 cm	0.52	0.29	2.69	3.43	1.66
2.1 cm	0.67	0.66	2.51	2.62	0.89
4.2 cm	1.92	1.83	2.13	2.37	0.56

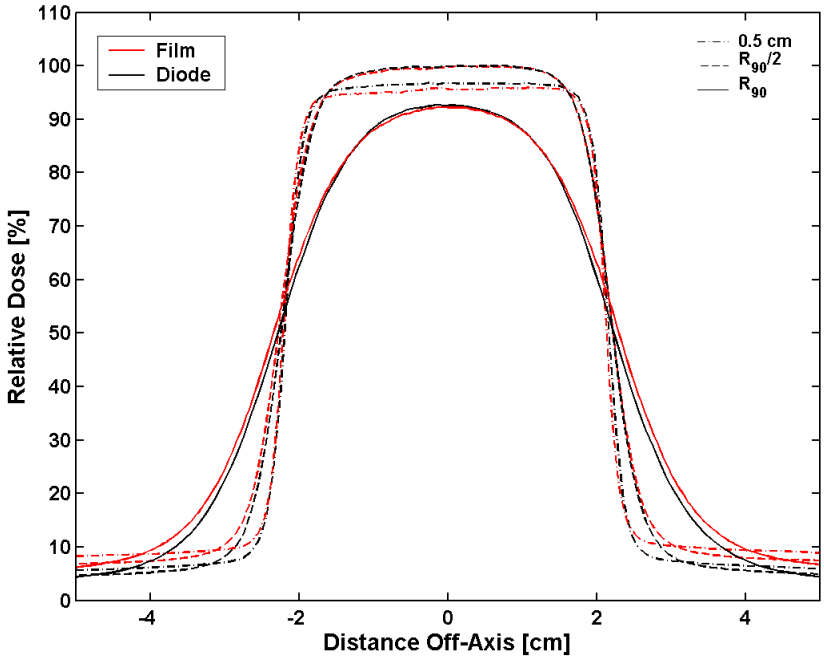

Figure 3.31: Off-axis dose profiles measured using RGF in the third prototype phantom compared to diode measurements for a 16 MeV, 4x4 cm^2 electron field. Depths shown are: 0.5 cm, $R_{90}/2$ = 2.05 cm, R_{90} = 4.1 cm.

2D dose distributions are shown in Figure 3.32, and 88.6 % of the film measured data points are within ± 2 % dose, ± 1 mm DTA to diode measurements. As the agreement criteria is

expanded to ± 2 %, ± 2 mm, and ± 3 %, ± 3 mm, the percentage of points within criteria is increased to 94.4 % and 99.5 %, respectively.

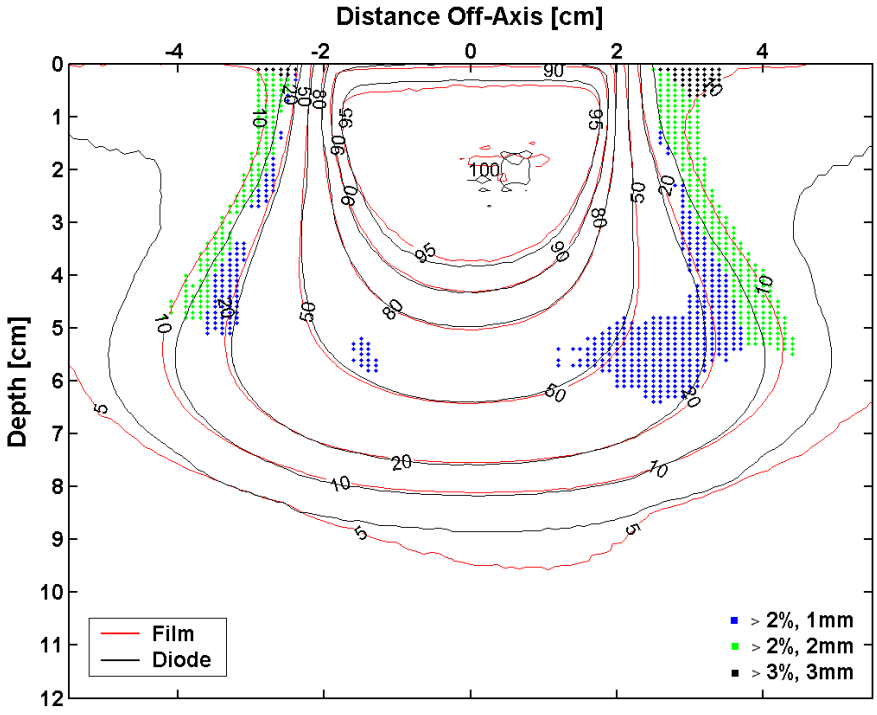

Figure 3.32: 2D dose distributions measured using RGF in the third prototype phantom compared to diode measurements for a 16 MeV, 4x4 cm^2 electron beam.

3.4.1.7 9 MeV, 4x4 cm^2

The RGF PDD measurement agrees within criteria to the diode PDD in all curve regions (c.f. Figure 3.33). Relative dose difference in the high-dose, low dose-gradient region are up to 1.6 %. In the high-gradient region the maximum DTA is 0.6 mm, and in the low-dose, low dose-gradient region relative dose differences are within 1.6 %.

Off-axis dose profiles are shown in Figure 3.34 and the maximum differences calculated for the regions of the curve are summarized in Table 3.13. Agreement is within criteria in the high-dose region of the curve for all depths. For the 0.5 cm, and 1.4 cm depth, film disagrees with diode measurements by a maximum of 1.05 mm and 1.09 mm DTA on the negative off-axis side, respectively. For the 2.8 cm depth, film differs from the diode by 1.3 mm DTA on the

positive off-axis side. In the low-dose region, film measurements overestimate diode measurements at the positive off-axis side for the 1.4 and 2.8 cm depth by 2.39 % and 2.16 % relative dose, respectively. Film underestimates diode measurements at the negative off-axis side for the 0.5 cm and 1.4 cm depths by 2.07 % and 2.89 % relative dose, respectively.

In the 2D dose distributions (c.f. Figure 3.35) 92.4 % of the film measured data points agree with diode measurements for the ± 2 % relative dose, and ± 1 mm DTA agreement criteria. As the agreement criteria is relaxed to ± 2 %, ± 2 mm, 98.5 % of the points agree with diode measurements, and 99.8 % of the RGF measured data points fall within ± 3 %, ± 3 mm agreement.

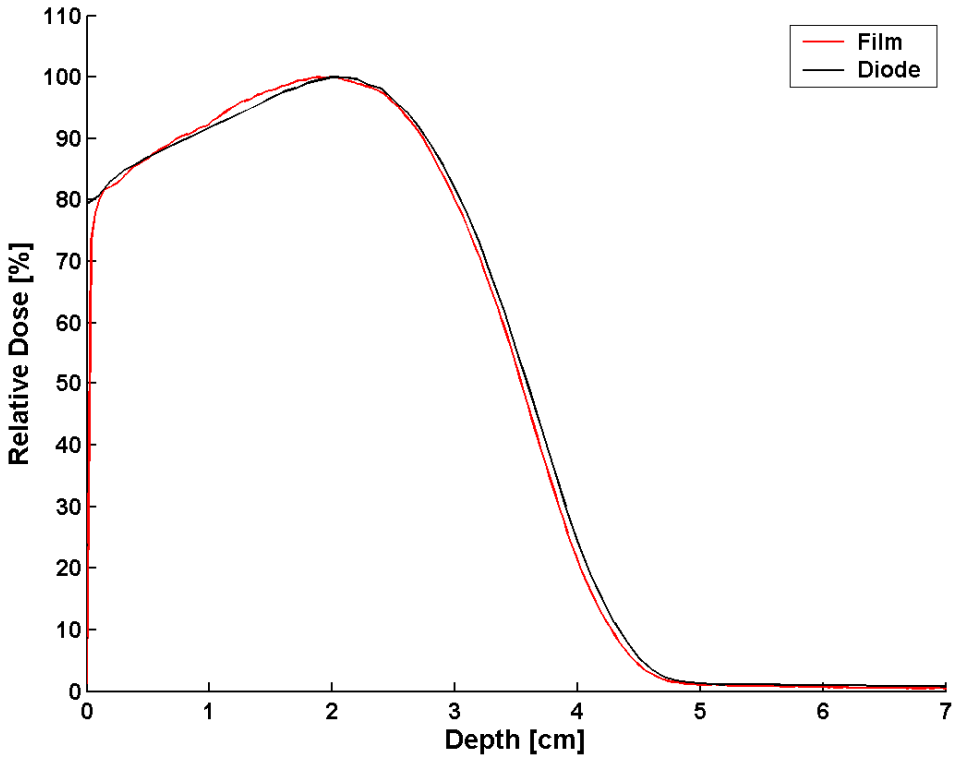

Figure 3.33: PDD measured using RGF in the third prototype phantom compared to diode measurements for a 9 MeV, 4x4 cm^2 electron field. Differences are 1.6 %, 0.60 mm, and 1.6 % in the high-dose, low dose-gradient; high-gradient; and low-dose, low dose-gradient regions, respectively.

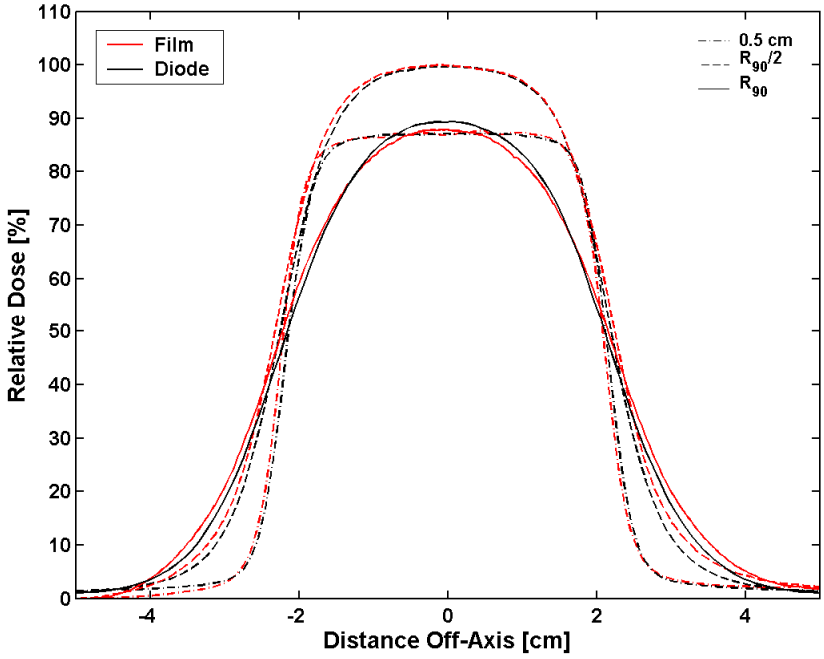

Figure 3.34: Off-axis dose profiles measured using RGF in the third prototype phantom compared to diode measurements for a 9 MeV, 4x4 cm^2 electron field. Depths shown are: 0.5 cm, $R_{90}/2$ = 1.35 cm, R_{90} = 2.7 cm.

Table 3.13: Maximum calculated differences between off-axis dose profiles measured using RGF in the third prototype phantom compared to diode measurements acquired in a water phantom for a 9 MeV, 4x4 cm^2 electron field. The sign (+/-) preceding column headers (excluding HDR) indicate position relative to the CAX.

Depth	-DTA [mm]	+DTA [mm]	-LDR [%]	+LDR [%]	HDR [%]
0.5 cm	1.05	0.61	2.07	1.13	0.75
1.35 cm	1.09	0.9	2.89	2.39	1.5
2.7 cm	1	1.3	1.96	2.16	1.56

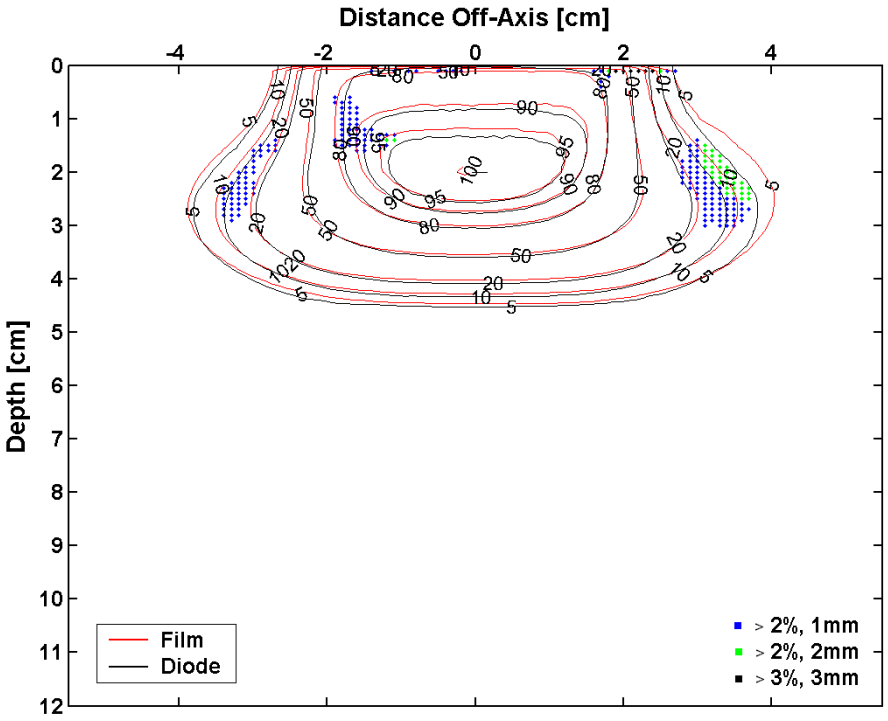

Figure 3.35: 2D dose distributions measured using RGF in the third prototype phantom compared to diode measurements for a 9 MeV, 4x4 cm^2 electron beam.

3.4.1.8 16 MeV, 2x2 cm^2

The 16 MeV, 2x2 cm^2 RGF measured PDD is in agreement to the diode PDD in the high-dose, low dose-gradient and low-dose, low dose-gradient regions of the curve (c.f. Figure 3.36). In these regions the maximum relative dose differences are 1.8 % and 1.1 %, respectively. In the high dose-gradient region of the curve, film measurements overestimate the diode by as much as 2.0 mm DTA.

Off-axis dose profiles are shown in Figure 3.37 and the maximum differences calculated for the regions of the curve are summarized in Table 3.14. Off-axis RGF measurements agree within criteria for the 0.5 and 1.35 cm depths in the high dose-gradient regions of the curve. For the 2.7 cm depth, film disagrees with diode measurements by 1.44 and 1.79 mm DTA for the negative and positive off-axis distances, respectively. Film overestimates diode measurements by > 2 % in the low-dose region of the curve for all depths measured with a maximum difference of

3.1 % relative dose measured for the 1.35 cm depth at the negative off-axis distance. In the high-dose region, the relative film dose underestimates the diode measurement for the 0.5 cm and 2.7 cm depths by 3.72 % and 3.57 %, respectively.

In the 2D dose distributions shown in Figure 3.38, 73.8 % of the film measured data points are in agreement with diode measurements for the ± 2 %, ± 1 mm agreement criteria. As the agreement criteria is expanded to ± 2 %, ± 2 mm, 84.8 % of the points agree with diode measurements, and 97.9 % of the RGF measured data points are in agreement for ± 3 %, ± 3 mm criteria.

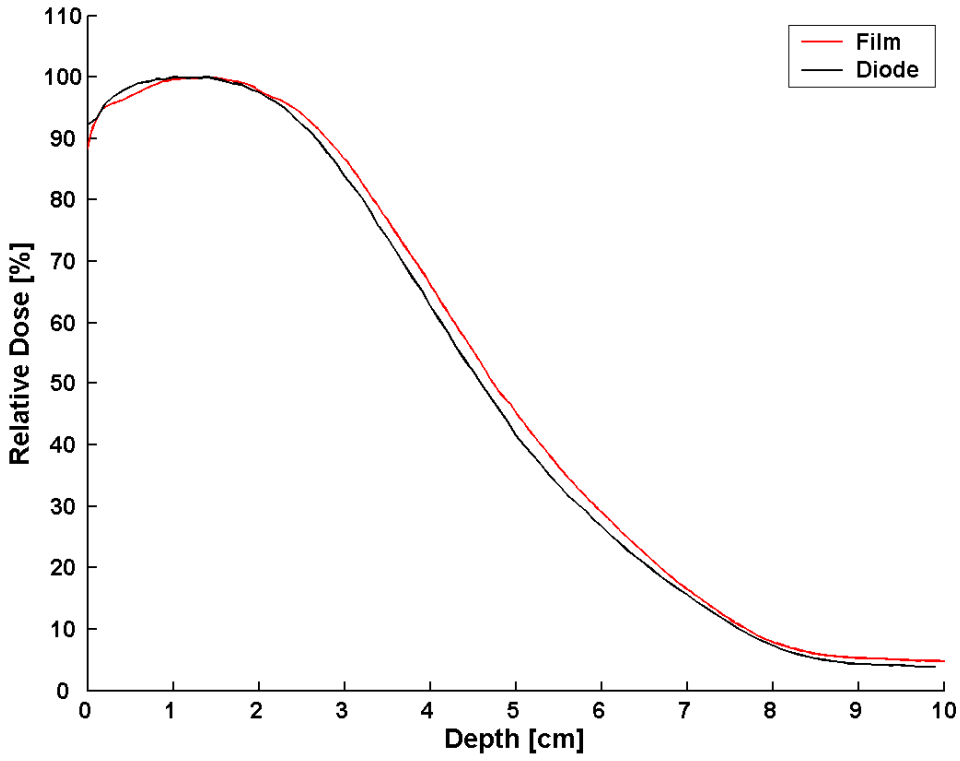

Figure 3.36: PDD measured using RGF in the third prototype phantom compared to diode measurements for a 16 MeV, 2x2 cm^2 electron field. Differences are 1.8 %, 2.00 mm, and 1.1 % in the high-dose, low dose-gradient; high-gradient; and low-dose, low dose-gradient regions, respectively.

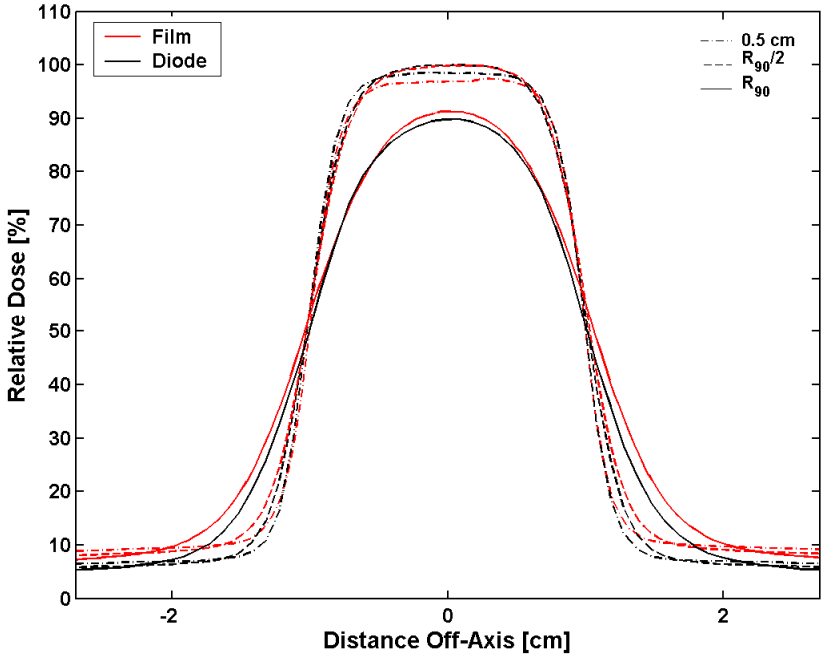

Figure 3.37: Off-axis dose profiles measured using RGF in the third prototype phantom compared to diode measurements for a 16 MeV, 2x2 cm^2 electron field. Depth's shown are: 0.5 cm, $R_{90}/2$ = 1.35 cm, R_{90} = 2.7 cm.

Table 3.14: Maximum calculated differences between off-axis dose profiles measured using RGF in the third prototype phantom compared to diode measurements acquired in a water phantom for a 16 MeV, 2x2 cm^2 electron field. The sign (+/-) preceding column headers (excluding HDR) indicate position relative to the CAX.

Depth	-DTA [mm]	+DTA [mm]	-LDR [%]	+LDR [%]	HDR [%]
0.5 cm	0.39	0.97	2.77	2.93	3.72
1.35 cm	0.78	0.66	3.11	3.02	1.52
2.7 cm	1.44	1.79	2.86	3.01	3.57

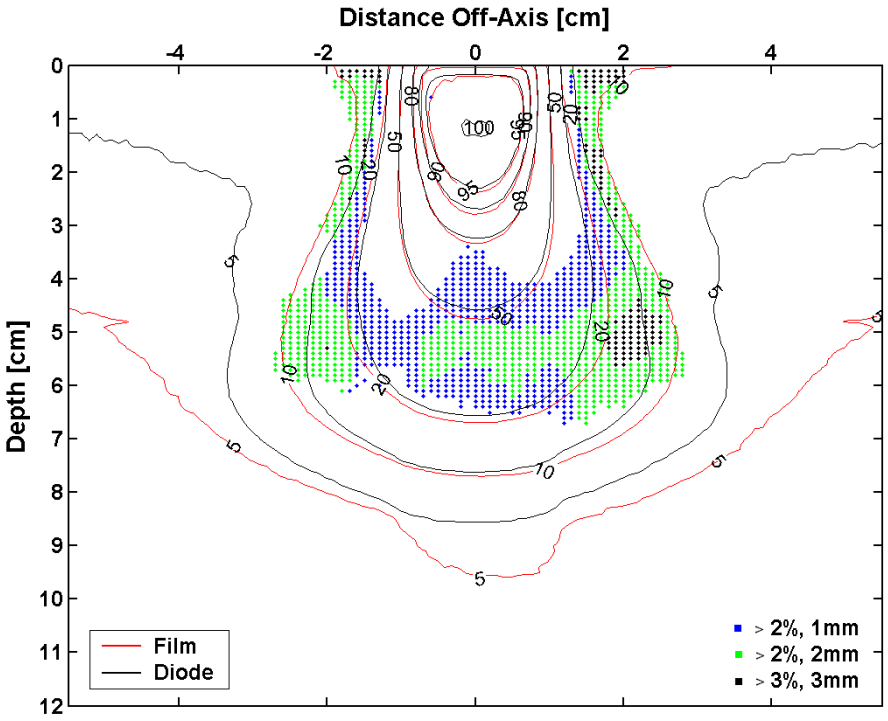

Figure 3.38: 2D dose distributions measured using RGF in the third prototype phantom compared to diode measurements for a 16 MeV, 2x2 cm^2 electron beam.

3.4.1.9 9 MeV, 2x2 cm^2

The RGF PDD measurement agrees within criteria to the diode measurement in all regions of the curve (c.f. Figure 3.39). In the high-dose, low dose-gradient region, relative dose differences are within 1.43 %. In the high dose-gradient region of the curve the DTA is within 0.68 mm, and in the low-dose, low dose-gradient region the maximum relative dose difference is 1.4 %.

Off-axis dose profiles are shown in Figure 3.40 and the maximum differences for the regions of the curve are summarized in Table 3.15. Film measurements agree within ± 2 % dose in the high-dose region at all depths. At the 0.5 cm and 0.9 cm depth, film measurements are within criteria, but at 1.8 cm film measurements disagree with diode by 1.86 mm and 1.72 mm DTA at the negative and positive off-axis sides, respectively.

2D dose distributions (c.f. Figure 3.41) show 78.5 % of the film measured data points in agreement with diode measurements for the ± 2 %, ± 1 mm agreement criteria. As the agreement criteria is expanded to ± 2 %, ± 2 mm, 90.4 % of the points agree with diode measurements, while 98.4 % of the points fall within ± 3 %, ± 3 mm agreement.

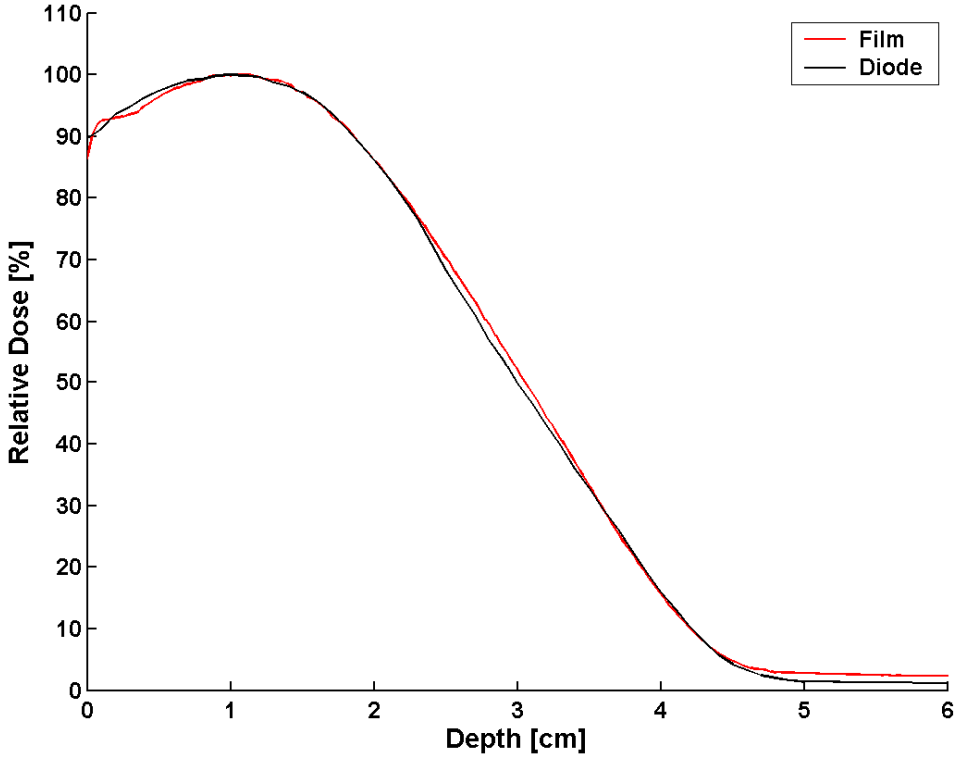

Figure 3.39: PDD measured using RGF in the third prototype phantom compared to diode measurements for a 9 MeV, 2x2 cm^2 electron field. Differences are 1.4 %, 0.68 mm, and 1.4 % in the high-dose, low dose-gradient; high-gradient; and low-dose, low dose-gradient regions, respectively.

Table 3.15: Maximum calculated differences between off-axis dose profiles measured using RGF in the third prototype phantom compared to diode measurements acquired in a water phantom for a 9 MeV, 2x2 cm^2 electron field. The sign (+/-) preceding column headers (excluding HDR) indicate position relative to the CAX.

Depth	-DTA [mm]	+DTA [mm]	-LDR [%]	+LDR [%]	HDR [%]
0.5 cm	0.8	0.59	4.47	3.72	1.33
0.95 cm	0.67	0.57	4.33	3.99	0.69
1.9 cm	1.86	1.72	4.03	4.59	0.62

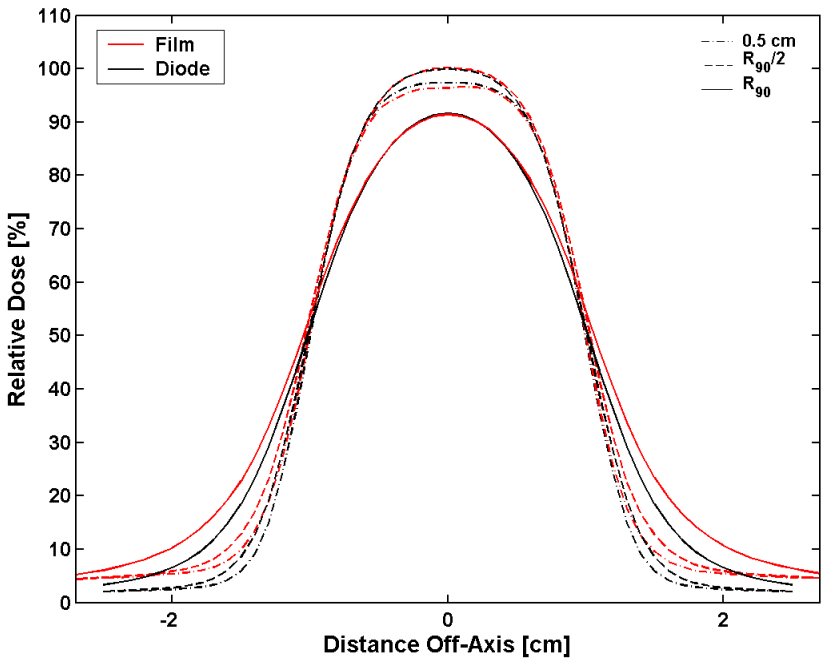

Figure 3.40: Off-axis dose profiles measured using RGF in the third prototype phantom compared to diode measurements for a 9 MeV, 2x2 cm^2 electron field. Depths shown are: 0.5 cm, $R_{90}/2$ = 0.95 cm, R_{90} = 1.9 cm.

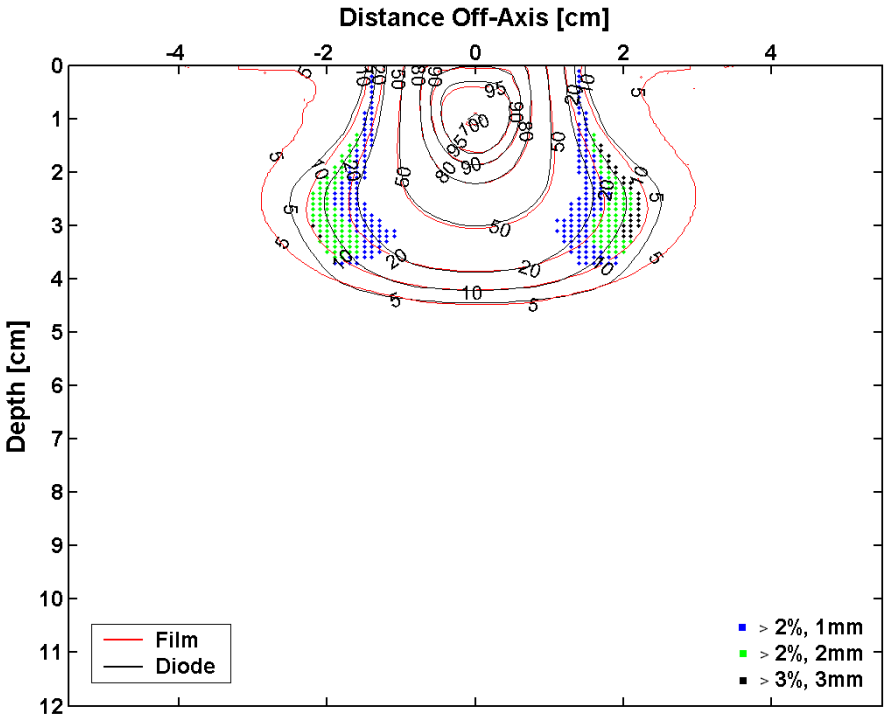

Figure 3.41: 2D dose distributions measured using RGF in the third prototype phantom compared to diode measurements for a 9 MeV, 2x2 cm^2 electron beam.

3.4.2 RCF Relative Dose Measurements

In sections 3.4.2.1 to 3.4.2.9, measured CAX PDD profiles, 1D off-axis dose profiles, and 2D dose distributions acquired using RCF in the third prototype phantom are compared to equivalent scanning diode measurements in water for 6-20 MeV, 15x15 cm^2 in addition to 9 and 16 MeV, 2x2 and 4x4 cm^2 electron fields. All film measurements were normalized to 100% at the CAX maximum and all data is unsmoothed. A discussion of presented RCF results is presented in Section 3.5.2.

3.4.2.1 20 MeV, 15x15 cm^2

In the measured PDD profiles shown in Figure 3.42 RCF measurements agree within criteria for all regions of the curve excluding the high-dose, low-dose gradient region where film underestimates the diode by as much as 4.7 %. In the high dose-gradient region, the DTA is within 0.89 mm, while in the low-dose, low dose-gradient region measured differences are within 0.6 %.

Off-axis dose profile measurements are shown in Figure 3.43, and a summary of the maximum differences in the regions of the curve is shown in Table 3.16. RCF measurements are within ± 2 % dose or ± 1 mm DTA for all depths in the high-gradient fall-off and low-gradient, low-dose regions excluding the 6.1 cm depth where the maximum DTA is 1.1 mm for the negative off-axis distances. In the high-dose region at 0.5 cm, film underestimates diode measurements by up to 6.5 % relative dose. At 3.05 cm and 6.1 cm, film underestimates diode measurements by 2.23 % and 2.48 % relative dose, respectively, for the positive off-axis distances.

In the 2D dose distributions shown in Figure 3.44, 90.1 % of the film measured data points are within ± 2 % relative dose, or ± 1 mm DTA. As the agreement criteria is expanded to ± 2 mm DTA, the percentage of points in agreement is also increased slightly to 90.3 %. For the

± 3 %, ± 3 mm agreement criteria, 95.0 % of the RCF measured data points are in agreement to diode measurements.

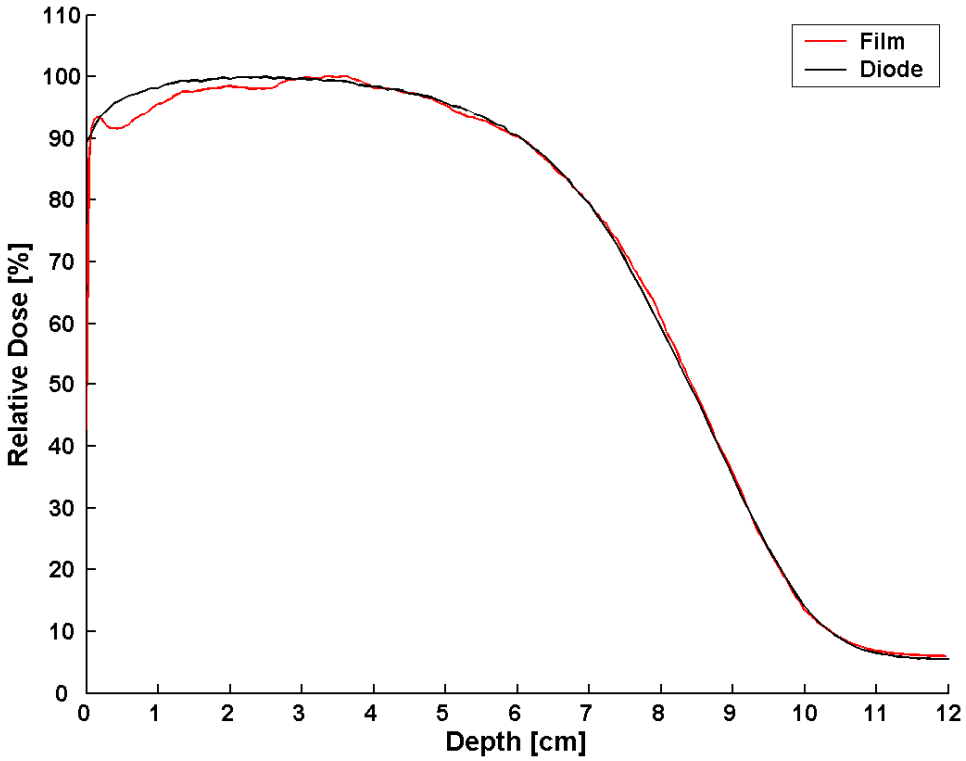

Figure 3.42: PDD measured using RCF in the third prototype phantom compared to diode measurements for a 20 MeV, 15x15 cm^2 electron field. Differences are 4.7 %, 0.89 mm, and 0.6 % in the high-dose, low dose-gradient; high-gradient; and low-dose, low dose-gradient regions, respectively.

Table 3.16: Maximum calculated differences between off-axis dose profiles measured using RCF in the third prototype phantom compared to diode measurements acquired in a water phantom for a 20 MeV, 15x15 cm^2 electron field. The sign (+/-) preceding column headers (excluding HDR) indicate position relative to the CAX.

Depth	-DTA [mm]	+DTA [mm]	-LDR [%]	+LDR [%]	HDR [%]
0.5 cm	0.95	0.85	1	0.93	6.56
3.05 cm	0.26	0.9	0.81	0.59	2.23
6.1 cm	1.1	0.86	0.61	0.7	2.48

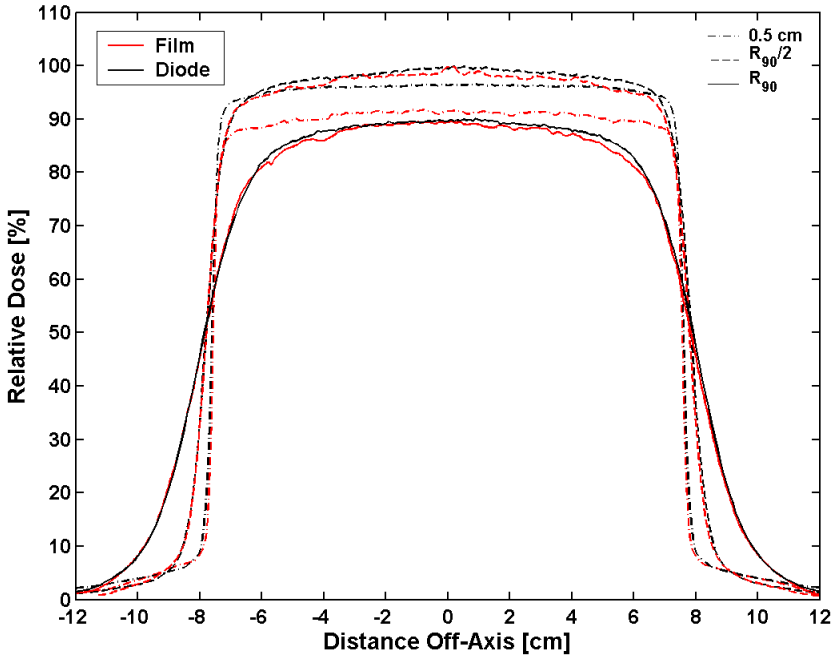

Figure 3.43: Off-axis dose profiles measured using RCF in the third prototype phantom compared to diode measurements for a 20 MeV, 15x15 cm^2 electron field. Depths shown are: 0.5 cm, $R_{90}/2$ = 3.05 cm, R_{90} = 6.1 cm.

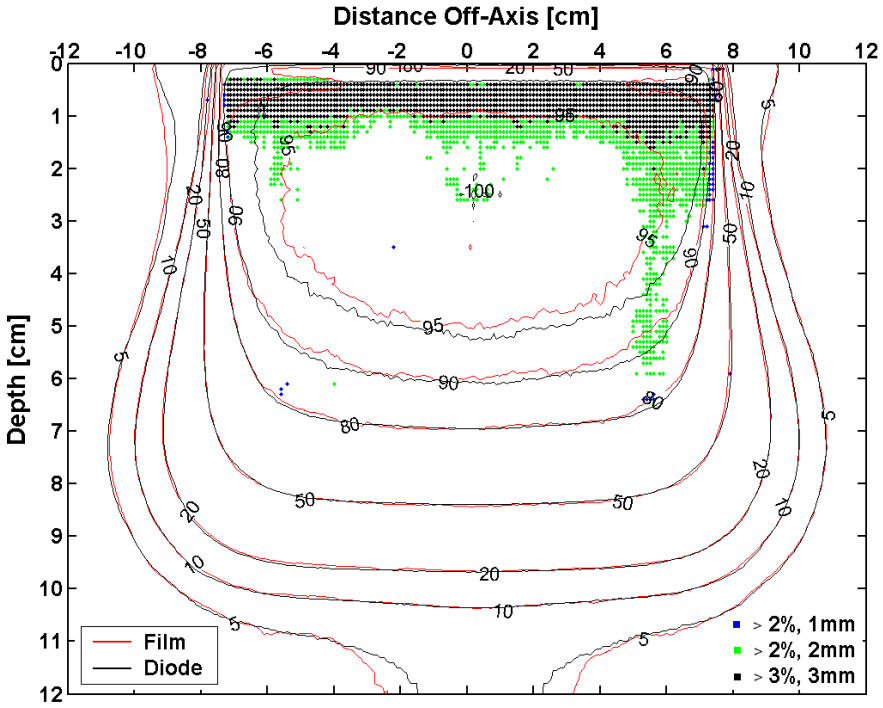

Figure 3.44: 2D dose distributions measured using RCF in the third prototype phantom compared to diode measurements for a 20 MeV, 15x15 cm^2 electron beam.

3.4.2.2 16 MeV, 15x15 cm^2

Differences are seen in the PDD measurements shown in Figure 3.45 where RCF underestimates the diode by up to 3.5%. The measurements are in agreement in the high dose-gradient and low-dose, low dose-gradient regions where the maximum differences are 0.87 mm DTA and 0.3 % relative dose, respectively.

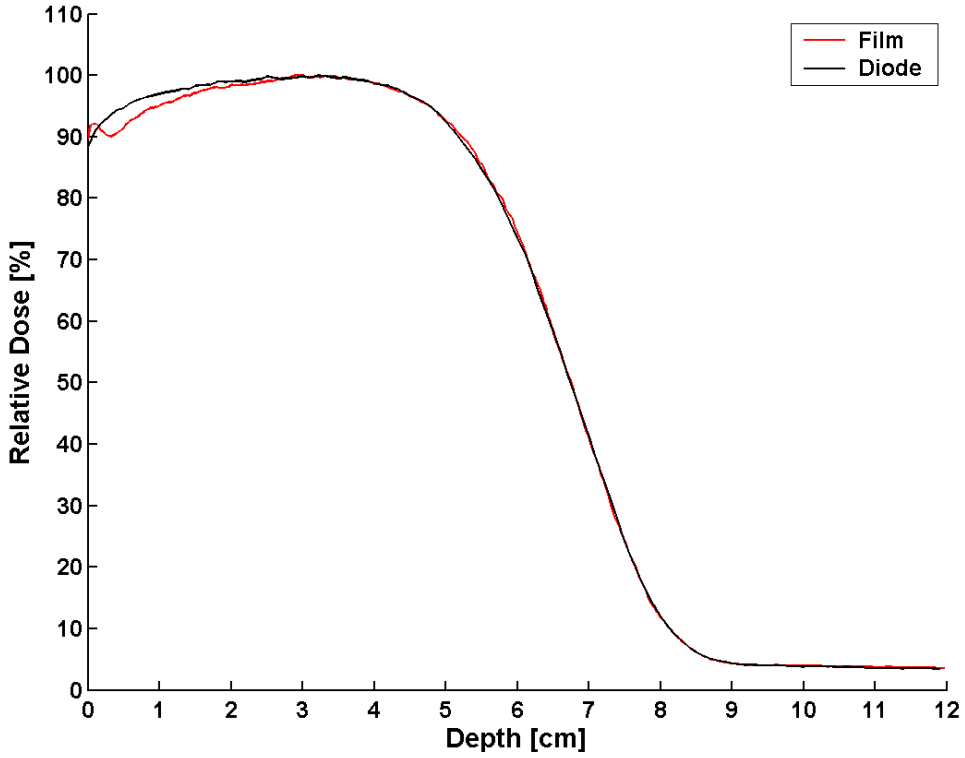

Figure 3.45: PDD measured using RCF in the third prototype phantom compared to diode measurements for a 16 MeV, 15x15 cm^2 electron field. Differences are 3.5 %, 0.87 mm, and 0.3 % in the high-dose, low dose-gradient; high-gradient; and low-dose, low dose-gradient regions, respectively.

Off-axis dose profiles are shown in Figure 3.46, and a summary of the maximum differences in the curve regions of the curve is shown in Table 3.17. RCF measurements are within ± 2 % dose or ± 1 mm DTA for all depths in the high-gradient fall-off and low-gradient, low-dose regions excluding the 5.3 cm depth where the maximum DTA is 1.73 and 1.9 mm for the negative and positive off-axis distances, respectively. In the high-dose region for the 0.5 cm

measurement depth, RCF underestimates diode measurements by up to 4.2 % relative dose. For the 5.3 cm measurement depth, RCF overestimates diode measurements by a maximum of 2.8 % relative dose.

In the 2D dose distributions shown in Figure 3.47, 91.3 % of the film measured data points fall within ± 2 % relative dose, or ± 1 mm DTA. As the agreement criteria is relaxed to ± 2 mm DTA, the percentage of points in agreement is also increased to 91.9 %, and for ± 3 %, ± 3 mm, 96.9 % of the RCF measured data points are in agreement.

Table 3.17: Maximum calculated differences between off-axis dose profiles measured using RCF in the third prototype phantom compared to diode measurements acquired in a water phantom for a 16 MeV, 15x15 cm^2 electron field. The sign (+/-) preceding column headers (excluding HDR) indicate position relative to the CAX.

Depth	-DTA [mm]	+DTA [mm]	-LDR [%]	+LDR [%]	HDR [%]
0.5 cm	0.33	0.2	1.39	0.98	4.15
2.6 cm	0.61	0.22	0.97	0.84	1.87
5.2 cm	1.73	1.9	1.03	0.9	2.83

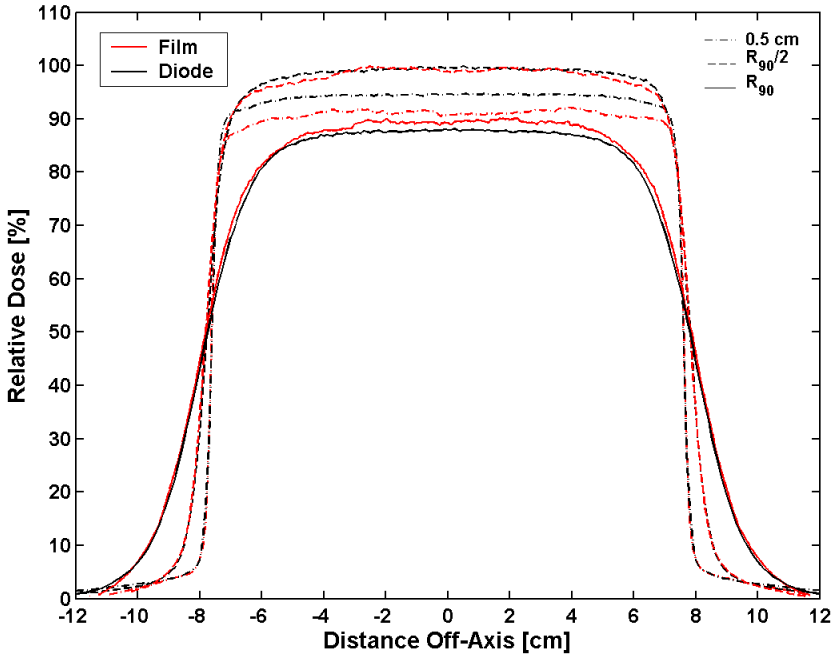

Figure 3.46: Off-axis dose profiles measured using RCF in the third prototype phantom compared to diode measurements for a 16 MeV, 15x15 cm^2 electron field. Depths are: 0.5 cm, $R_{90}/2$ = 2.6 cm, R_{90} = 5.2 cm.

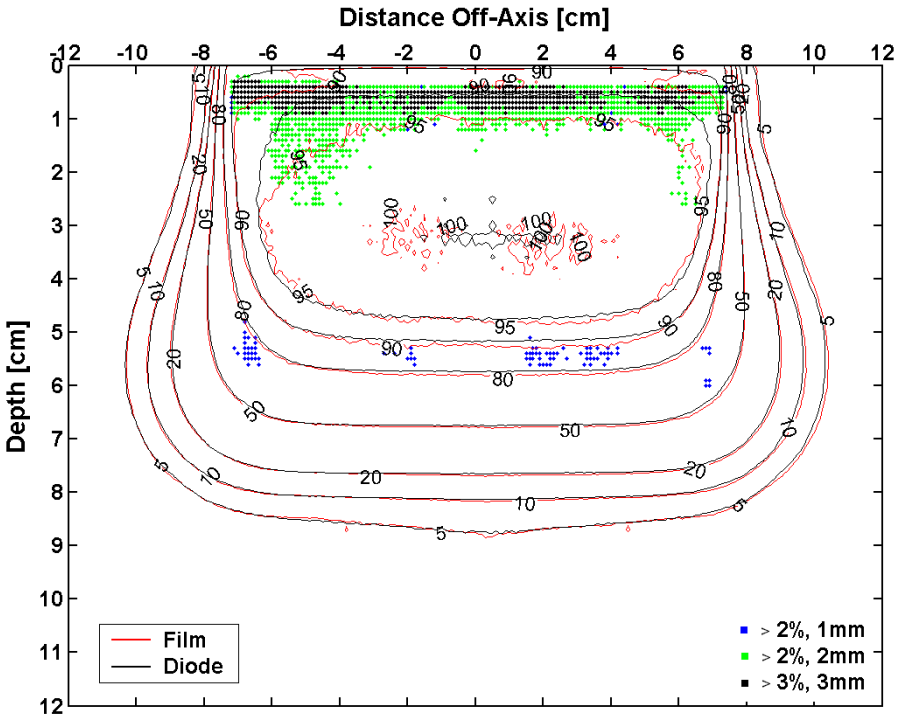

Figure 3.47: 2D dose distributions measured using RCF in the third prototype phantom compared to diode measurements for a 16 MeV, 15x15 cm^2 electron beam.

3.4.2.3 12 MeV, 15x15 cm^2

The RCF measured PDD profile shown in Figure 3.48 underestimates the diode measurement by a maximum of 3.9 % relative dose in the high-dose, low-dose gradient region of the curve. Agreement is within criteria in the high dose-gradient region where the maximum DTA is 0.63 mm, and in the low-dose, low dose-gradient region where relative dose differences are within 0.8 %.

Off-axis dose profile comparisons are shown in Figure 3.49, and the differences calculated for each depth and region of the curve are summarized in Table 3.18. Profiles are within ± 2 % dose or ± 1 mm DTA for all depths in the high-gradient fall-off and low-gradient, low-dose regions excluding the 4.0 cm depth where the maximum DTA is 1.22 and 1.47 mm for the negative and positive off-axis distances, respectively. In the high-dose region at 0.5 cm, film

underestimates diode measurements by up to 4.03 % relative dose. At the 4.0 cm measurement depth, film overestimates diode measurements by a maximum of 2.65 % relative dose.

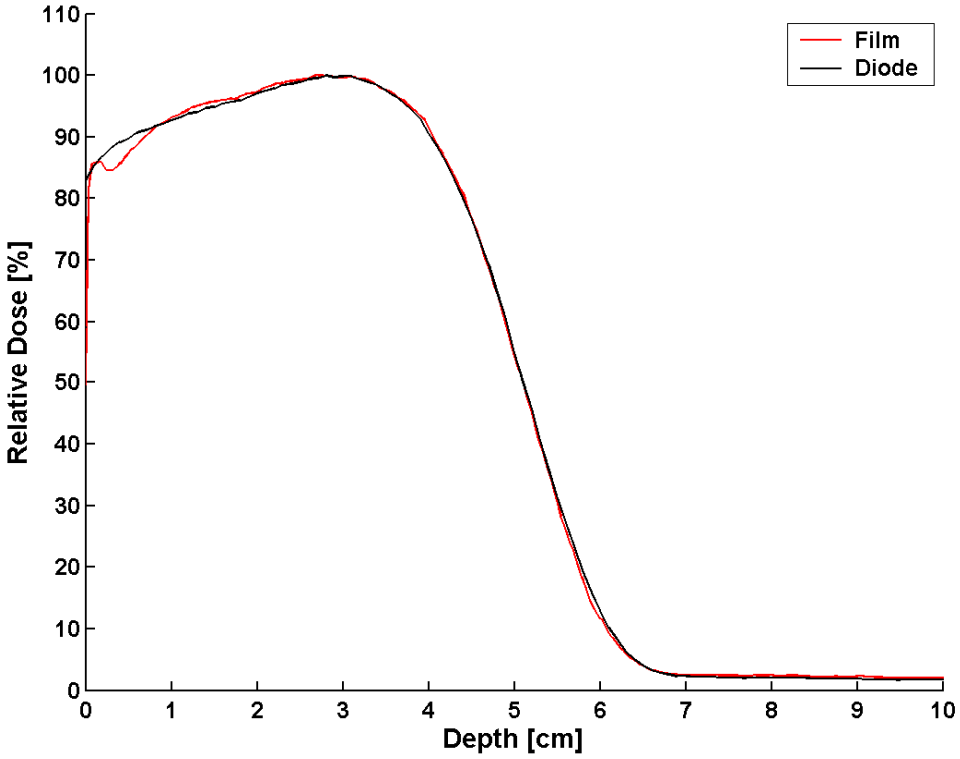

Figure 3.48: PDD measured using RCF in the third prototype phantom compared to diode measurements for a 12 MeV, 15x15 cm^2 electron field. Differences are 3.9 %, 0.63 mm, and 0.8 % in the high-dose, low dose-gradient; high-gradient; and low-dose, low dose-gradient regions, respectively.

Table 3.18: Maximum calculated differences between off-axis dose profiles measured using RCF in the third prototype phantom compared to diode measurements acquired in a water phantom for a 12 MeV, 15x15 cm^2 electron field. The sign (+/-) preceding column headers (excluding HDR) indicate position relative to the CAX.

Depth	-DTA [mm]	+DTA [mm]	-LDR [%]	+LDR [%]	HDR [%]
0.5 cm	0.87	0.52	1.71	0.8	4.03
2.0 cm	0.81	0.2	0.9	0.5	1.84
4.0 cm	1.22	1.17	0.97	0.8	2.65

The 2D dose distributions (c.f. Figure 3.50) show 95.47 % of the film measured data points falling within ± 2 % relative dose, or ± 1 mm DTA. As the agreement criteria is expanded

to ± 2 mm DTA, the percentage of points in agreement is also increased slightly to 96.89 % while 99.63 % of the data points are within ± 3 %, ± 3 mm.

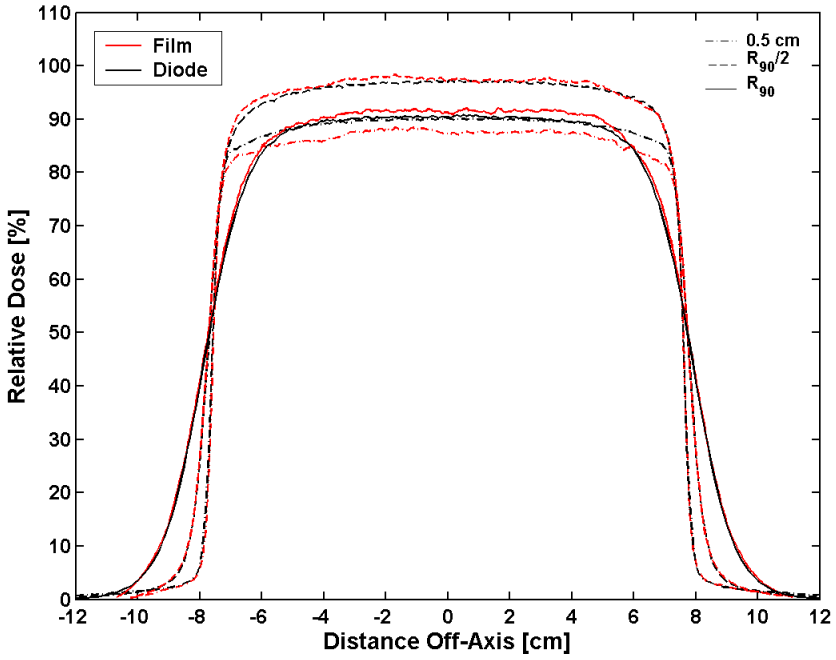

Figure 3.49: Off-axis dose profiles measured using RCF in the third prototype phantom compared to diode measurements for a 12 MeV, 15x15 cm^2 electron field. Depths shown are: 0.5 cm, $R_{90}/2$ = 2.0 cm, R_{90} = 4.0 cm.

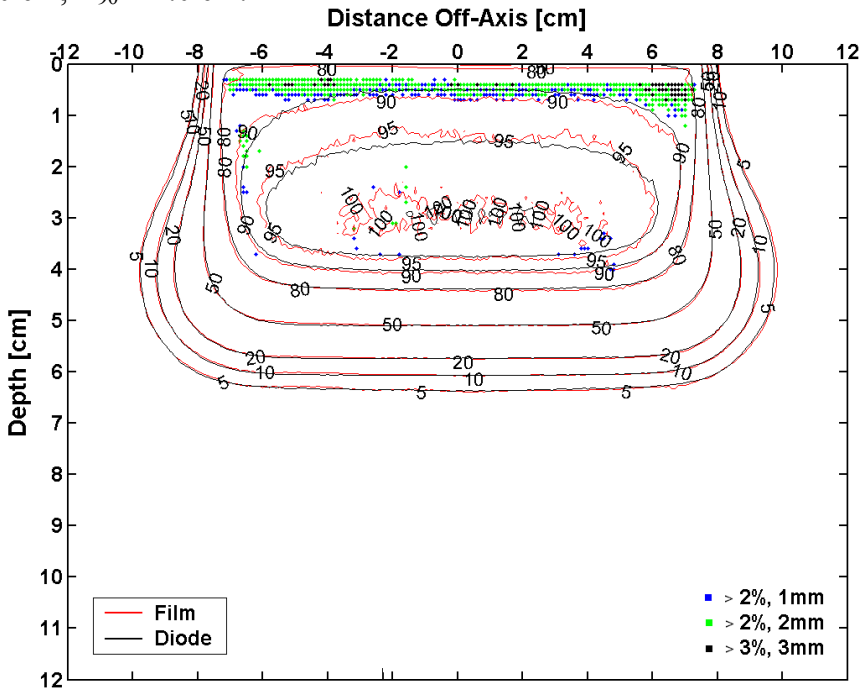

Figure 3.50: 2D dose distributions measured using RCF in the third prototype phantom compared to diode measurements for a 12 MeV, 15x15 cm^2 electron beam.

3.4.2.4 9 MeV, 15x15 cm^2

Measured PDDs agree within criteria in all regions of the curve (c.f. Figure 3.51). The maximum relative dose difference in the high-dose, low dose-gradient region of the PDD is 2.0%. In the high dose-gradient region the DTA is within 0.6 mm and in the low-dose, low dose-gradient region the maximum dose difference is 0.6 %.

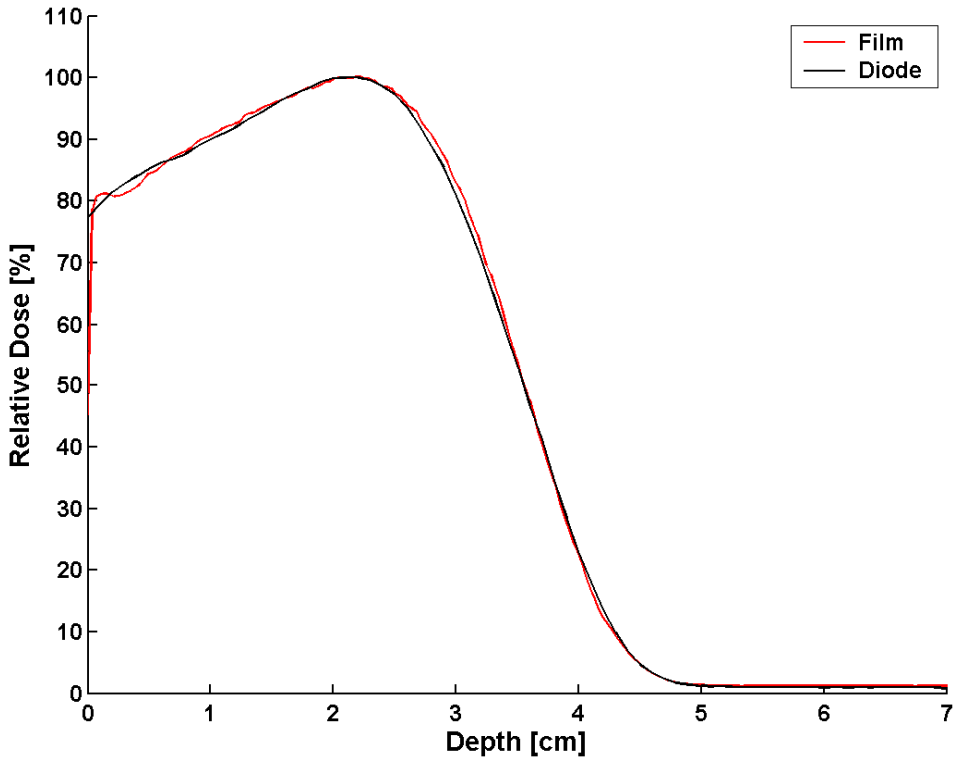

Figure 3.51: PDD measured using RCF in the third prototype phantom compared to diode measurements for a 9 MeV, 15x15 cm^2 electron field. Differences are 2.0 %, 0.60 mm, and 0.6 % in the high-dose, low dose-gradient; high-gradient; and low-dose, low dose-gradient regions, respectively.

Off-axis dose profiles are shown in Figure 3.52 and a summary of the maximum differences for each depth and curve region is presented in Table 3.19. RCF measurements are in agreement with the diode in the high-gradient and low-dose regions of the curve for all depths except the 2.8 cm depth where the film disagrees with diode measurements by 1.05 mm and 1.58

mm DTA for the negative and positive off-axis distances, respectively. Relative dose differences of 2.3 % are seen in the high-dose region of the curve at 0.5 cm as the film measured profile underestimates the diode at the edges of the high-dose region. At the 1.4 cm depth, there is a spike where the film overestimates the diode by 2.5 % at - 2 cm off-axis. Film also overestimates diode measurements by up to 3.7 % at 2.8 cm.

Table 3.19: Maximum calculated differences between off-axis dose profiles measured using RCF in the third prototype phantom compared to diode measurements acquired in a water phantom for a 9 MeV, 15x15 cm^2 electron field. The sign (+/-) preceding column headers (excluding HDR) indicate position relative to the CAX.

Depth	-DTA [mm]	+DTA [mm]	-LDR [%]	+LDR [%]	HDR [%]
0.5 cm	0.31	0.33	0.8	0.89	2.31
1.4 cm	0.46	0.45	1.18	1.34	2.45
2.8 cm	1.05	1.58	0.98	1.95	3.7

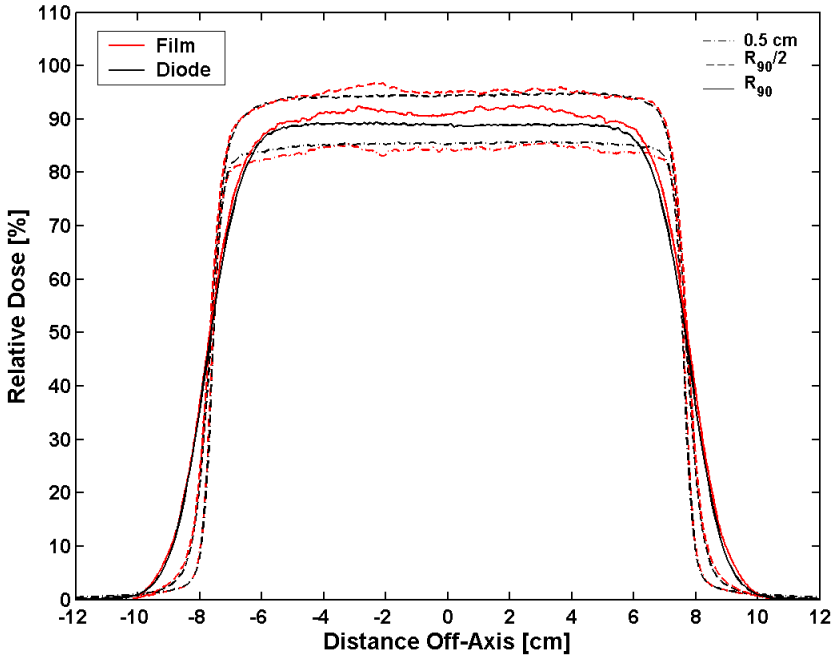

Figure 3.52: Off-axis dose profiles measured using RCF in the third prototype phantom compared to diode measurements for a 9 MeV, 15x15 cm^2 electron field. Depths shown are: 0.5 cm, $R_{90}/2$ = 1.4 cm, R_{90} = 2.8 cm.

As shown in Figure 3.53, 98.3 % of the RCF measured data points fall within the ± 2 %, ± 1 mm agreement criteria. As the criteria is expanded to ± 2 %, ± 2 mm, 99.74 % of the points

are in agreement, and that percentage is increased to 100 % for the ± 3 %, ± 3 mm agreement criteria.

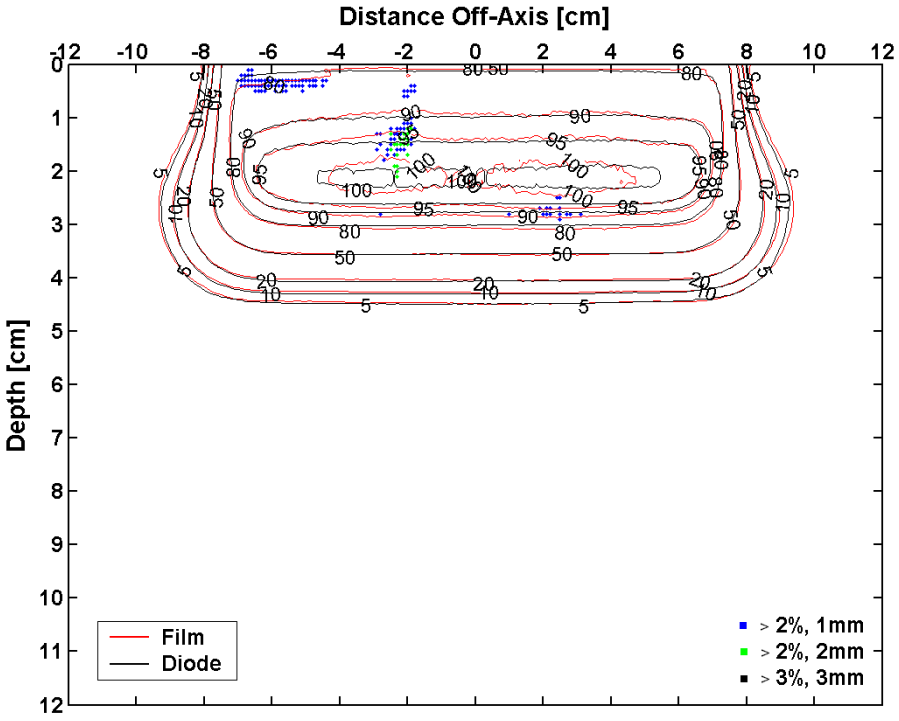

Figure 3.53: 2D dose distributions measured using RCF in the third prototype phantom compared to diode measurements for a 9 MeV, 15x15 cm^2 electron beam.

3.4.2.5 6 MeV, 15x15 cm^2

The RCF measured PDD agrees with diode measurements within criteria in all regions of the curve (c.f. Figure 3.54). The maximum relative dose difference in the high-dose, low dose-gradient region of the PDD is 1.9 %. In the high dose-gradient region the DTA is within 0.15 mm, and in the low-dose, low dose-gradient region the maximum relative dose difference is 0.9 %.

Off-axis dose profiles are shown in Figure 3.55 and a summary of the maximum differences for each depth and curve region is shown in Table 3.20. RCF measurements are in agreement within criteria to diode measurements in the fall-off and low-dose regions for all depths. Relative dose differences of 3.4 % are seen in the high-dose region of the curve at the 0.5

cm depth as the film measured profile underestimates the diode for the positive off-axis distances.

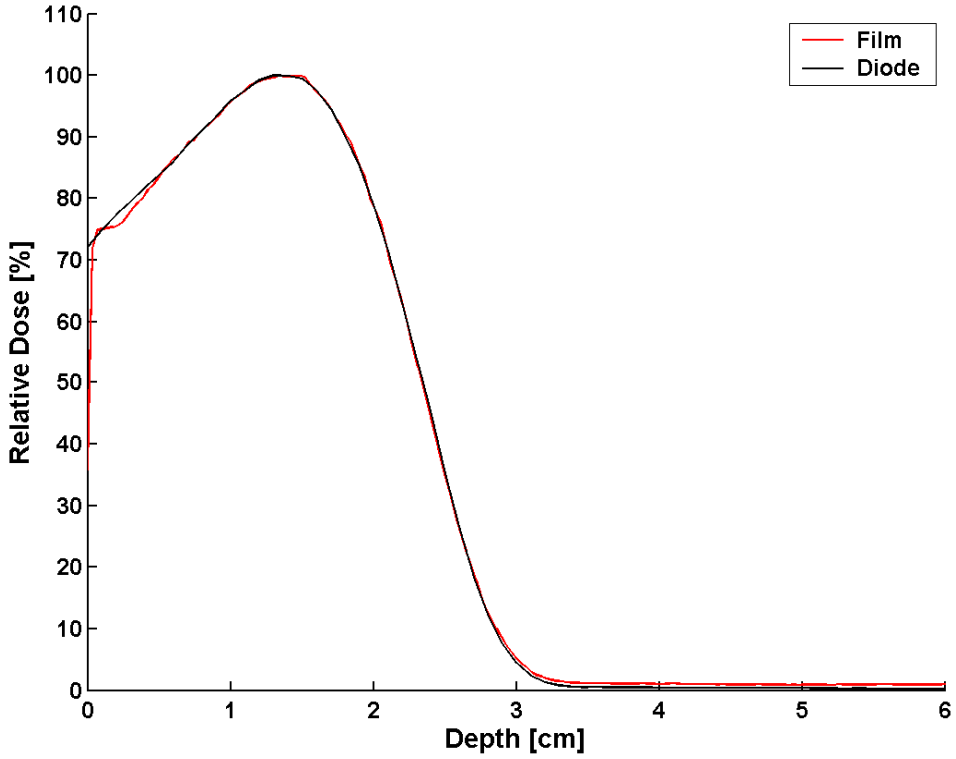

Figure 3.54: PDD measured using RCF in the third prototype phantom compared to diode measurements for a 6 MeV, 15x15 cm^2 electron field. Differences are 1.9 %, 0.15 mm, and 0.9 % in the high-dose, low dose-gradient; high-gradient; and low-dose, low dose-gradient regions, respectively.

Table 3.20: Maximum calculated differences between off-axis dose profiles measured using RCF in the third prototype phantom compared to diode measurements acquired in a water phantom for a 6 MeV, 15x15 cm^2 electron field. The sign (+/-) preceding column headers (excluding HDR) indicate position relative to the CAX.

Depth	-DTA [mm]	+DTA [mm]	-LDR [%]	+LDR [%]	HDR [%]
0.5 cm	0.79	0.51	0.67	1.44	3.39
0.9 cm	0.84	0.5	0.87	1.36	2.02
1.8 cm	0.64	0.95	0.36	2.0	1.96

2D dose distributions (c.f. Figure 3.56) show 97.7 % of the data points falling within the ± 2 %, ± 1 mm agreement criteria. As the criteria is relaxed to ± 2 %, ± 2 mm, 99.76 % of the

points are in agreement and the percentage of in agreement is increased to 100 % for ± 3 %, ± 3 mm.

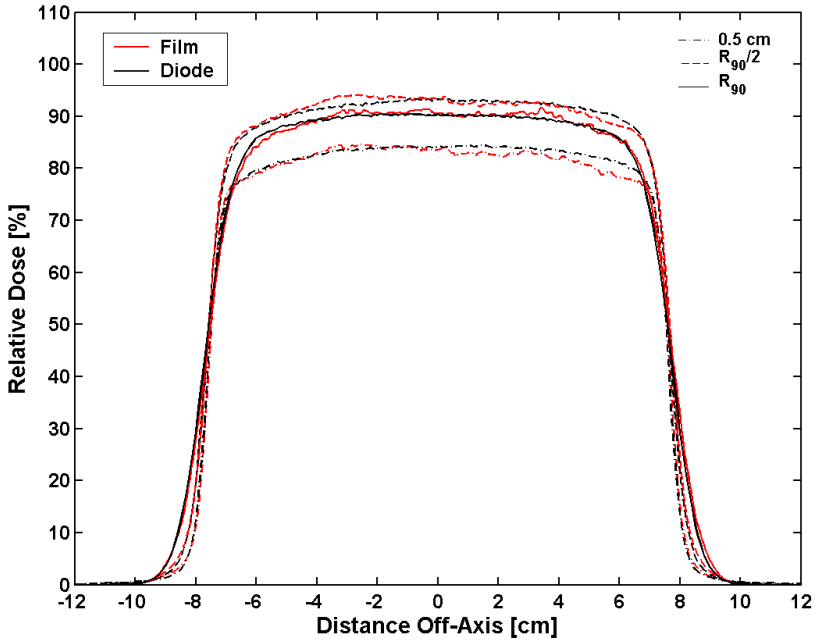

Figure 3.55: Off-axis dose profiles measured using RCF in the third prototype phantom compared to diode measurements for a 6 MeV, 15x15 cm^2 electron field. Depths shown are: 0.5 cm, $R_{90}/2$ = 0.9 cm, R_{90} = 1.8 cm.

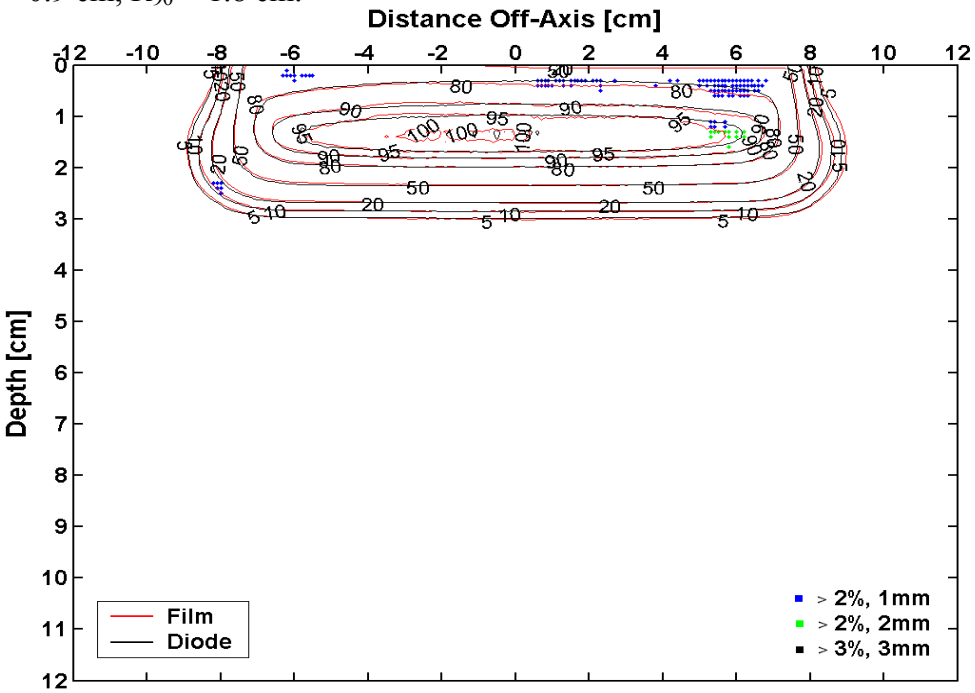

Figure 3.56: 2D dose distributions measured using RCF in the third prototype phantom compared to diode measurements for a 6 MeV, 15x15 cm^2 electron beam.

3.4.2.6 16 MeV, 4x4 cm^2

The film measured PDD shown in Figure 3.57 agrees within criteria to diode measurements in both the high-gradient, and low-dose, low dose-gradient regions of the curve where differences are up to 0.83 mm DTA and 0.7 % relative dose, respectively. In the high-dose, low dose-gradient region of the curve, film underestimates diode measurements by a maximum of 6.1 %.

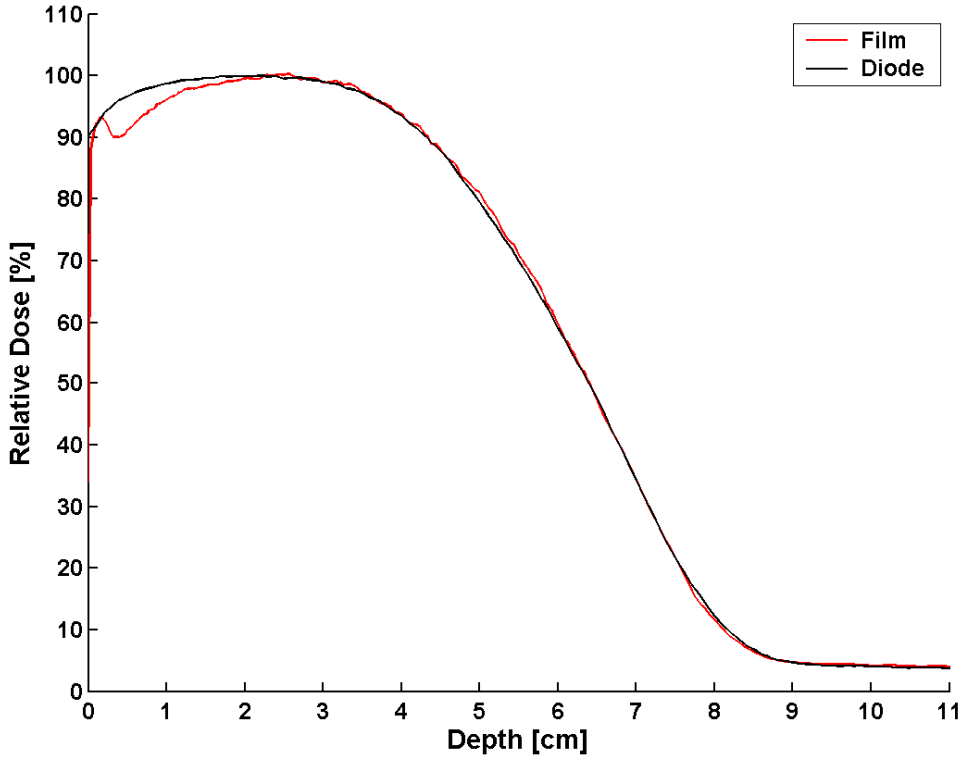

Figure 3.57: PDD measured using RCF in the third prototype phantom compared to diode measurements for a 16 MeV, 4x4 cm^2 electron field. Differences are 6.1 %, 0.83 mm, and 0.7 % in the high-dose, low dose-gradient; high-gradient; and low-dose, low dose-gradient regions, respectively.

Off-axis dose profiles are shown in Figure 3.58, and the maximum differences for each depth and curve region are presented in Table 3.21. Measurements are in agreement for all depths in both the high-gradient and low-dose regions of the curve. In the high-dose region of the

curve, film underestimates diode measurements at the 0.5 and 2.05 cm depths by a maximum of 7.0 % and 3.18 % relative dose, respectively.

2D dose distributions presented in Figure 3.59 show 95.1 % of the film measured data points agreeing with diode measurements within ± 2 % relative dose or ± 1 mm DTA. As the agreement criteria is expanded to ± 2 %, ± 2 mm, the number of points in agreement is slightly increased to 95.3 %. For the ± 3 %, ± 3 mm criteria, 97 % of the film measured data points agree with diode measurements.

Table 3.21: Maximum calculated differences between off-axis dose profiles measured using RCF in the third prototype phantom compared to diode measurements acquired in a water phantom for a 16 MeV, 4x4 cm^2 electron field. The sign (+/-) preceding column headers (excluding HDR) indicate position relative to the CAX.

Depth	-DTA [mm]	+DTA [mm]	-LDR [%]	+LDR [%]	HDR [%]
0.5 cm	0.26	0.62	1.49	1.3	7.0
2.1 cm	0.61	0.51	1.32	1.2	3.18
4.2 cm	0.78	0.57	1.3	1.12	1.5

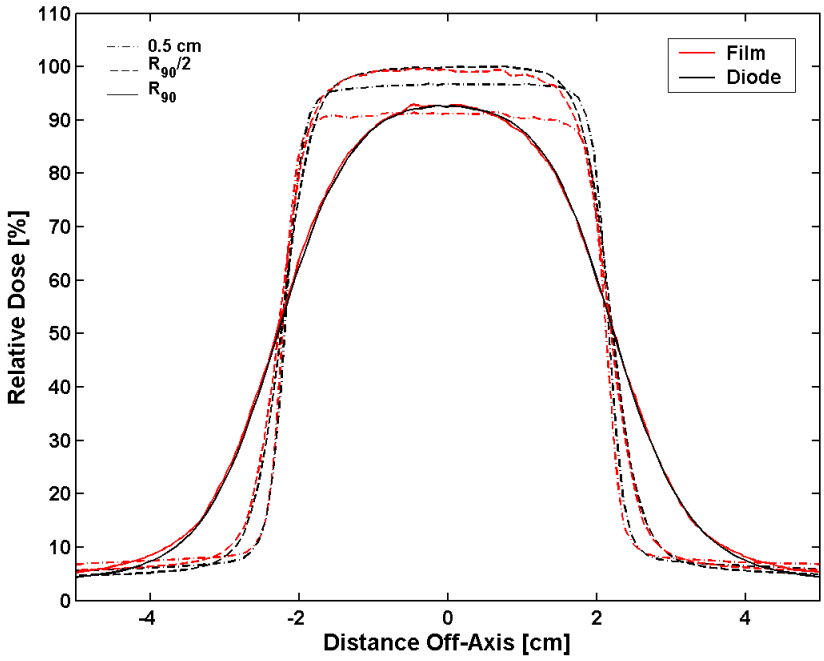

Figure 3.58: Off-axis dose profiles measured using RCF in the third prototype phantom compared to diode measurements for a 16 MeV, 4x4 cm^2 electron field. Depths shown are: 0.5 cm, $R_{90}/2$ = 2.1 cm, R_{90} = 4.2 cm.

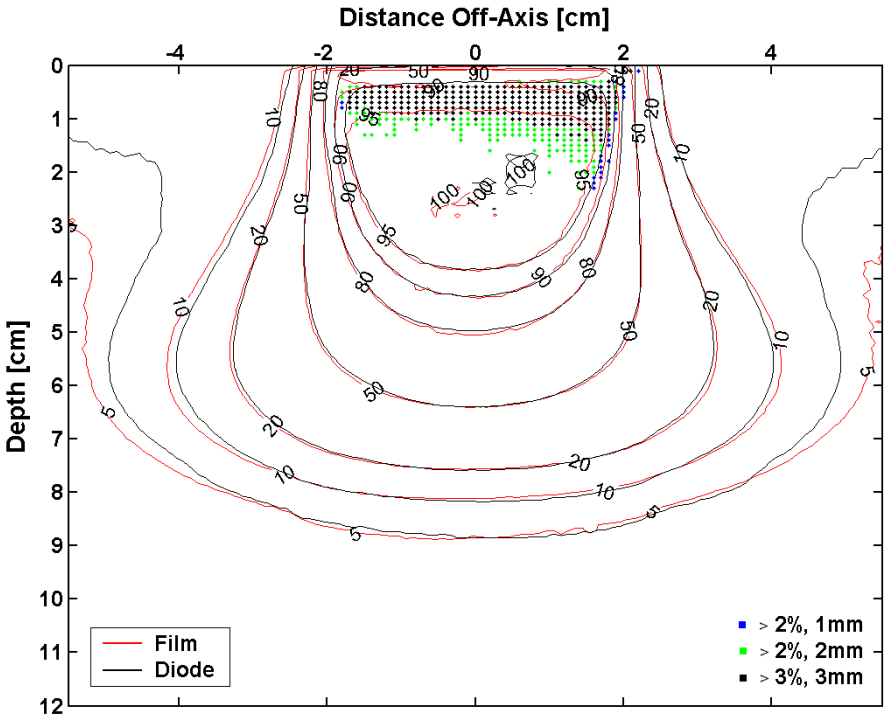

Figure 3.59: 2D dose distributions measured using RCF in the third prototype phantom compared to diode measurements for a 16 MeV, 4x4 cm^2 electron beam.

3.4.2.7 9 MeV, 4x4 cm^2

PDD comparisons are shown in Figure 3.60 and agreement is within criteria in both the high-gradient, and low-dose, low dose-gradient regions of the curve where the maximum differences are 0.65 mm DTA and 1.6 % relative dose, respectively. In the high-dose, low dose-gradient region of the curve, film underestimates diode measurements by as much as 3.6 %.

Off-axis dose profiles are shown in Figure 3.61, and a summary of the maximum differences for each depth and curve region is presented in Table 3.22. Film measurements are in agreement for all depths in both the high-gradient and low-dose regions of the curve. In the high-dose region of the curve, film underestimates diode measurements at 0.5 cm by a maximum of 2.77 % relative dose.

2D dose distributions presented in Figure 3.62 show 95.3 % of the film measured data points agreeing with diode measurements within ± 2 % relative dose or ± 1 mm DTA. As the

agreement criteria is expanded to ± 2 %, ± 2 mm, the number of points in agreement is slightly increased to 97.8 %. For the ± 3 %, ± 3 mm criteria, 100 % of the film measured data points agree with diode measurements.

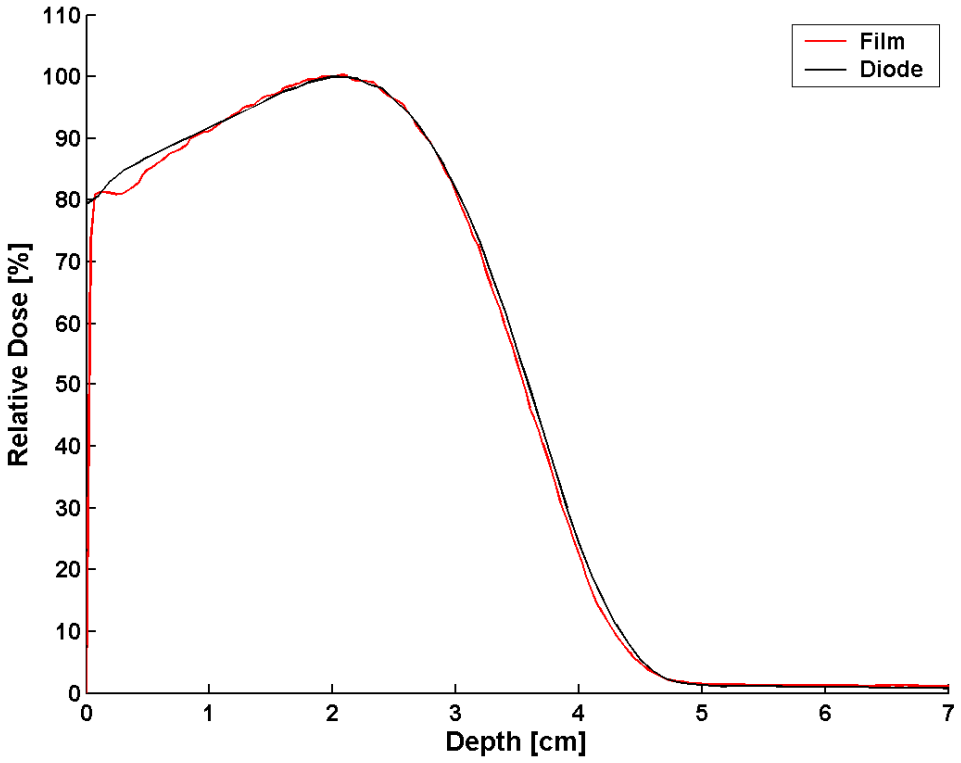

Figure 3.60: PDD measured using RCF in the third prototype phantom compared to diode measurements for a 9 MeV, 4x4 cm^2 electron field. Differences are 3.6 %, 0.65 mm, and 1.6 % in the high-dose, low dose-gradient; high-gradient; and low-dose, low dose-gradient regions, respectively.

Table 3.22: Maximum calculated differences between off-axis dose profiles measured using RCF in the third prototype phantom compared to diode measurements acquired in a water phantom for a 9 MeV, 4x4 cm^2 electron field. The sign (+/-) preceding column headers (excluding HDR) indicate position relative to the CAX.

Depth	-DTA [mm]	+DTA [mm]	-LDR [%]	+LDR [%]	HDR [%]
0.5 cm	0.23	0.67	1.2	1.45	2.77
1.35 cm	0.35	0.48	1.36	1.48	1.88
2.7 cm	0.67	0.95	1.32	1.44	1.29

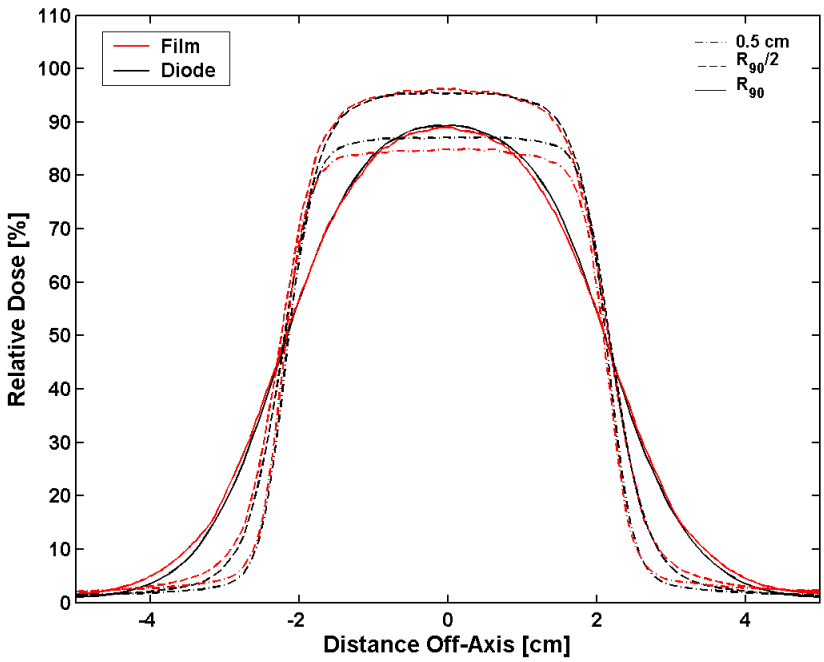

Figure 3.61: Off-axis dose profiles measured using RCF in the third prototype phantom compared to diode measurements for a 9 MeV, 4x4 cm^2 electron field. Depths shown are: 0.5 cm, $R_{90}/2$ = 1.35 cm, R_{90} = 2.7 cm.

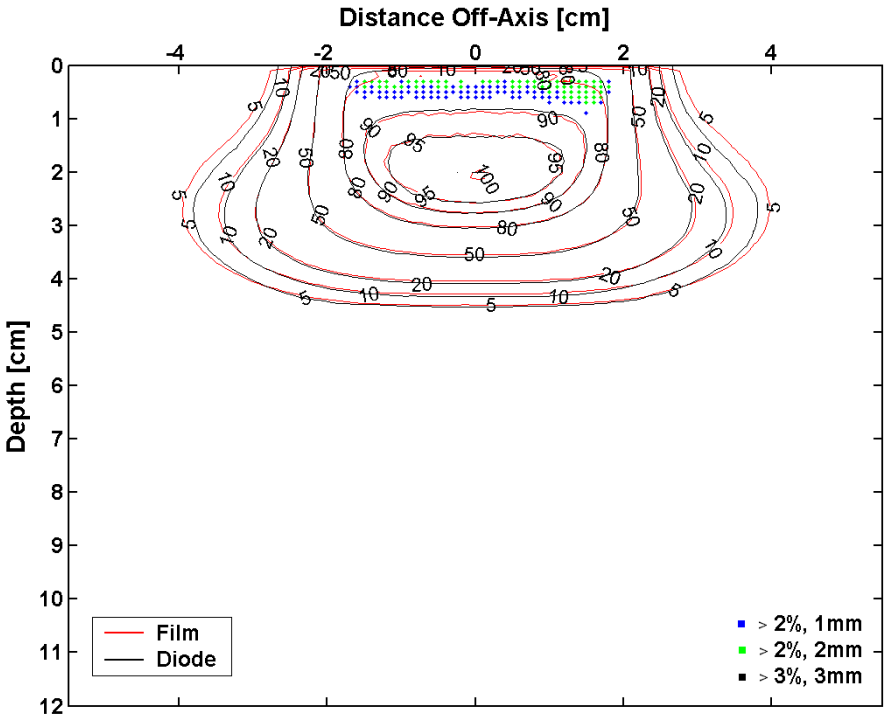

Figure 3.62: 2D dose distributions measured using RCF in the third prototype phantom compared to diode measurements for a 9 MeV, 4x4 cm^2 electron beam.

3.4.2.8 16 MeV, 2x2 cm2

The film measured PDD shown in Figure 3.63 disagrees with diode measurements in both the high-dose, low dose-gradient, and high dose-gradient regions of the curve where the maximum differences are 5.8 % relative dose and 1.6 mm DTA, respectively. In the low-dose, low dose-gradient region of the curve, film is within criteria and relative dose differences are do not exceed 0.5 %.

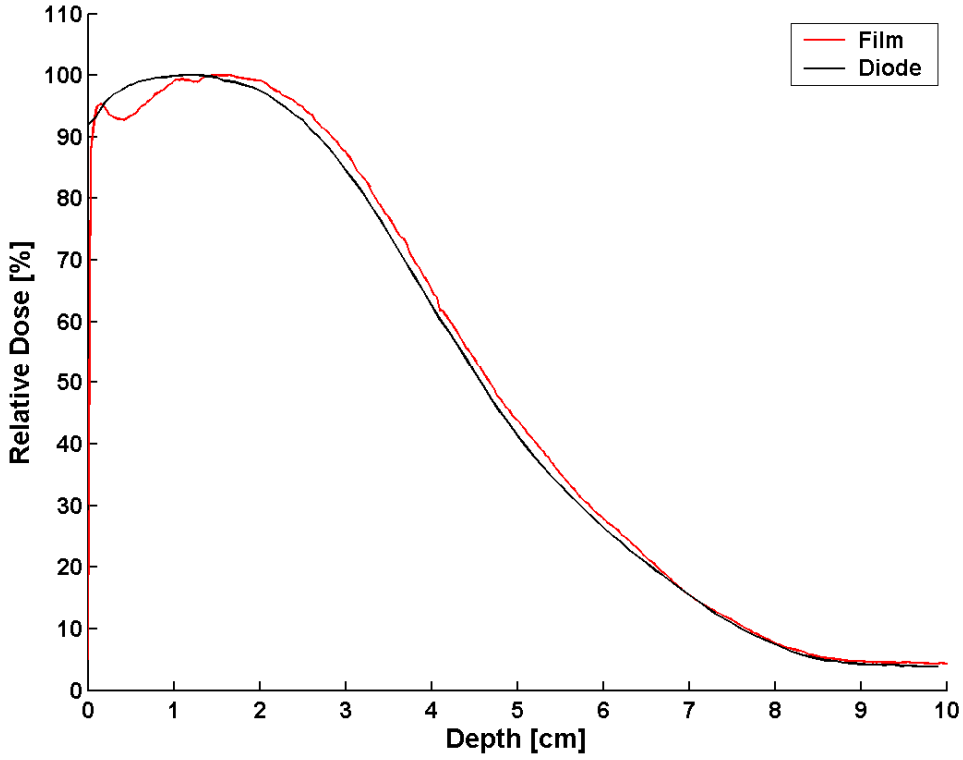

Figure 3.63: PDD measured using RCF in the third prototype phantom compared to diode measurements for a 16 MeV, 2x2 cm^2 electron field. Differences are 5.8 %, 1.60 mm, and 0.5 % in the high-dose, low dose-gradient; high-gradient; and low-dose, low dose-gradient regions, respectively.

Off-axis dose profiles are shown in Figure 3.64, and a summary of the maximum calculated differences for each depth and curve region is presented in Table 3.23. Film measurements are in agreement for all depths in both the high-gradient and low-dose regions of

the curve. In the high-dose region of the curve, film underestimates diode measurements for the 0.5 and 2.7 cm depths by a maximum of 6.02 % and 3.02 % relative dose, respectively.

In the resulting 2D dose distributions shown in Figure 3.65, 95.7 % of the film measured data points agree with diode measurements within ± 2 % relative dose or ± 1 mm DTA. As the agreement criteria is relaxed to ± 2 %, ± 2 mm, the percentage of points in agreement is increased to 98.3 %. For the ± 3 %, ± 3 mm criteria, 98.7 % of the film measured data points agree with diode measurements.

Table 3.23: Maximum calculated differences between off-axis dose profiles measured using RCF in the third prototype phantom compared to diode measurements acquired in a water phantom for a 16 MeV, 2x2 cm^2 electron field. The sign (+/-) preceding column headers (excluding HDR) indicate position relative to the CAX.

Depth	-DTA [mm]	+DTA [mm]	-LDR [%]	+LDR [%]	HDR [%]
0.5 cm	0.19	0.59	1.43	1.32	6.02
1.35 cm	0.28	0.45	1.57	1.36	1.94
2.7 cm	0.72	0.5	1.58	1.39	3.02

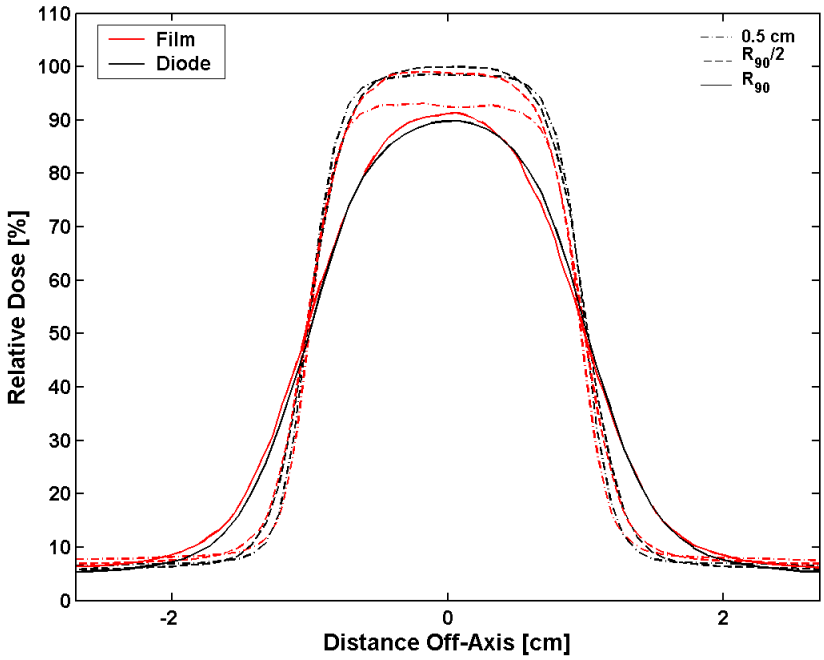

Figure 3.64: Off-axis dose profiles measured using RCF in the third prototype phantom compared to diode measurements for a 16 MeV, 2x2 cm^2 electron field. Depths shown are: 0.5 cm, $R_{90}/2$ = 1.35 cm, R_{90} = 2.7 cm.

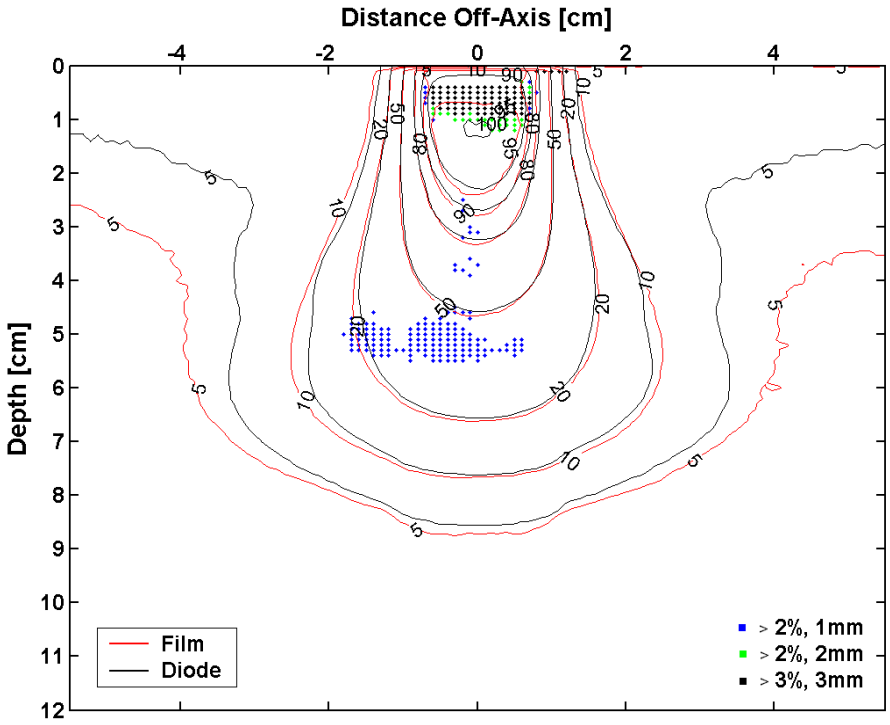

Figure 3.65: 2D dose distributions measured using RCF in the third prototype phantom compared to diode measurements for a 16 MeV, 2x2 cm^2 electron beam.

3.4.2.9 9 MeV, 2x2 cm2

PDD measurements shown in Figure 3.66 are in agreement in both the high dose-gradient, and low-dose, low dose-gradient regions of the curve where differences are up to 0.6 mm DTA and 1.0 % relative dose, respectively. In the low-dose, low dose-gradient region of the curve, film underestimates diode measurements by a maximum of 4.9 %.

Off-axis dose profiles are shown in Figure 3.67, and a summary of the maximum calculated differences for each depth and curve region is presented in Table 3.24. Film measurements are in agreement for all depths in the high-gradient region of the curve. In the low-dose region, film overestimates diode measurements for both the 0.5 and 0.9 cm depths by 2.03 % and 2.07 % relative dose, respectively. In the high-dose region of the curve, film underestimates diode measurements at 0.5 cm by a maximum of 4.43 %.

2D dose distributions presented in Figure 3.68 show 93.4 % of the film measured data points agreeing with diode measurements within ± 2 % relative dose or ± 1 mm DTA. As the agreement criteria is expanded to ± 2 %, ± 2 mm, the percentage of RCF measured data points in agreement to diode measurements is slightly increased to 97.2 %. For the ± 3 %, ± 3 mm criteria, 99.7 % of the film measured data points agree with diode measurements.

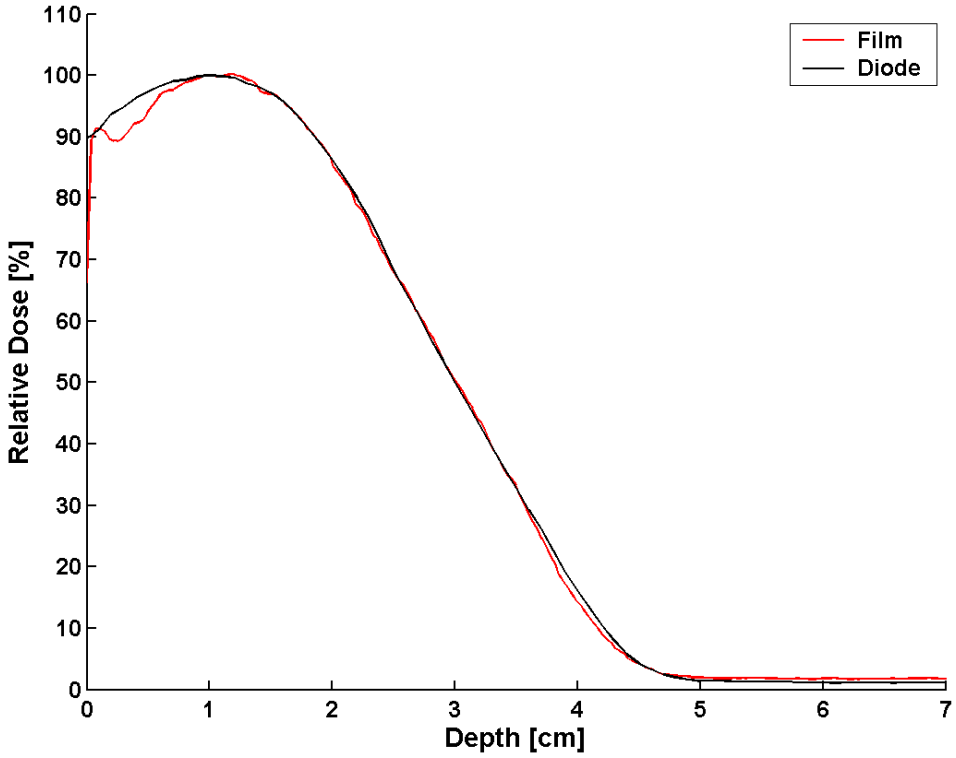

Figure 3.66: PDD measured using RCF in the third prototype phantom compared to diode measurements for a 9 MeV, 2x2 cm^2 electron field. Differences are 4.9 %, 0.60 mm, and 1.0 % in the high-dose, low dose-gradient; high-gradient; and low-dose, low dose-gradient regions, respectively.

Table 3.24: Maximum calculated differences between off-axis dose profiles measured using RCF in the third prototype phantom compared to diode measurements acquired in a water phantom for a 9 MeV, 2x2 cm^2 electron field. The sign (+/-) preceding column headers (excluding HDR) indicate position relative to the CAX.

Depth	-DTA [mm]	+DTA [mm]	-LDR [%]	+LDR [%]	HDR [%]
0.5 cm	0.45	0.51	1.06	2.03	4.43
0.95 cm	0.23	0.19	0.99	2.07	1.8
1.9 cm	0.61	0.74	1.19	1.86	1

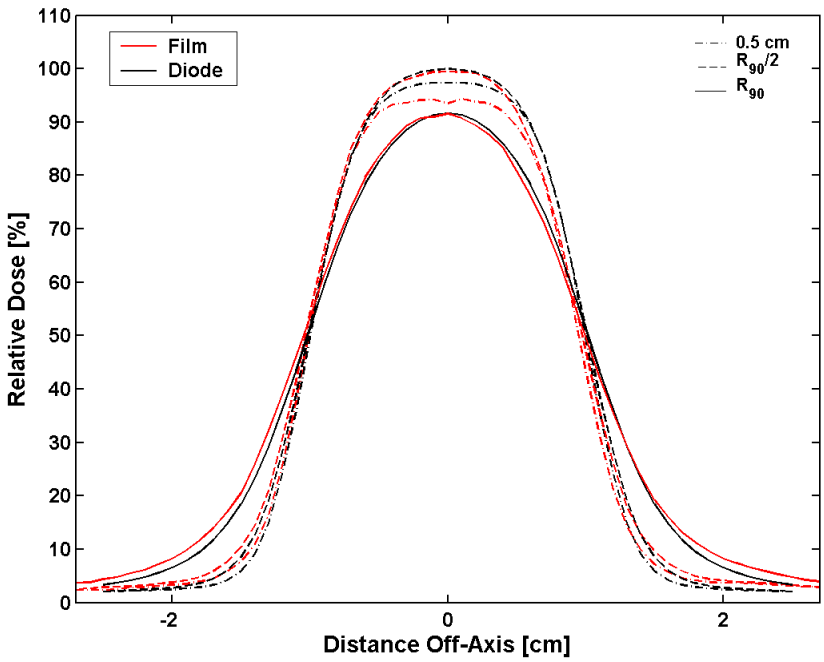

Figure 3.67: Off-axis dose profiles measured using RCF in the third prototype phantom compared to diode measurements for a 9 MeV, 2x2 cm^2 electron field. Depths shown are: 0.5 cm, $R_{90}/2$ = 0.95 cm, R_{90} = 1.9 cm.

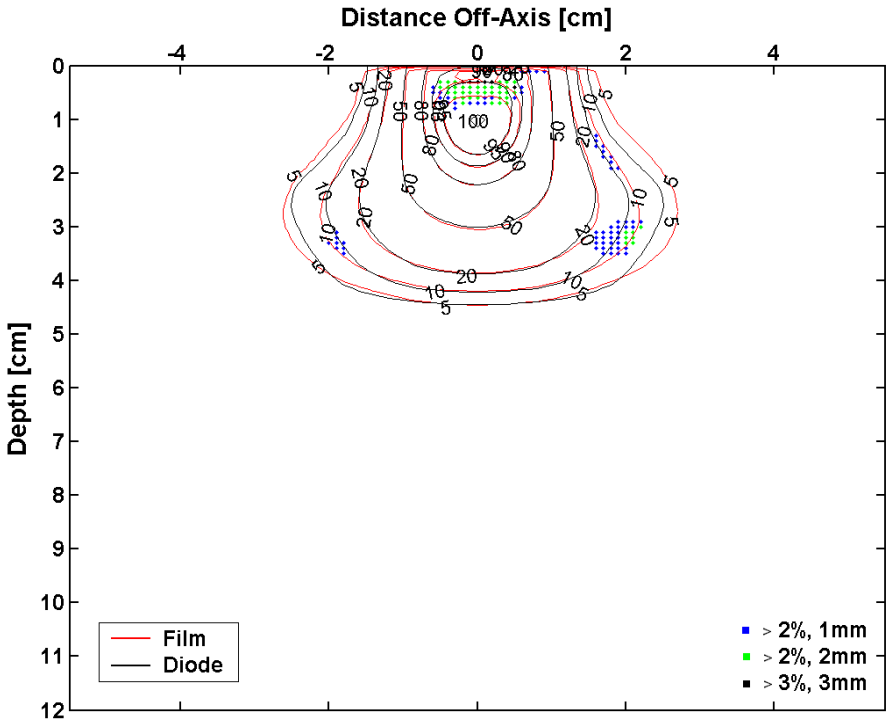

Figure 3.68: 2D dose distributions measured using RCF in the third prototype phantom compared to diode measurements for a 9 MeV, 2x2 cm^2 electron beam.

3.5 Summary of Results

3.5.1 Radiographic Film

3.5.1.1 Central-Axis, Percent Depth-Dose Profiles

All PDDs measured using RGF were in agreement within criteria in all regions of the curve except for the 16 MeV, 2x2 cm^2 electron field where film measurements overestimate diode measurements in the high-gradient region by a maximum of 2 mm DTA. A summary of the differences between RGF and diode measurements for all fields measured the three curve regions is shown in Table 3.25. The difference seen in the 16 MeV, 2x2 cm^2 field is possibly due to the RGF over responding to low energy electrons scattered off of the Cerrobend cut-out used to define the field size. Errors made by the author could have contributed to this disagreement as well.

Table 3.25: Summary of maximum differences between RGF and diode measurements in the three regions of the curve.

Energy [MeV]	Field Size [cm^2]	D>90%	90%>D>10%	D<10%
6	15x15	1.9 %	0.43 mm	1.4 %
9	15x15	1.6 %	0.28 mm	1.4 %
12	15x15	1.3 %	0.33 mm	0.8 %
16	15x15	1.7 %	0.44 mm	0.4 %
20	15x15	1.3 %	0.82 mm	0.3 %
9	4x4	1.6 %	0.60 mm	1.6 %
16	4x4	1.3 %	0.74 mm	0.9 %
9	2x2	1.4 %	0.68 mm	1.4 %
16	2x2	1.8 %	2.00 mm	1.1 %

3.5.1.2 2D Dose Distributions

At least 98 % of RGF measured data points acquired in the third prototype phantom using the 15x15 cm^2 field size were in agreement within criteria to diode measurements for all energies. A summary of the percentage of points in agreement for each field measured is presented in Table 3.26. Major differences are seen for 9, 12, and 16 MeV at the 90 % and 95 %

isodose contours for off-axis distances between -6 to -8 where film measurements overestimate diode measurements by ≈ 2 – 3 %. These differences are possibly due to a change in the symmetry of the electron field produced by the linear accelerator between film and diode measurements as they were acquired on dates more that one month apart. However, these differences do not exceed ± 3 % relative dose or ± 3 mm DTA as 100 % of the RGF data points for all energies (15x15 cm^2) agree within criteria to diode measurements.

For the 4x4 cm^2 and 2x2 cm^2 field sizes, film measurements consistently overestimate diode measurements for both 9 and 16 MeV in the low-dose region off-axis by over 3 %. This discrepancy is likely due to the XV film over responding to low energy x-ray's that are scattered through the Cerrobend cut-outs used to define the field size. These x-ray's are attenuated by the Cerrobend cut-outs which are not as thick as the collimating jaws used to define the field size for the 15x15 cm^2 field. Also, errors in the low dose region of the calibration curves may have attributed to these discrepancies. The dose differences between RGF and diode measurements are larger for the 2x2 cm^2 field for both 9 and 16 MeV.

Table 3.26: Percentage of points passing the specified agreement criteria for all RGF fields measured.

Energy [MeV]	**Field Size [cm^2]**	**< 2%, 1mm**	**< 2%, 2mm**	**< 3%, 3mm**
6	15x15	99.0 %	99.7 %	100.0 %
9	15x15	99.1 %	99.7 %	100.0 %
12	15x15	98.1 %	98.2 %	100.0 %
16	15x15	99.1 %	99.3 %	100.0 %
20	15x15	99.8 %	99.9 %	100.0 %
9	4x4	92.4 %	98.5 %	99.8 %
16	4x4	88.6 %	94.4 %	99.5 %
9	2x2	78.5 %	90.4 %	98.4 %
16	2x2	73.8 %	84.8 %	97.9 %

3.5.2 Radiochromic Film

3.5.2.1 Central-Axis, Percent Depth-Dose Profile

All RCF measured PDDs underestimate diode measurements in the high-dose, low dose-gradient region of the curve. A table summarizing the agreement for the three regions of the PDD is presented in Table 3.27.

Table 3.27: Summary of maximum differences between RCF and diode measurements for the three regions of the curve.

Energy [MeV]	Field Size [cm^2]	D>90%	90%>D>10%	D<10%
6	15x15	1.9 %	0.15 mm	0.9 %
9	15x15	2.0 %	0.60 mm	0.6 %
12	15x15	3.9 %	0.63 mm	0.8 %
16	15x15	3.5 %	0.87 mm	0.3 %
20	15x15	4.7 %	0.89 mm	0.6 %
9	4x4	3.6 %	0.65 mm	1.6 %
16	4x4	6.1 %	0.83 mm	0.7 %
9	2x2	4.9 %	0.60 mm	1.0 %
16	2x2	5.8 %	1.60 mm	0.5 %

This discrepancy is believed to be due in part to misalignment of the film edge at the phantom surface. Alignment of RCFs was more difficult than for RGF's as the adjustable cam onto which the RCF spacer was seated created a pivot point which allowed the film to rotate since the films width is smaller than the dimensions of the film cassette recess. Also, RCF is not cut perfectly straight at the film edge by the manufacturer. Often the film edge was curved making it impossible to align the entire film edge. These alignment difficulties contributed to as much as a 6.1 % relative dose difference in the high-dose, low dose-gradient region for the 16 MeV, 4x4 cm^2 field.

The PDDs for all fields measured agreed with diode measurements in the high-gradient and low-dose, low dose-gradient regions of the PDD except for the 16 MeV, 2x2 cm^2 field where the film measurement overestimated the diode by 1.6 mm DTA. Since this overestimation of

dose is also observed for equivalent RGF measurements, error in the diode measurement was suspected. To test this theory, the diode PDD was compared to an equivalent PDD in the MBPCC beam commissioning database. The agreement at R_{50} between the two measurements was within 0.05 mm suggesting that the diode measurement acquired in this study is accurate. Therefore, this difference may likely be attributed to measurement error by the author.

3.5.2.2 2D Dose Distributions

Major differences seen between RCF and diode measurements in the 2D dose distributions are due to differences in the PDDs. For all fields measured, at least 90 % of the RCF data points agree within criteria when compared to diode measurements. A summary of the percentage of measured data points in agreement is presented in Table 3.28.

Table 3.28: Percentage of points passing the specified agreement criteria for all RCF fields measured.

Energy [MeV]	Field Size [cm^2]	< 2%, 1mm	< 2%, 2mm	< 3%, 3mm
6	15x15	97.7 %	99.8 %	100.0 %
9	15x15	98.3 %	99.7 %	100.0 %
12	15x15	95.5 %	96.9 %	99.6 %
16	15x15	91.3 %	91.9 %	96.9 %
20	15x15	90.1 %	90.3 %	95.0 %
9	4x4	95.3 %	97.8 %	100.0 %
16	4x4	95.1 %	95.3 %	97.0 %
9	2x2	93.4 %	97.2 %	99.7 %
16	2x2	95.7 %	98.3 %	98.7 %

The best agreement was seen for the 9 MeV, 15x15 cm^2 field where 98.3 % of the data points met agreement criteria. This is due to agreement of the RCF and diode measured PDD in the high-dose, low dose-gradient region of the curve. The 6 MeV, 15x15 cm^2 field also showed comparable agreement in this region and the results for the 2D dose distribution were similar (97.7 % of points within criteria). The 20 MeV, 15x15 cm^2 field resulted in the worst agreement with only 90.1 % of the RCF measured data points agreeing with diode measurements within

criteria. This is due to the underestimation of dose at the film surface extending the deepest for this field. Slight differences are seen off-axis for all energies, but do not exceed ± 3 % relative dose or ± 3 mm DTA. These differences may be due to an inconsistent response of the scanner used in the digitization of the films.

3.5.2.3 Investigation of Surface Dose Discrepancy for RCF Measurements

It was postulated that in addition to alignment errors of the film edge at the phantom surface, the dose differences may also be due to artifacts incumbent of the RCF at the film's edge, or due to unknown depth-dependencies exhibited by the RCF. To investigate the effect seen at the RCF edge, two tests were carried out. The first test investigated the possibility of an artifact introduced at the RCF edge due to manufacturing processes. To test this theory, a 2-cm thick slab of Plastic Water was placed on top of the third prototype phantom, set to 100-cm SSD, and irradiated by a 16 MeV, 15x15 cm^2 electron beam. The film was allowed to develop, and the PDD was plotted with the surface of the film placed at 2-cm depth. The resulting PDD measurement compared to the normal irradiation for a 16 MeV, 15x15 cm^2 electron field in the third prototype phantom is shown in Figure 3.69. At the surface of the film irradiated with the build-up placed atop the phantom, the artifact is not seen as in the normally irradiated film, and the measurement does not underestimate the relative dose. This result rules out the idea that an effect may be present at the RCF edge.

For the second test, the depth-dependency of RCF was examined by irradiating cut pieces of RCF perpendicular to the electron beam (16 MeV, 15x15 cm^2) at depths of 0, 0.5, 1.0, 1.5, 2.0, 2.5, 3, and 5.5 cm. The exposed films were allowed to develop and were digitized and calibrated according to Sections (2.4.2 and 2.4.4). The calibrated dose values were then normalized to the dose value measured at 3 cm and the resulting relative dose values were to the edge-on irradiated PDD (c.f. Figure 3.70). The shapes of the PDD measured by the perpendicular

and edge-on irradiated films are the same. The perpendicular irradiations also underestimate the true value of the PDD within the first several cm. This result suggests a depth-dependency inherent in the RCF film.

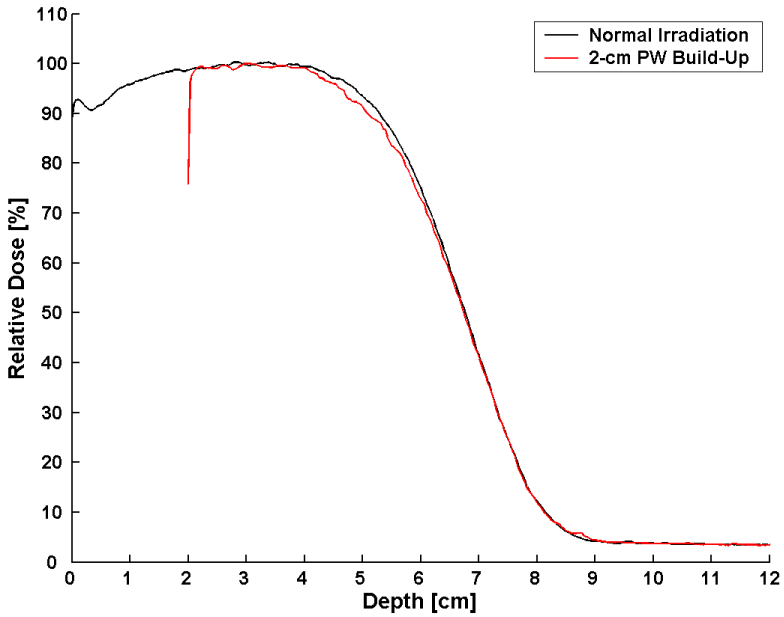

Figure 3.69: RCF irradiated with 2-cm of Solid Water build-up placed on top of the third prototype film phantom (16 MeV, 15x15-cm^2, 100-cm SSD).

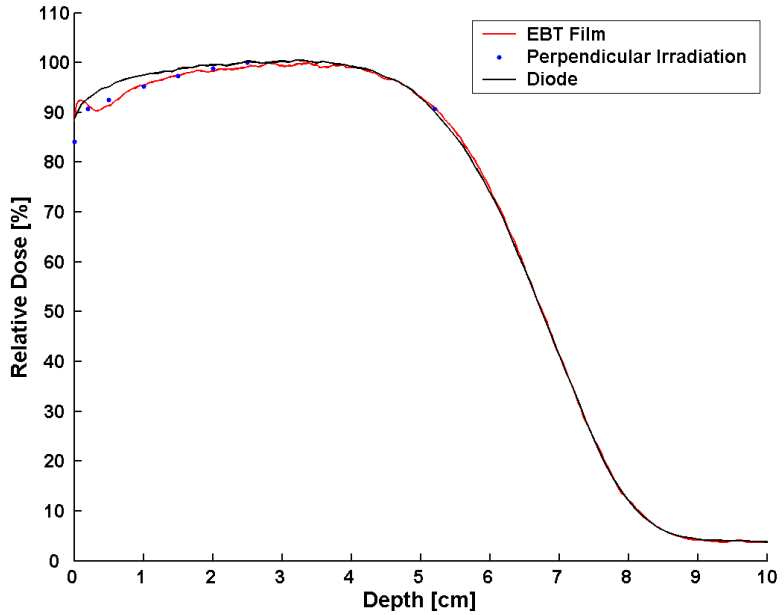

Figure 3.70: Perpendicular dose measurements acquired using RCF at 0.5-cm depth increments between 0 – 3 cm and one at 5.5 cm compared to RCF irradiated edge-on in the third prototype phantom (16 MeV, 15x15-cm^2).

Chapter. 4 Conclusions and Recommendations

4.1 Conclusions

The results of this research did not support the hypothesis that a clinically practical solid water-equivalent electron beam dosimetry film phantom can be created that produces relative dose measurements, using both radiographic and radiochromic films, that are in agreement within ± 2 % relative dose, or ± 1 mm DTA to equivalent measurements acquired using a scanning diode in a water phantom.

Use of the third prototype phantom as designed with RGF does not support the hypothesis due to difficulties with air gaps forming between the film and phantom, alignment of the film edge at the phantom surface, and Cerenkov irradiation produced in varying magnitudes throughout the phantom. However, the hypothesis was supported by using the third prototype phantom with manual modifications using RGF. The modifications consisted of using black photographic paper between the film and phantom as well as securing a C-clamp around the phantom body to compress the film cassette and expel any air present between the film and phantom cassette.

Similar difficulties concerning film-edge alignment and the presence of air gaps were expected while using RCF and were thought to be possibly worse due to the higher variation in RCF dimensions. Therefore, RCF was only tested in the third prototype phantom with manual modifications. Under these circumstances, the hypothesis was not supported due to systematic underestimation of the percent depth-dose measurements for depth near the surface (depths < 2 cm). The cause of this systematic error is attributed to both film-edge alignment inaccuracies as well as a perceived depth-dependency of the RCF.

4.2 Clinical Applications of Current Work

First, clinical use of the current third prototype film phantom as designed with bare RGF is not possible due to two major design shortcomings: the production of non-uniform magnitudes of Cerenkov radiation within the phantom due to milling of the Solid Water, and the presence of small air gaps between the film and phantom. However, utilizing appropriate adjustments, black photographic paper between bare film and Solid Water and the use of a C-clamp to compress air between film and phantom can be used with RGF for relative dosimetry of electron beams with reasonable accuracy (± 2 % relative dose, ± 1 mm DTA for CAX PDD). Second, the phantom may also be used with RCF for relative dose measurements so long as the differences in RCF and diode measurements along the CAX PDD are noted. For electron beam commissioning, RCF measured off-axis ratio's may be used in conjunction with a diode measured CAX PDD to reconstruct 2D dose distributions. This method has been previously suggested by (Shiu *et al.* 1989)) and is beneficial in reducing necessary beam-on time associated with electron beam commissioning.

4.3 Recommendations for Future Work

Future work relating to this study should focus on improving the design of the film phantom. First, a film phantom should be designed that eliminates the formation of air gaps within the film cassette. An improved design may utilize a phantom body that uniformly compresses the film cassette when secured, opposed to the current design where the compression bolts are located at the phantom's corners. Second, two separate film cassettes should be constructed, one matching the dimensions of 10"x12" RGF, and a second matching the dimensions of 8"x10" RCF. Both film cassettes should facilitate fine adjustment of the *en face* film edge since significant differences in the dimensions between films taken from different manufacturing lots for are present for both types of film.

Third, the film cassette should not be constructed in a manner resulting in an optically non-uniform inner-cassette surface contacting the film. Fourth, the design of the adjustable cam presented in this study is not optimal and should be modified. The current cam design creates a single contact point between the film and cam which allows for skewing of the film within the cassette. This design may be improved by utilizing a flat cam surface to abut against the downstream edge of the film and eliminate skewing of the film. Lastly, as the clinical use of RCF continues to grow, further investigation should include the most recent film model (EBT2), which might display improved film uniformity and depth-dependency.

References

Almond, P. R., P. J. Biggs, B. M. Coursey, W. F. Hanson, M. S. Huq, R. Nath, and D. W. Rogers. 1999. AAPM's TG-51 protocol for clinical reference dosimetry of high-energy photon and electron beams. *Med Phys* 26 (9):1847-70.

Bos, L. J., C. Danciu, C. W. Cheng, M. J. Brugmans, A. van der Horst, A. Minken, and B. J. Mijnheer. 2002. Interinstitutional variations of sensitometric curves of radiographic dosimetric films. *Med Phys* 29 (8):1772-80.

Bova, F. J. 1990. A film phantom for routine film dosimetry in the clinical environment. *Med Dosim* 15 (2):83-5.

Das, I. J., C. W. Cheng, R. J. Watts, A. Ahnesjo, J. Gibbons, X. A. Li, J. Lowenstein, R. K. Mitra, W. E. Simon, and T. C. Zhu. 2008. Accelerator beam data commissioning equipment and procedures: report of the TG-106 of the Therapy Physics Committee of the AAPM. *Med Phys* 35 (9):4186-215.

Dutreix, J., and A. Dutreix. 1969. Film dosimetry of high-energy electrons. *Ann N Y Acad Sci* 161 (1):33-43.

Fritsch, F.N., and R.E. Carlson. 1980. Monotone Piecewise Cubic Interpolation. *SIAM Journal on Numerical Analysis* 17 (2):8.

Fujisaki, T., H. Saitoh, T. Hiraoka, A. Kuwabara, S. Abe, and T. Inada. 2003. Contribution of Cerenkov radiation in high-energy x-ray and electron beam film dosimetry using water-substitute phantoms. *Phys Med Biol* 48 (6):N105-9.

Gammex, Inc. *Certified Therapy Grade Solid Water Data Sheet* 2009.

Gerbi, B.J., J. A. Antolak, F. C. deibel, D.S. Followill, M. G. Herman, P.D. Higgins, M.S. Huq, D.N. Mihailidis, and E.D. Yorke. 2009. Recommendations for clinical electron beam dosimetry: supplement to the recommendations of Task Group 25. *Medical Physics*.

Hogstrom, K. 1991. *The role of high energy electrons in the treatment of cancer : 25th Annual San Francisco Cancer Symposium, San Francisco, Calif., February 9-11, 1990*. Edited by J. M. Vaeth, J. Meyer and T. Karger, *Frontiers of radiation therapy and oncology vol. 25*. Basel ; New York: Karger.

Hogstrom, K.R. 2003. Electron beam therapy: dosimetry, planning, and techniques. In *Principles and Practice of Radiation Oncology*, edited by C. Perez, I. Brady, H. E. and R. Schmidt-Ullrick. Baltimore: Lippinkott, Williams, and Wilkins.

Khan, F. M., K. P. Doppke, K. R. Hogstrom, G. J. Kutcher, R. Nath, S. C. Prasad, J. A. Purdy, M. Rozenfeld, and B. L. Werner. 1991. Clinical electron-beam dosimetry: report of AAPM Radiation Therapy Committee Task Group No. 25. *Med Phys* 18 (1):73-109.

Khan, Faiz M. 2003. *The physics of radiation therapy*. 3rd ed. Philadelphia: Lippincott Williams & Wilkins.

Menegotti, L., A. Delana, and A. Martignano. 2008. Radiochromic film dosimetry with flatbed scanners: a fast and accurate method for dose calibration and uniformity correction with single film exposure. *Med Phys* 35 (7):3078-85.

Niroomand-Rad, A., C. R. Blackwell, B. M. Coursey, K. P. Gall, J. M. Galvin, W. L. McLaughlin, A. S. Meigooni, R. Nath, J. E. Rodgers, and C. G. Soares. 1998. Radiochromic film dosimetry: recommendations of AAPM Radiation Therapy Committee Task Group 55. American Association of Physicists in Medicine. *Med Phys* 25 (11):2093-115.

Pai, S., I. J. Das, J. F. Dempsey, K. L. Lam, T. J. Losasso, A. J. Olch, J. R. Palta, L. E. Reinstein, D. Ritt, and E. E. Wilcox. 2007. TG-69: radiographic film for megavoltage beam dosimetry. *Med Phys* 34 (6):2228-58.

Perrin, D., K. Hogstrom, and D. Cheek. 2007. Cerenkov Light from Phantom Cassettes in Absolute Dose Measurements Using Radiographic Film. *Med Phys* 34 (6):2629.

PTW. 2009. Therapy Detectors Data Sheet.

Savitzky, A., and M.J.E. Golay. 1964. Smoothing and Differentiation of Data by Simplified Least Squares Procedures. *Analytical Chemistry* 36 (8):12.

Shiu, A. S., V. A. Otte, and K. R. Hogstrom. 1989. Measurement of dose distributions using film in therapeutic electron beams. *Med Phys* 16 (6):911-5.

Tapley, Norah duV. 1982. *Clinical applications of the electron beam*. Malabar, Fla.: R.E. Krieger Pub. Co.

Ten Haken, R. K., B. A. Fraass, and R. J. Jost. 1987. Practical methods of electron depth-dose measurement compared to use of the NACP design chamber in water. *Med Phys* 14 (6):1060-6.

Wong, P. F. 1987. Comparison of electron beam depth-dose and off-axis profiles measured with various detectors in water and plastic. *M.S. Thesis*. The University of Texas.

Appendix: Drawings of the Prototype Film Phantoms Used in This Study

Detailed drawings of the prototype film phantom body and film cassette are presented in this appendix. All dimensions are in centimeters.

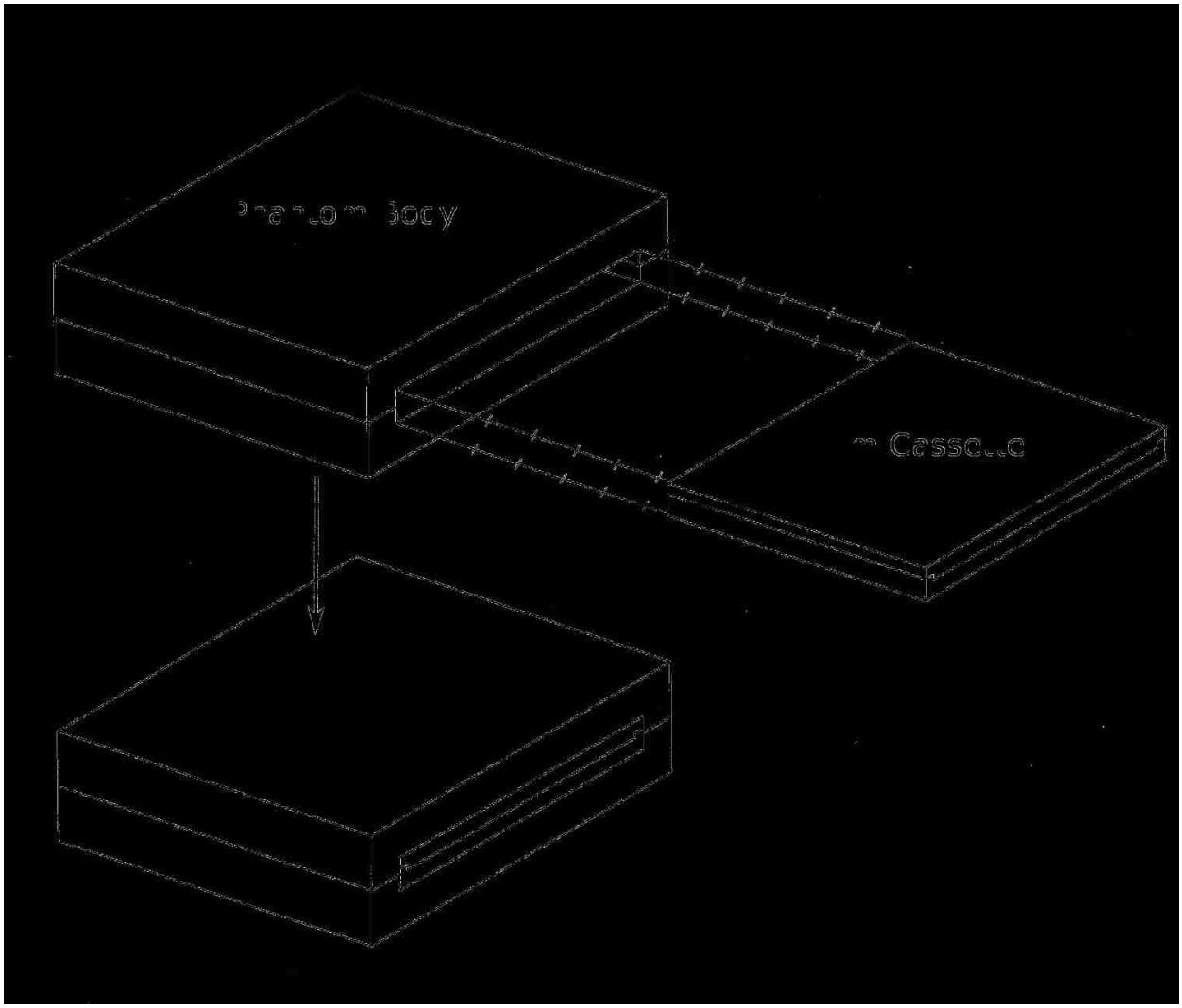

Figure A. 1: Prototype film phantom concept used for all prototypes in this study. The film cassette houses bare radiographic film and is secured within the phantom body by thumb bolts located at the phantom body corners. The thumb bolts were omitted in this drawing.

(a)

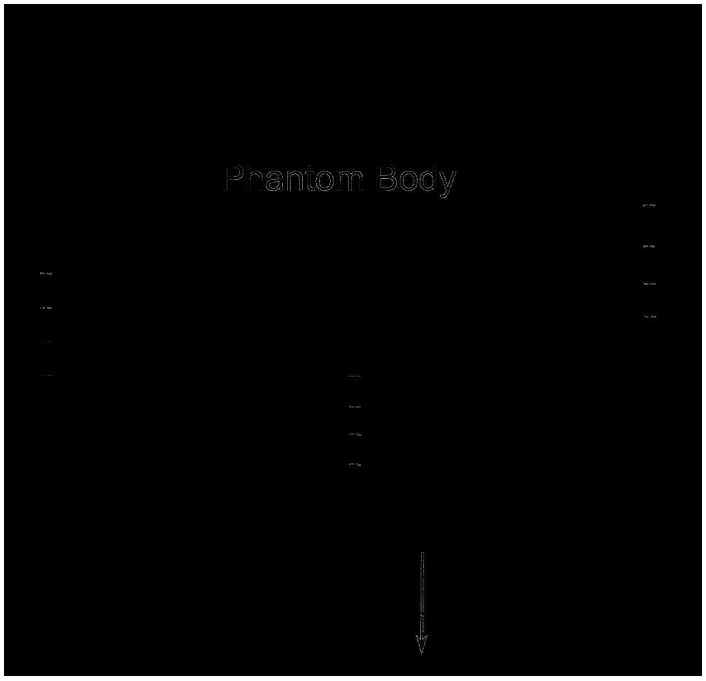

(b)

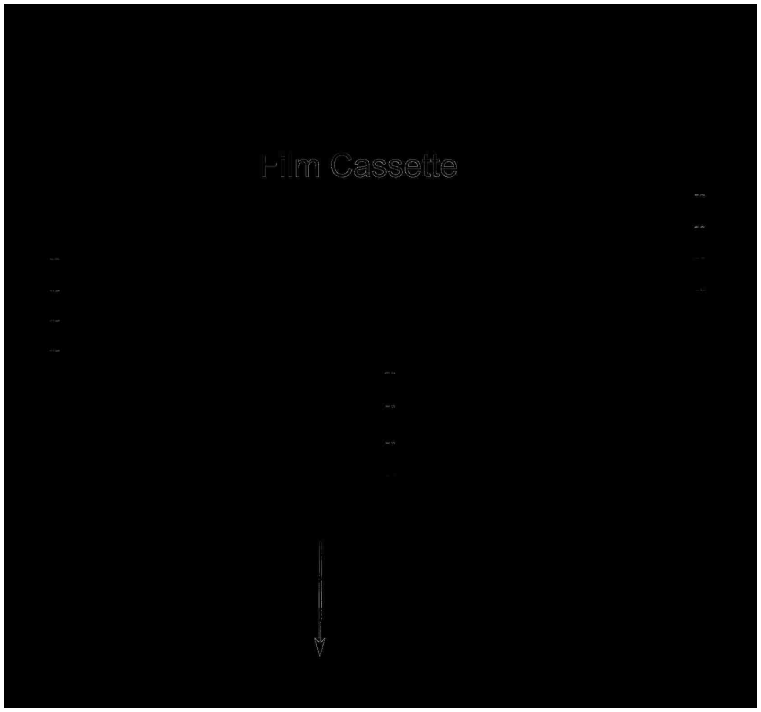

Figure A. 2a and 2b: Exploded views of the prototype phantom body and film cassette, respectively. The thumb bolts have been omitted on the phantom body drawing.

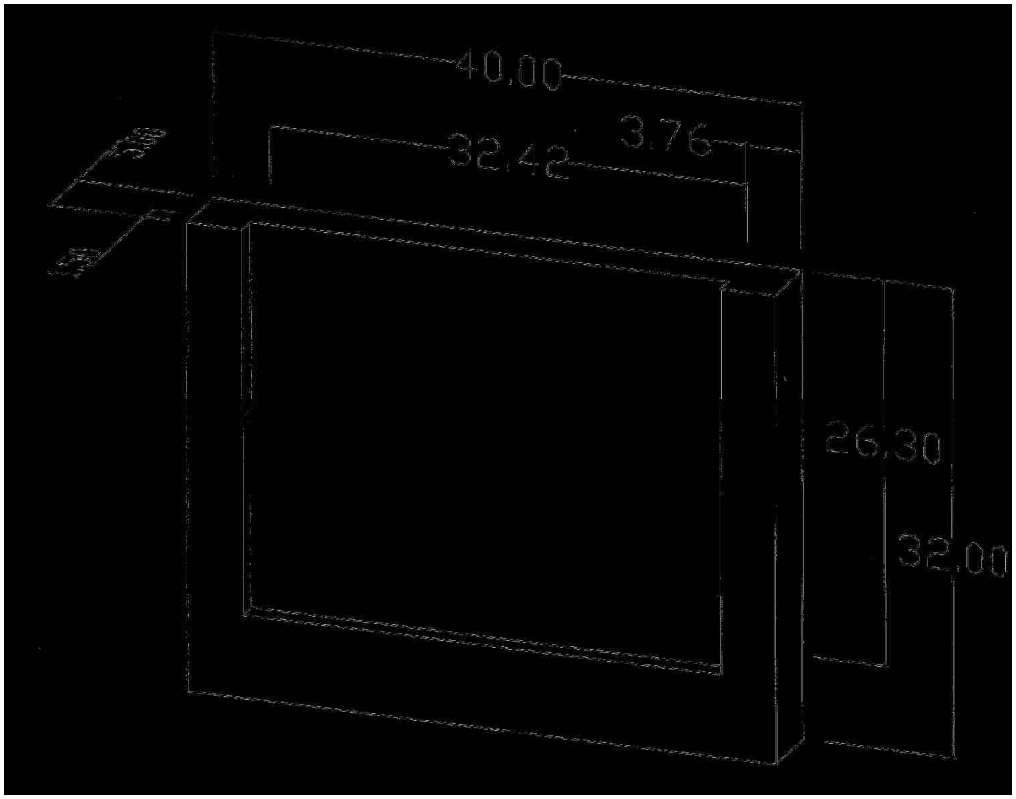

Figure A. 3: One half of the 1st prototype film phantom body. The two halves were identical. The compression bolts at the corners of the phantom body were not included in this drawing.

(a) (b)

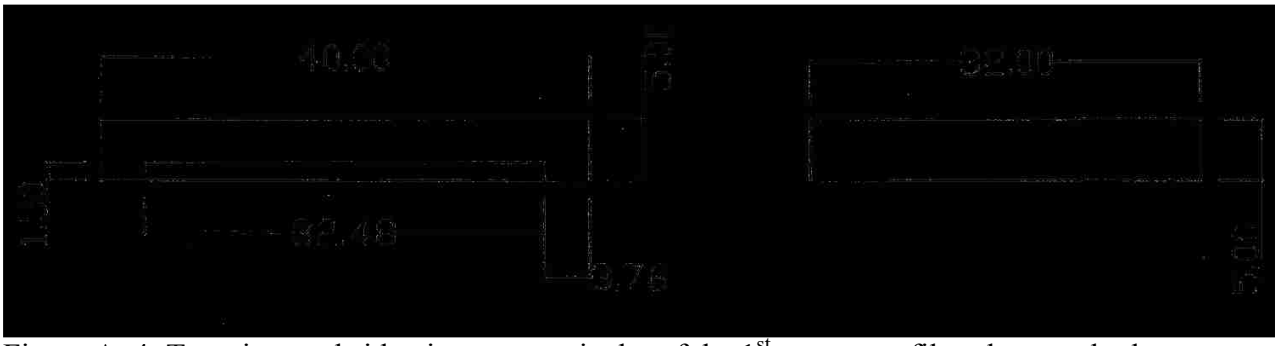

Figure A. 4: Top view and side view, respectively, of the 1st prototype film phantom body.

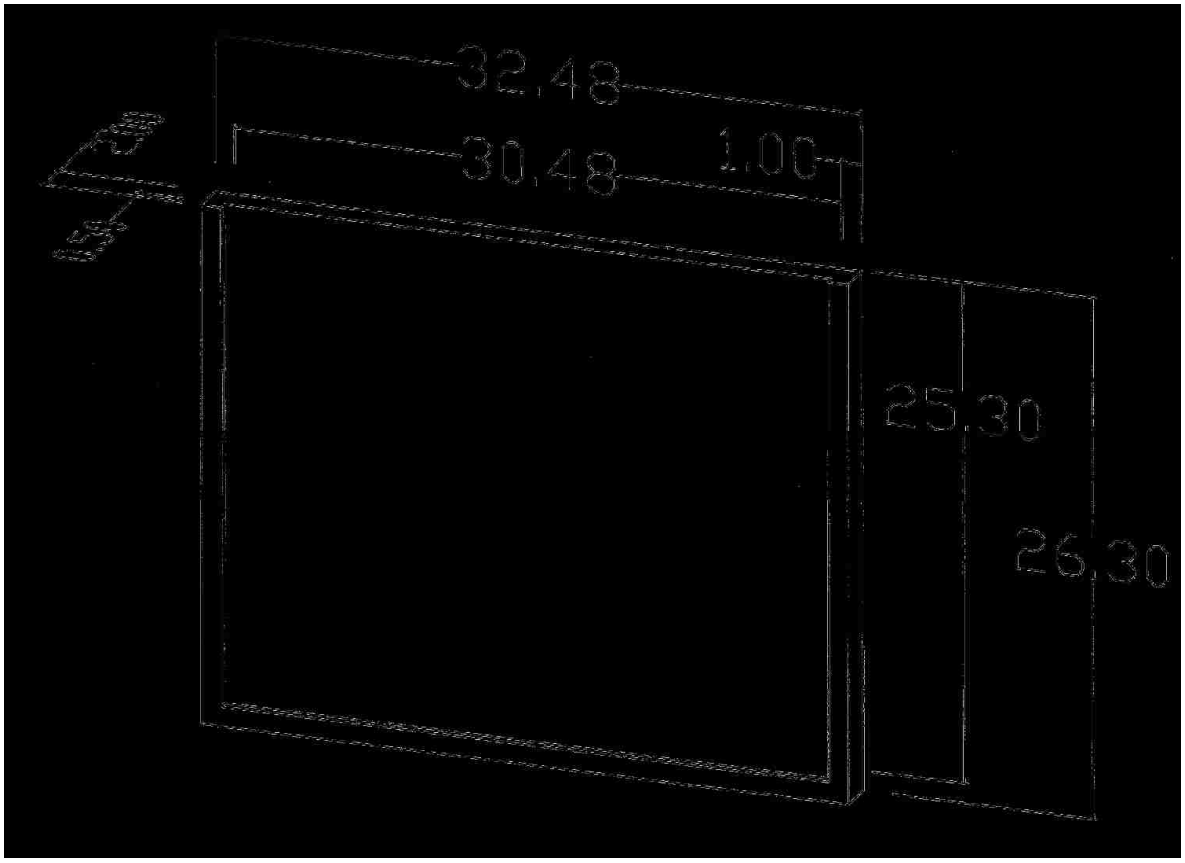

Figure A. 5: Female half of the 1st prototype film phantom cassette. The recess is designed to hold 10"x12" radiographic film.

(a) (b)

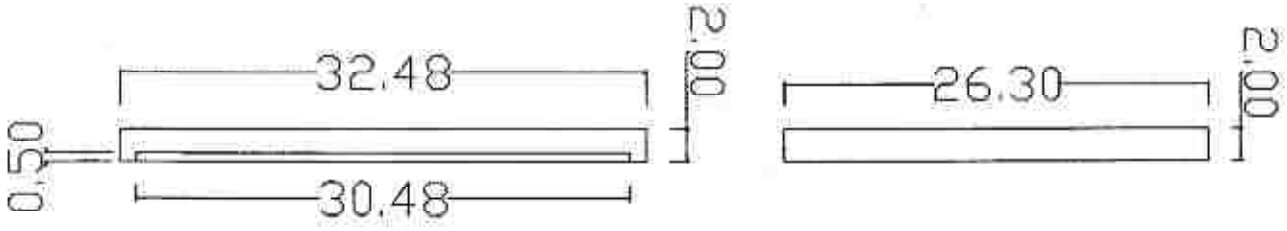

Figure A. 6: Top view and side view, respectively, of the female half of the 1st prototype film phantom cassette.

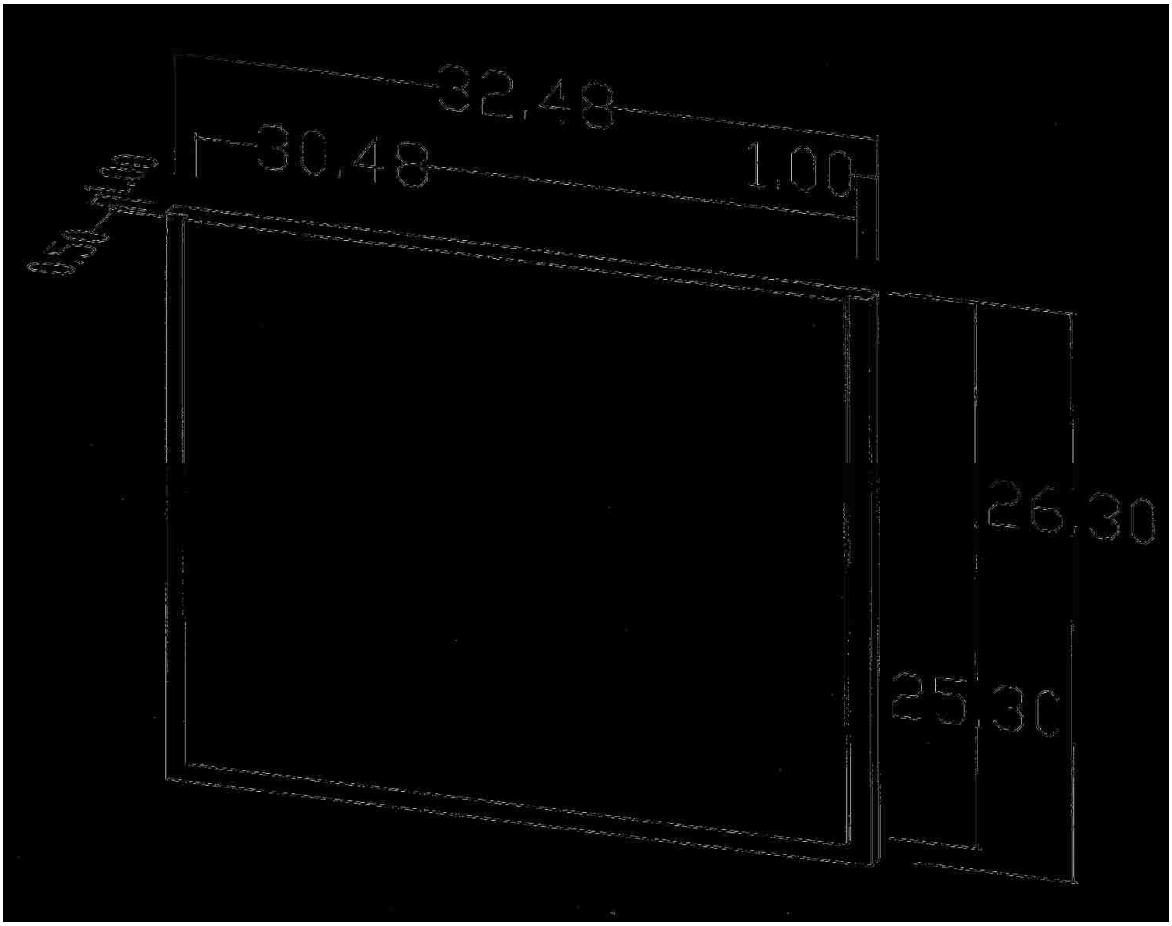

Figure A. 7: Male half of the 1st prototype's film cassette which holds the film firmly in place in the recessed half of the film cassette.

(a) (b)

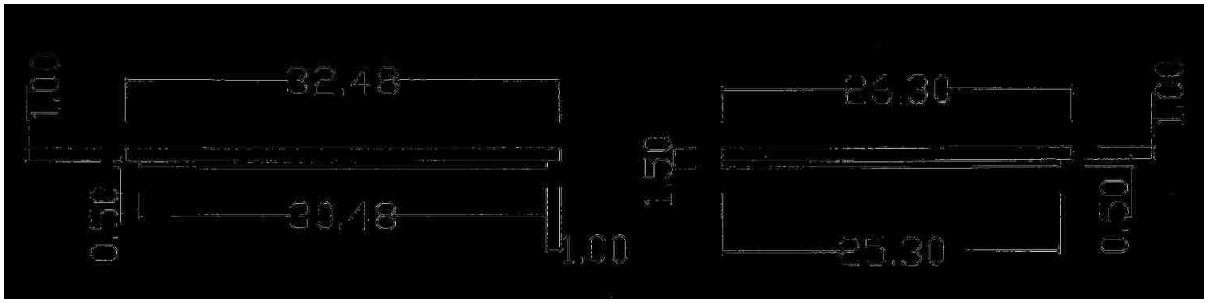

Figure A. 8a and 7b: Top view and side view, respectively, of the male half of the 1st prototype film phantom cassette.

Vita

Chad Robertson was born in Baton Rouge, Louisiana, in 1984 where he lived with his parents and one sister until high school graduation. He completed his Bachelor of Science degree in biomedical engineering with a concentration in pre-med from Louisiana Tech University in Ruston, Louisiana, where he lived from 2002 – 2006. In the fall of 2006 he began his graduate education in medical physics at Louisiana State University. He currently plans to begin a career as a clinical medical physicist.